Study of dielectric and optical properties of agro-food wastes derived glasses and glass ceramics

A

Thesis

Submitted for the partial fulfillment

of the requirements for the award of the degree of

Doctor of Philosophy

By

Gaurav Sharma

(Registration No. 901412004)

Under the supervision of

Dr. Kulvir Singh

(Professor & Associate Dean RSP)

THAPAR INSTITUTE
OF ENGINEERING & TECHNOLOGY
(Deemed to be University)

School of Physics and Materials Science
Thapar Institute of Engineering and Technology,
Patiala-147004 (Punjab), India
(A Deemed University declared under Section 3 of the UGC Act, 1956)

February-2020

Declaration

I hereby certify that the work which acknowledged in thesis entitled "**Study of dielectric and optical properties of agro-food wastes derived glasses and glass ceramics**" in the partial fulfillment of requirements for the award of the degree of **DOCTOR OF PHILOSOPHY** in School of Physics and Materials Science, Thapar Institute of Engineering and Technology, Patiala (Punjab), India is an authentic record of my own research work carried out under the supervision of Dr. Kulvir Singh. The content embodied in this thesis has not been submitted in part or full to any other university or institute for the award of any degree.

(Gaurav Sharma) Dated: 03-11-2020

(Regn. no. **901412004**)

It is certified that the above statement made by the student is correct to the best of my knowledge and belief.

(Dr. Kulvir Singh)

Professor, School of Physics and Materials Science

Thapar Institute of Engineering and Technology,

Patiala-147004 (Punjab), India.

Acknowledgment

The Ph.D period is not just a degree begging course but a short journey of learning. On the completion of this beautiful period of time, I would like to express my feelings for all the people, who made this journey easy and ever-memorable for me. Words are not enough to express my heartfelt gratitude towards my research supervisor, **Dr. Kulvir Singh,** Professor and Associate Dean RSP, Thapar Institute of Engineering and Technology, Patiala. He has been with me, along the way, with esteemed guidance, parental care and immeasurable patience and forgiveness toward my guilt. He not only guided me for research but socially and spiritually too. I expect that his love will keep showering to my life throughout.

I express my gratitude to **Dr. Prakash Gopalan,** honorable director, Thapar Institute of Engineering and Technology, Patiala, for providing me the necessary infrastructure and lab facilities without them, this work could not be possible.

I am deeply thankful to **Dr. O. P. Pandey,** Senior Professor and Head of the School of Physics and Materials Science for his continuous attention and hard concern about my research work. His timely suggestions and admonishment polished my research skills. I am deeply obliged to **Dr. Puneet Sharma. Dr. B.N. Chudasama, Dr. S.D. Tiwari,** and **Dr. Amjad Ali,** who always resolve any technical or practical problems that I faced during the experimentation, they monitored my ongoing work very keenly and suggested pin point solutions to my research queries during the progress reports. I am also deeply thankful to **Dr. Manoj Kumar Sharma, Dr. DP Singh, Dr. Sumendu Jana, Dr. BN Chudasama and Dr. BC Mohanty** for providing the research atmosphere in the department. I must acknowledge **Dr. Gurbinder Kaur, Dr. Jayant Kolte, Dr. Samita Thakur, Dr. Paramjyot Jha, Dr. S.S. Danewalia, Dr. Chandni Khurana, Dr. Bhupinder Kaur, Dr. Suresh Kumar,** for their extensive scientific discussions time to time. All the staff members and operators of SAI Labs (Thapar Institute of Engineering and Technology, Patiala), SAIF (Panjab University, Chandigarh), other instrumentation laboratories and centers and the research scholars of various departments and schools of Thapar Institute of Engineering and Technology, Patiala are also acknowledged, who always offered their precious time and services for any characterization or related help. A special word of thanks goes to, Ms. Neelam Sadana **Mr. P.K. Singh, Mr. Gurjant Singh, Mr. Indermani Mishra, Mr. S.P. Verma, Mr. Lalji Verma, Ms. Aman Kaur Randhawa, Mr. Param Kumar, Ms. Aman Kaur** and for their valuable official and technical support.

Colleagues have a special place of respect in my heart; they helped me understanding research terminology and introduced me to the data analysis techniques. I am thankful to my lab mates

Ms. Neetu Bansal, Savidh Khan, Paramvir Kaur, Shivani Punj, Manmeet Kaur, Trisha Walia, Taranvir Kaur and Vimi Dua for providing me a very constructive and conducive environment in the lab. **Dr. Praveen Jha, Kaushlendra Pandey, Piyush Sharma, Santhosh K. Mahadevan,** and all my colleagues have always acted like my brothers to help me thoroughly during experimental work. **Dr. Devender Kumar and Dr. S.K. Arya** stood like a mentor during the hard days of my Ph.D research. They always acted as a bridge between me and my supervisor. I cannot forget the extreme love and help that I got from my contemporary research fellows, **Pradeep Bhatia, Raveena Chaudhary, Amandeep Kaur, Kaveri Ajravat** and many others.

I dedicate this thesis to my loving family. My mother **Late Smt. Rameshwari Sharma**, my father **Shri Begram Sharma** and my sisters, who dreamt of the highest degree of education in the family. Because of their blessings, I could complete this piece of work. I could not forget my wife **Rashmi Sharma,** and my heartbeat son and daughter **Atharva Sharma and Sanskriti Sharma**, who sacrificed their most valuable time for the completion of my work. They all were always there to support every way, every day throughout the work. During my research work, I shared an enjoyable time with hundreds of friends. However, it is impossible to name every person in limited words. I humbly apologize for the same. I heartedly thank every person, which is not listed above but contributed to this thesis in one or another way.

Above all my beloved Sadguru Sant Rajendra Ji Maharaj always motivated me through his inner voice to do deeds for God. All that I pray to get from him are strength, patience, encouragement, help, love, care, etc. always.

G Sharma

(Gaurav Sharma)

Dated: 03-11-2020

Contents

List of publication

1. Gaurav Sharma, M. Kaur, S. Punj, and K. Singh, Biomass as a sustainable resource for value-added modern materials: a review, ***Biofuels, Bioproducts and Biorefining,*** 13 (2020) 1-23 **(4.53)**

2. Gaurav Sharma, K. Singh, Dielectric and optical properties of glasses and glass-ceramics synthesized from agro-food wastes, ***Materials Chemistry & Physics,*** 246 (2020) 122754 **(3.40)**

3. Gaurav Sharma and K. Singh, Agro-waste ash and mineral oxides derived glass-ceramics and their interconnect study with Crofer 22 APU for SOFC application, ***Ceramics International,*** 45 (2019) 20501-20508 **(3.83)**

4. Gaurav Sharma and K. Singh, Recycling and utilization of agro-food waste ashes; syntheses of the glasses for semiconductor applications, ***Journal of Materials Cycle and Waste Management,*** 21 (2019) 801-809 **(1.97)**

5. Gaurav Sharma, S. K. Arya, and K. Singh, Optical and thermal properties of glasses and glass-ceramics derived from agricultural wastes, ***Ceramics International,*** 44 (2017) 947-952 **(3.83)**

6. S.S. Danewalia, Gaurav Sharma, S. Thakur and K. Singh, Agricultural wastes as a resource of raw materials for developing low-dielectric glass-ceramics, ***Scientific Reports,*** 6 (2016) 24617 **(3.99)**

7. Gaurav Sharma and K. Singh, Dielectric properties of the glass-ceramics derived from agro-food wastes, **(Revision submitted)**

8. Gaurav Sharma and K. Singh, Agricultural waste ashes as new sustainable and renewable source of silicate glasses and ceramics **(To be communicated)**

9. Gaurav Sharma and K. Singh, Catalytic properties of the agro-food waste ashes to remove the heavy metals from waters. **(To be submitted)**

Other publications

10. Praveen Jha, S.S. Danewalia, Gaurav Sharma and K. Singh, Antimicrobial and bioactive phosphate-free glass-ceramics for bone tissue engineering applications, ***Journal of Materials & Engineering C,*** 86 (2017) 9-17 **(5.88)**

11. S.S. Danewalia, S. Khan, S. Dhillon, N. Bansal, Gaurav Sharma, K. Singh, Effect of transition metals on crystallization and conducting properties of SiO_2–CaO–Na_2O–P_2O_5–MO (where MO–TiO_2, MnO_2, Fe_2O_3, and ZnO) glass–ceramics, ***Ionics,*** 26 (2019) 2959-2967 **(2.39)**

12. S. Sharma, M. Rastogi, Gaurav Sharma, K. Singh, Durg Rai, Electrical properties of different Mukhi rudraksha beads: a comparative analysis, ***Materials Today: Proceedings,*** **(2019)** **(Under review)**

13. Jasmeet Kaur Gill, **Gaurav Sharma,** O.P. Pandey, B.N. Chudasama and K. Singh, Effect of secondary phase on optical and conductivity properties of Sr^{2+}/Ca^{2+} doped $La_{1-x}Sr_xNbO_4$ ($0 \leq x \leq 0.4$) system, **Physica B: Cond. Mat** **(Under review)**

List of oral and poster presentation in national and international conferences

1. Poster presented on "Optical and dielectric properties of agricultural wastes derived glasses/glass-ceramics" International conference on Electroceramics **(Expo-2016)** held at Limoges, France 27-29th June, 2016. **(Best Poster Presentation award)**
2. Poster presented on "Properties of agricultural waste derived glasses/glass-ceramics" in an academy of microscope science & technology **(AMST-16)** held at Thapar University, Patiala, Punjab, from 24-27th February, 2016. **(Best Poster Presentation award)**
3. Oral presentation on "Utilizations of the agro-food wastes derived glasses and glass-ceramics for optoelectronic applications" in international conference on electron microscopy & allied analytical techniques **(EMAAT-2019**) at Kufri, Himachal Pradesh, from 7-9th June, 2019. **(Best Oral Presentation award)**
4. Oral presentation on "Glass-ceramics synthesized using agro-food waste ashes and their numerous properties" in international academy of physical sciences **(IAPS)** on '**innovations in physical sciences'** in Campus, CCS University, Meerut from 9-11th August, 2019.
5. Presented the poster in **(IFSM-2018)** international conference held in Shivalik view hotel Chandigarh from 16-20th March, 2018.
6. Poster presented on "Structural and optical properties of agricultural-food waste-derived glasses/glass-ceramics" in an international conference held at Budapest, Hungary on 9-13th July, 2017.
7. Presented poster in national conference **RACMP-2018** held in Kurukshetra University from 12-13th October, 2018.
8. Attended the workshop on based "**Characterization techniques''** held on 27-29th October, 2015 in Thapar University, Patiala, Punjab.
9. Attended the "**Summer School-2016**" on Electroceramics-16 held at Limoges, France 22-25th June, 2016.
10. Attended the "**Summer School-2017**" Innovative technologies in the field of ceramic manufacturing" held at Budapest, Hungary 7-8th July, 2017.

List of abbreviations

BA	Barley ash
BP	Banana peel
CCA	Coconut ash
CH	Coconut husk
CHA	Corn husk ash
CPG	Controlled porous silicate glass
CS	Cotton stalk
CTE	Coefficient of thermal expansion
CRT	Cathode ray tube
DTA	Differential thermal analysis
DSC	differential scanning calorimetry
ECPC	Eggshell derived calcium phosphate cement
EDS	Energy dispersive spectroscopy
E_g	Band gap energy
EM	Electromagnetic waves
ESP	Eggshell powder
E_u	Urbach energy
FTIR	Fourier transforms infrared spectroscopy
H	Hours
H	Heat-treated hours
HApNP	Hydroxyapatite nanoparticles
ICDD	International center of diffraction data
ICP-MS	Inductively coupled plasma mass-spectroscopy
LDPE	Low-density polyethylene
LEDs	Light-emitting diodes
M	Molecular weight
MH	Maize husk
MOD	Mineral oxides derived sample
NBOs	Non-bridging oxygens
ODC	Oxygen defect center
OPC	Ordinary portland cement
PL	Photoluminescence
PS	Peanut shell
PSA	Peanut shell ash
PVA	Polyvinyl alcohol
PCL	Polycaprolactone
RB	Rice bran
RH	Rice husk
RHA	Rice husk ash
RT	Room temperature
SBA-15	Santa barbara acid-15
SBF	Simulated body fluid
SCB	Sugarcane bagasse
SCBA	Sugarcane bagasse ash
SCL	Sugarcane leave
SCLA	Sugarcane leave ash
SEM	Scanning electron microscopy

SG	Silica gel
SLG	Soda lime glass
SOFCs	Solar oxides fuel cells
STE	Self-trapped exciton
T_c	Crystallization temperature
T_g	Glass transition temperature
T_m	Melting temperature
V_m	Molar volume
WA	White ash
WS	Wheat straw
Wt%	Weight percentage
WSA	Wheat straw ash
XPS	X-ray photoelectron spectroscopy
XRD	X-ray diffraction

List of figures

List of tables

Abstract

Glasses play a very important role in modern life due to their applications in electronics, medical, communication, microwave, optoelectronics, etc.[1–4] Basically, glasses are completely disordered materials, which exhibit lack of the periodic arrangement of atoms.[5] However, they look like mechanically solid. According to Zachariasen's and Sun's criteria, some selected materials can only form glasses after rapid cooling from their molten state.[1,6] The properties of the glasses depend on their initial composition, their amount and local arrangement of the structural units. So, proper selection of glass composition could be tailored the properties according to need and application. In recent times, researchers have been reported that the ashes of appropriate agro-food wastes could use as the resources materials to synthesize the oxide glasses and glass-ceramics for numerous applications.[7,8] Since, some of the ashes of agricultural waste contain SiO_2 as the major component along with minor alkali and alkaline-earth metals oxides, which are essential constituents to modify the properties of silicate glasses.[9,10] Therefore, ashes of the agro-food waste could be used to synthesize the inexpensive silicate-based glasses and glass-ceramics to check their suitability in various applications.[11–13] Various synthesis techniques have been employed such as sol-gel, solid-state reaction, and melt-quench to synthesize glasses and glass-ceramics.[14,15] In the present study, the melt-quench technique is used to synthesize the glasses/glass-ceramics from various agro-food wastes ashes. For this purpose, Rice husk ash (RHA), sugarcane leave ash (SCLA), wheat straw ash (WSA), peanut shell ash (PSA) and eggshell powder (ESP) are taken as the initial ingredients. Above mentioned ashes/powder exhibit SiO_2, CaO, MgO, as major components along with Na_2O, TiO_2, K_2O, and Fe_2O_3 as minor components or traced elements.[16–20] These waste ashes exhibit more or less similar constituents, which are required to synthesize silicate glasses and glass-ceramics. However, RHA, SCLA, and WSA have required very high temperature for melting, since, the ashes of these agro-wastes contain up to ~70 weight percentage (wt%) of silica along with some

other element oxides. The addition of ESP in different ashes not only modifies the network of the silicate structure but also decreases the melting point; since ESP has ~97-98 wt% (CaO) with a small amount of alkali oxides such as Na_2O, K_2O, which act as the modifiers in silicate glasses. So, appropriate wt% of RHA, SCLA, PSA, WSA and ESP have been used to synthesize the glasses and glass-ceramics for the present study. The as-quenched glasses and glass-ceramics are characterized and tested using various experimental techniques. The present work of the thesis includes the characterization of these agro-food waste ashes derived glasses and glass-ceramics to study their structural, thermal, optical, and dielectric properties for better applications such as non-linear optics, wide-band gap semiconductors and light-emitting diodes (LEDs), substrate for the solar-energy production, microelectronics. Some selected glasses are used for interaction study with interconnecting materials to check their applicability as the sealant materials in solid oxide fuel cells (SOFCs). Based on the above properties, This thesis work has been divided into six chapters along with references.

Chapter 1 deals with a brief introduction related to the production of different wastes and their disposable process in developing countries. Rapid growth of population, the demand for food is increased day by day, which inherently responsible to create more and more wastes. It is well-known that the rest of the consuming part of any kind of staple food or vegetable is considered as the agro or biowastes. Now a day, agricultural-food wastes are found in the excess amounts due to a lack of knowledge and scientific methods to dispose of them properly. Presently, these wastes are being used as conventional applications like animal feed, mud houses, bio-fertilizers, etc. In recent times, these wastes have been used in civil construction and power generation as fuel.[21,22] During heat-generation in power plants, sugarcane industries, and other small scale industries. The ashes of the agro-food waste have been produced as secondary by-products. These secondary bio-products are used as resource materials like RHA, SCLA, WSA to prepare the glasses and glass-ceramics due to contained silica with other trace elements.[23] Silica is

required a higher melting temperature to convert glass. On the other hand, ESP is a direct source of CaO with a small amount of trace elements, which act as the modifier and reduced the melting temperature of the final melts of the above ashes. The role of different components presented in agro-food wastes is discussed as the glass former, modifier and intermediate oxides and their influences on various properties of glasses. Furthermore, different methods of glass and their applications in modern life have also been summarized. In the last, the chapter ends with the motivation of the present study.

Chapter 2 reviews the literature and gives an idea about the agro-food waste ashes derived glasses and glass-ceramics. Normally, the agro-food wastes have been used in various applications. The advancement in various techniques/methods for the effective use of agro-food wastes is also discussed. Based on the advancement and available the objectives of the present study are given at the end of this chapter.

Chapter 3 is related to synthesize and characterization details of glasses and glass-ceramics. The glasses were prepared by taking the required stoichiometric amounts of different agro-food waste ashes in the wt%. These ashes were first sintered at 1000 °C for 2 h and mixed together using an agate mortar-pestle to make a homogenous mixture. Then, ashes and ESP were mixed and melted at 1550 °C followed by quenching in the air on copper plates. The synthesis parameters and characterization of the as-prepared glasses and glass-ceramics have been discussed in detail in this chapter. Four different glass series have been synthesized using different agro-food wastes ashes/powder. In these series, the different sources of silica along with variable ESP (CaO) content are chosen. The technical details of the various characterization and testing techniques are given. These techniques X-rays diffraction (XRD), differential thermal analyzer (DTA), thermo-gravimetric analyzer (TGA), Dilatomerty, UV-Visible spectroscopy, Fourier-transform infrared spectroscopy (FTIR), Photoluminescence spectroscopy (PL), Scanning electron microscopy (SEM) with attached energy dispersive

spectroscopy (EDS), X-ray photoelectron spectroscopy (XPS) and impedance analyzer are used in this chapter.

Chapter 4 the interpretations of the data obtained from various characterization techniques have been discussed. It has been found that the glasses and glass-ceramics could be made using the different components of the waste ashes. Physical properties like color appearance, density and molar volume of the samples have been calculated and discussed in light of variation in compositions. The direct band gap decreases by adding the ESP on the cost of RHA/SCLA/WSA. Optical studies indicate that Urbach energy increases with ESP content in all the selected glasses. Mass loss with respect to temperature is observed very less, which shows the good thermal stability of the samples. CTE lies from 6-16×10^{-6}/K, which could be exploited to use the selected sample as the sealant in solid oxide fuel cells (SOFCs). The obtained results are also discussed and compared with mineral oxides derived glasses and glass-ceramics of similar composition. The dielectric properties of agro-food waste ashes are comparable as obtained glasses from mineral oxides.

Chapter 5 contains the conclusions drawn from the present research work and offers recommendations for future direction. Interestingly, agro-food waste ashes derived glasses and glass-ceramics are having comparable or better thermal, optical and dielectric properties. These materials are not only inexpensive but also open new avenues of research and innovations. Most of the ashes of the agro-food waste-derived glasses exhibit an optical band gap in the wide semiconductor range. So, these developed materials find applications in the field of the energy sector. Some glasses and glass-ceramics are shown independent dielectric behaviors with temperature and frequency, which can be used in microelectronic and semiconductor devices. Some of the samples are shown better sealing properties at various thermal cycles as compared to similar mineral-derived glasses and glass-ceramics.

These waste ashes derived glasses and glass-ceramics can be used as biomaterials, catalytic materials to remove toxic and heavy metal from drinking water. Most importantly, agro-food waste ashes are sustainable and abundantly available. So, in the future, these wastes can be used as resource materials to generate many cost-effective value-added engineering materials.

Chapter 1 Introduction

1.1 Background

Food demands are increasing due to increasing the population of the world in every passing day. Unused portions of the agricultural products and foods are considered as agro-food wastes. These wastes are creating not only environmental problems but also management related problems, particularly, in developing and agrarian-based economy countries. Major and common agricultural wastes are husk, straw fibers, hulls, shells, bagasse, leaves, etc.[24–27] Usually, these wastes are biodegradable in nature. Self-biodegradation of these wastes is time-dependent. It is varying from waste to waste. However, during this process, they also create pollution up to some extent in water bodies and atmosphere. Lack of effective and safe ways to manage these wastes leads to a direct impact on human health.[28] This problem is very severe in developing countries, particularly highly populated agrarian-based economy countries. It is increased in many folds when the burning of these agro-food waste residues are taken place in open-air that releases greenhouse gases such as carbon dioxides, carbon monoxide, oxides of sulfur and nitrogen.[29,30] The release of these gases causes acid rain, ozone layer depletion, and many other environment-related problems. Thus, effective environmental-friendly and scientific ways are required to manage and dispose of these wastes properly. Apart from the conventional use of the wastes in recent times, researchers have suggested that these wastes could be used as a resource to convert them into value-added materials according to the need and applications.

1.2 Common agro-food wastes

Most of the agrarian countries, particularly, south Asian countries are generating large amount of agricultural wastes such as rice husk (RH) or paddy, maize husk (MH), sugarcane bagasse (SCB), sugarcane leave (SCL) and wheat straw (WS), vegetables waste, food products, tea, oil production, jute fiber, peanut shell (PS), coconut husk (CH), cotton stalk (CS), and others. Similarly, eggs are

also produced and used at a large scale due to common food across the globe. Eggshells (ES) mostly dumped in open areas, without any proper treatment, which created environmental problems. According to the world health organization, 1200 million tons of agro-food wastes are generated every year, in India. Agricultural wastes are conventionally used as animal food, heat generation in power plants, small scale industries, and compost fertilizers, etc. In addition to this, currently, a lot of efforts are being made to use agro-food wastes to generate fuels, catalysts, etc.[31–33] Therefore, it is imperative to know the chemical and physical properties of agro-food wastes in order to find their use for appropriate applications.

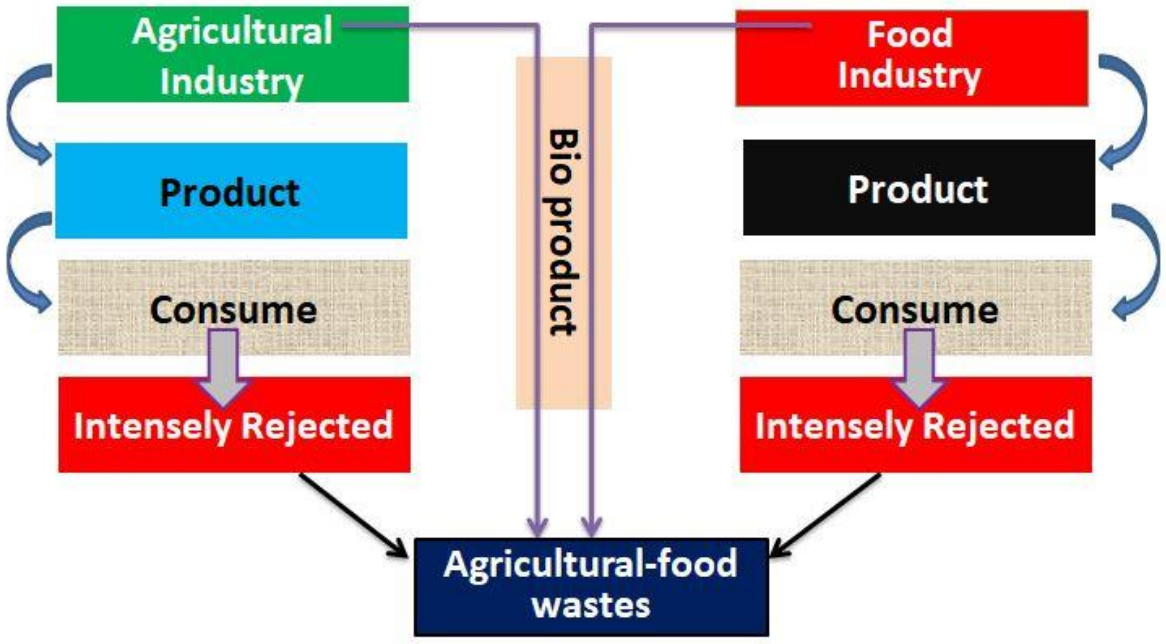

Fig. 1.1 Agro-food wastes generation from agricultural and food industry

Moreover, properties like surface area, small particle size are also important for many applications like wastewater treatment, degradation of organic dyes and photo catalyst. Few characteristics (compositions, cellulose, lignin, C, H, O, N, S, etc.) of common agro-food wastes like RH, SCL, SCB, WS, PS, and ES are given in table 1.1.

Table 1.1 Chemical and physical properties of RH,[34] SCL,[35,36] SCB,[35,37] ES,[38,39] WS,[40] and PS[41]

Waste ⟶ / Constituents (wt%) ↓	RH	SCL	SCB	ES	WS	PS
Cellulose	31.30	27.64	31	30	35.30	45.0
Hemi-celluloses	24.30	19.15	23	50	37.50	26.81
Lignin	14.30	11.95	21	15	7.90	33.60
C	45.28	-	58.14	42.90	44.88	37-55
H	5.51	-	8.05	5.70	6.16	-
O	45.10	-	34.57	38.25	-	-
N	0.67	14	0.69	0.62	1.32	-
S	0.29	2.20	0.19	0.16	0.20	-
Crude protein	-	-	1.59	3.50	-	-
Crude fat	-	-	-	1.30	-	2.7-6
Ash contents	11.70	-	4.34	7.90	5	3.46

1.3 Conventional applications of agro-food wastes

Many agro-food wastes could be fed to animals without any modification in them. It does not require any fermentation or treatment for the aforementioned use. Additionally, these agricultural wastes are being used to make biocomposites and biofertilizers to enhance the fertility of the land.[16,42] It has been found that composted RH, dry SCL, etc., can help to improve the growth of plants as they increase soil fertility by improving the organic content in the soil.[43] The agro-waste products viz. wheat bran, mustard oil cake, cicerbrown husk, PS, and tea waste have been composted to form biodegradable value-added products like biofertilizers.[16,44] SCB has cellulose, hemicellulose and few% of lignin, which generates a little amount of residual ash after fiery.[45,46] Due to the degradation of some materials, it contains few nutrients and can be used as fertilizer for crop growth.[47] Significant changes have been observed in the growth of different crops when bio compost is used as a fertilizer grown. These crops' growth is depended on climate and cultivation conditions in different countries.[48] Omatola *et al.*[49] concluded that agricultural wastes such as RH can be used as chemical fertilizers, insecticides, pesticides, etc.

Several biowastes like RH, SCL, WS could be used as the source of energy and have to meet the energy demands of a nation.[50] Presently, in India, some of the wastes are used to generate the energy directly or indirectly by burning of biomasses as depicted in Fig. 1.2. Agro-food wastes have a higher amount of organic components, hence; they can act as a potential source of renewable energy to generate biofuels.

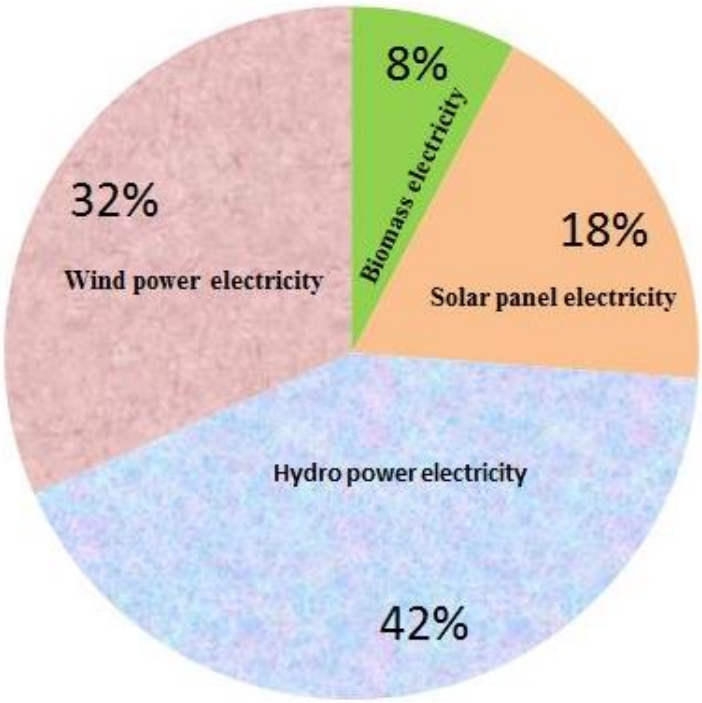

Fig. 1.2 Biomass used in energy production in India

Thermo-chemical processes like pyrolysis are being used to obtain fuels from biomass and the value of the surface area of activated carbon obtained from pyrolysis of RH by different chemical activation methods, which is presented in table 1.2. Zhang *et al.*[51] attempted to achieve the highest possible gas yield from microwave pyrolysis of RH using Ni, Fe, and Cu as catalysts. It was found that the nickel (Ni) catalyst produces the highest gas yield. Another possible use of agricultural wastes like RH is produced silica, which found ~80-90% silica depending upon the processing parameters.[9,52]

Table 1.2 Bio-oil yield from different reactors and optimum conditions for obtaining the highest yield with references

Reactor	Bio-oil yield	Optimum conditions
Fixed bed reactor[53]	>40%	Pyrolysis temperature >500 °C, A heating rate >200 °C/min, Holding time >2min, Condensation temperature <-10 °C and Particle size <0.50 mm.
Fluidized bed reactor[54]	~60%	Pyrolysis temperature between 400-450 ^{o}C
Downdraft circulating fluidized bed reactor[55]	53.2%	Pyrolysis temperature of 550 ^{o}C
Conical spouted bed reactor[56]	70%	Pyrolysis temperature of 450 ^{o}C

Further, pure silicon nanoparticles can also be synthesized from RH, which has a lot of applications in electronics and energy sectors.[57] Kavitha *et al.*[58] found that direct pyrolysis of RH can produce SiC, which has many applications because of the low coefficient of thermal expansion (CTE), good oxidation resistance and excellent abrasion/wear resistance. Adebisi *et al.*[59] highlighted that the importance of using agricultural wastes to produce nanosized solar grade silicon, which involves lesser cost as compared to extract from the conventional methods, in addition to the above applications of different agricultural wastes. Advent in process technology, the agro-food wastes are used to extract some other valuable elements and compounds, directly. In general, two distinct stages are mainly used to decompose the existing wastes like RH, SCL, and WS. Carbonization, basically during the carbonization process, rice paddy is combusted at more than 300 °C to decompose the volatile matter from it, which also releases combustible gas and tar. De-carbonization is actually a process, in which, RH is combusted at a very high temperature (~1400°C) for combustion of the carbon char from RH. Different techniques like sol-gel, co-precipitation, and simple acid and alkaline treatments are being used to extract various % of silica from RH wastes, as shown in Fig. 1.3.

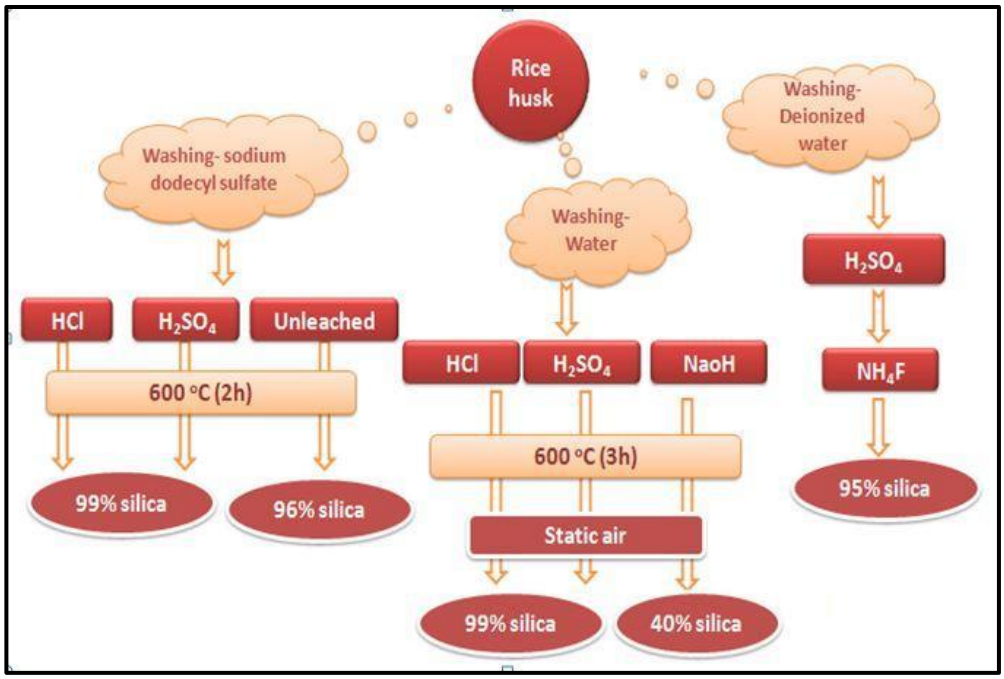

Fig. 1.3 Different techniques used for the extraction of silica from RH

Apart from the extracting of silica from the agro-food wastes directly; there are many other possible uses of the wastes. The residues of these wastes are also used to generate the heat in the boiler, sugar mills; small scale industries and household applications particularly in low per capita income countries. Ashes of the agro-waste are considered as the second-generation byproducts, which used in above mentioned small scale industries. These ashes are usually dumped in open fields or places, which led to polluting the water and environment due to their small particle sizes, lightweight and high porosity, etc. Ashes of different agro-food wastes contain different elements in oxide form. The content of these oxides is tabulated in table 1.3 for common agro-food waste ashes. The contents of the oxides are variable (±5%) depending on processing temperature and region from where the agro-food wastes are collected.

1.4 Chemical constituents of agro-food waste ashes

Agro-food waste ashes may find some applications in different fields of engineering such as civil construction, fertilizers, extraction of valuable elements or elements oxides, etc. The effective,

systematic and scientific uses of these ashes not only provide good value-added materials but also get rid of management-related problems of these ashes.

Table 1.3 Various wastes ashes in oxides and their weight percentage (wt%) in rice husk ash (RHA), sugarcane leave ash (SCLA), corn husk ash (CHA), peanut shell ash (PSA), wheat straw ash (WSA), barley ash (BA), coconut ash (CCA), eggshell powder (ESP) and banana peel (BP)[7,10,60,61]

Wastes → / Components ↓	RHA	SCBA	CHA	PSA	WSA	BA	CCA	ESP	BP
SiO_2	91.03	65.8	35.7	29.3	73.95	62.04	25.68	0.54	6.6
CaO	1.95	4.2	5.80	21.9	5.21	4.48	4.08	98.03	3.2
MgO	0.81	1.7	9.91	6.7	1.83	2.16	5.38	0.41	1.3
K_2O	3.18	7.5	20.1	25.7	11.51	19.27	31.23	-	67.6
Na_2O	0.08	0.6	5.10	0.1	-	0.44	8.40	0.41	-
Al_2O_3	0.35	5.5	0.40	3.7	0.91	0.19	1.74	0.46	0.3
Fe_2O_3	-	3.3	0.30	1.3	1.51	0.17	2.65	0.15	0.2
P_2O_5	-	-	22.5	-	-	2.52	-	-	3.4
SO_3	-	2.0	-	3.2	-	1.42	0.71	-	-
TiO_2	-	-	-	-	1.92	0.02	-	-	-
MnO	-	-	-	-	-	-	0.05	-	-
Cl	-	-	-	-	-	-	0.61	-	-

SCLA, WSA, RHA and other agricultural wastes ashes contain 22% carbon-content, with variable 30-78% SiO_2 along with K_2O, Na_2O, MgO, P_2O_5 and some other trace elements.[17,62,63] Content of various metal and metalloid oxides depends on the region, fertilizers used during plant growth, quality of soil, burning atmosphere and processed temperature of different agricultural wastes. The chemical composition of common agro-food waste ashes along with food wastes are given in table 1.3. As observed from the table, the most common inorganic component is SiO_2, apart from alkali and alkaline-earth metal oxides along with some trace transitions elements oxides. Based on the presence of different metals and metalloid oxides; these ashes could be used in cement and civil construction, glasses and glass-ceramics, silicate-based ceramics directly or indirectly.

1.5 Different agro-food waste ashes and their uses

Different agro-food waste ashes are used for various applications. These applications are, particularly, in the field of civil engineering, materials science, and electronics, etc.[64,65]

1.5.1 Cement and civil constructions

Cement and construction industries are utilizing agro-food waste ashes to enhance the properties of cement. Many researchers have found that by adding RHA, SCLA, WSA and some other residue ashes of the wastes into cement, the mechanical properties such as durability and compressive strength of the cement are improved.[66,67] RHA is partially filled in cement concrete, which improves the properties of the concrete.[68] Banger *et al.*[69] suggested that the strength of the concrete can be improved after adding sugarcane bagasse ash (SCBA) up to 10 wt%. Dhengare *et al.*[70] studied the effects of the use of SCBA on the mechanical strength of concrete by partial replacement of cement at the ratio of 0%, 10%, 15%, and 20%, by weight. The addition of the 10 wt% RHA in the composite is improved the compressive strength, fire and acid resistance of the as-prepared composite, which is suitable for making bearing bricks for the buildings.[71] Ali *et al.*[72] reported that 10-50 wt% of RHA added with alumina is created more porosity and new phases like cristobalite, corundum (Al_2O_3 related phase), etc., which increases the tensile and compressive strength of the concrete. Mehta[73] concluded that when RHA is replaced with cement up to 50 wt%, higher compressive strength than that of ordinary portland cement (OPC) concrete can be achieved. Javed *et al.*[18] have investigated that after using fibre waste, RHA, lime soda powder as the filler in cement, the lightweight concrete blocks are formed with better mechanical properties. The water absorption and bulk density of these concrete blocks can be reduced by adding RHA. Cisse *et al.*[74] reported that the addition of RHA into cement, the physicomechanical performance of the final products are improved. RHA added cement has a lower cost as compared to using other types of additions in the cement. Jauberthie *et al.*[75] also reported that the polozon of the agro wastes could

be used for making lower-cost cement and agro waste based silica can be used in many other applications such as filler in the road concrete.

1.5.2 Filler in synthetic rubber, ink, and cosmetics

RHA, SCLA could be used as the silica to increase mechanical properties such as hardness, tear strength, resilience, tensile strength of the rubber and ink industries. Due to the high surface area of agro-food waste ashes, these are used as the vulcanizing rubber filler up to a certain limit. Nanohybrid silica was fabricated from RHA and further used as filler in dentistry due to the low surface area (30 m^2/g) with good mechanical properties like hardness, flexural and compressive strength.[76] Tangboriboon *et al.*[77] found the 96% CaO with other inorganic contents, which are used as rubber filler to make thermal insulation materials in the various devices.

1.5.3 Extraction of elements and compounds

Recently, agro-food waste ashes are taking considerable attention from the scientific community in view of their potential use as the fruitful products in various applications. Since, most of the agro-food wastes contain silica, calcium carbonate, alkaline earth metal oxides, and some trace elements oxides, direct or after some modification of these ashes can be used particularly as bioactive materials, heating elements silicon carbide (SiC), crucible and other silicate-based materials. In addition to this, the ashes of the agricultural waste could be used directly to synthesize silicate-based glasses and glass-ceramics for different engineering applications such as substrates for solar cells, microelectronic applications due to their lower dielectric constant with the wide range of the temperature and frequency independence.[78,79] However, to synthesize glasses from only RHA (SiO_2:90-94%) requires a higher melting temperature i-e. more than 1600 ºC, so, the proper selection of other wastes like ESP, which contain CaO would not only reduce the melting point of RHA based glasses but also modify the properties of the as-prepared glasses, accordingly. Since, silica is the major component of RHA, a number of glass compositions could be synthesized from RHA based silica for their optical and electronic applications. Calcium silicates like

$Ca_2SiO_4/Ca_3Si_2O_7$ act as suitable host materials for producing glasses and glass-ceramics added with alkali, alkaline-earth metal and rare-earth-doped phosphors for light-emitting diodes (LEDs), lasers, etc.[80]

1.5.4 Bioactive materials and bioglasses

Different bioglasses and bio-ceramics are being developed focusing on a variety of biomedical applications (Fig. 1.4.).[81–85] Bioglass being one of its subsets is used in different applications such as orthopedics and dentistry etc.[86–88] Attempts are currently being made to replicate its composition using agro-food wastes ashes. RHA has been used to prepare amorphous silica as the resources for making bioactive materials. Three types of amorphous silica namely brown ash (BA), white ash (WA) and silica gel (SG) have been prepared from rice husk. BA can be prepared by burning husk at 700 °C and it contains about 96% silica. WA contains 99.78% silica, which can be prepared by combustion and further acid treatments. SG can be prepared from BA through extraction of silica and acid neutralization process. Bioactivity of these different ashes are evaluated and reported at different temperatures i.e. 900 °C for BA, 1100 °C for SG and 1200 °C for WA after dipping into simulated body fluid (SBF) and Tris buffer solution. BA and SG ceramics show more bioactivity than WA ceramics. This is due to the formation of silanol (Si-OH) groups on the surface of the silica particles in the presence of the hydrolysis process.[89] In the case of SG, hydrolysis might be more straightforward due to the inherent gel formation of materials. WA shows the low response for bioactivity due to the presence of some impurities when treated at high temperatures (~1200 °C). The effect of sintering temperature on the mechanical and physical properties of bioactive glasses prepared from agro-food wastes is presented in table 1.4. Textural properties in biomaterials also play an important role in the fabrication of the apatite layer. Increment in the specific surface area and pore volume of bioactive glasses may greatly accelerate the apatite layer formation and enhance the bioactive behavior.[90,91] ES waste has been used to synthesize nanocrystalline HAp by microwave, wet chemical, hydrothermal and mechanochemical processing

methods. Different processing methods influence HAp parameters such as particle size, crystalline size, surface area, pH factor, and morphology, physical and mechanical properties. All these parameters directly influence the bioactivity of the materials. Eggshell derived calcium phosphate cement (ECPC) has superior physical and biological properties than the synthetically derived calcium phosphate cement. This is due to the presence of trace ions in ECPC, as reported by Jayasree *et al.*[92] However, the main limitation of calcium hydroxide cement is low bioactivity.[93] Nano ESP is recently being used to enhance bioactivity and alkalinity of calcium hydroxide materials, due to more Ca^{2+} ions is being released in the medium. The presence of some trace elements such as Ca, P, and Mg in ESP may have also played a role in apatite formation and stabilization on the surface.[94]

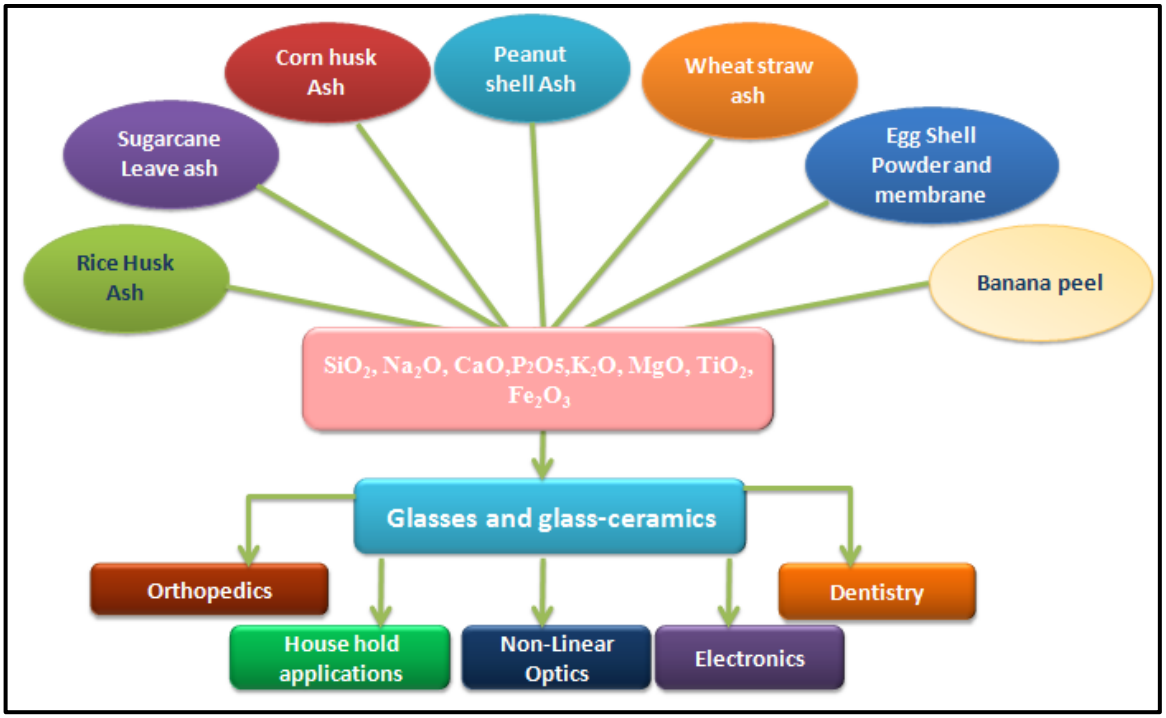

Fig. 1.4 Different oxides are present in the agro-food waste ashes, hence, these can be used to synthesize glasses and glass-ceramics and find use in a variety of applications

Table 1.4 Bioactive properties of silica-based glasses and glass-ceramics derived from RHA at different sintering temperature

Comp-osition	Sintering temperature	Methods	Phases	Density (g/cc)	Conclusion	Ref.
SiO_2-Na_2O-CaO	> 700 °C	Sol-gel	Three phases Combetite-I, $Na_6Ca_3Si_6O_{18}$ & $Na_2Ca_2Si_2O_7$	2.20	-	[79,95]
	At 900 to 1000 °C	Sol-gel	Combetite-I, small amount of combetite-II, $Na_4Ca_4Si_6O_{18}$	-	Good bioactivity, biodegradability	-
	>1050 °C	Sol-gel	-	-	Degradability, bioactivity decreases, show cracks, strength become lower	-
SiO_2-Na_2O-CaO-P_2O_5	At 650 to 700 °C	Melt-quench	hexagonal $Na_2Ca_2Si_3O_9$ $Ca_3Si_2O_7$	-	-	[96]
	At 1050 °C	Melt-quench	$Ca_3Si_2O_7$	2.27	Good bioactivity without affecting of the crystalline phases	-

1.5.5 Glasses and glass-ceramics

Glasses and glass-ceramics are being used in the field of engineering and medical science such as window glasses, sealing materials in solid oxide fuel cells, non-linear optics, lasers, a substrate in solar energy production, hyperthermia treatment of cancer, testing glass slides, automobiles, etc.[3,97–105] Normally, these glasses and glass-ceramics are synthesized using different mineral oxides.[106,107] Based on different components of glasses, these could be categorized as the glass formers, modifiers, and intermediates oxides. All components should have some specific properties to act as formers, modifiers, and intermediates as given in table 1.5. There are few well-known glass formers such as silica (SiO_2), phosphate oxide (P_2O_5) and boric oxide (B_2O_3), which act as glass network former in oxide glasses. In addition to the above-mentioned formers, there are some other oxides that work as conditionally glass formers such as GeO_2, Bi_2O_3, As_2O_3, Sb_2O_3 TeO_2,

Al_2O_3, Ga_2O_3, and V_2O_5, under certain circumstances. There are some other elements also called intermediate oxides, whose behavior is completely depending on their percentage (%) in the glass composition. Intermediate oxides could act as glass formers or modifiers.[1] Along with this, there is some such compounds that also alter the properties of the glasses and make it better applicants for further uses after adding up to the certain limit. Alkali and alkaline-earth metals are known as the glass modifiers, which mainly influence the overall properties of the main components.

Table 1.5 Classification of glass formers, modifiers, and intermediates based on their bond strength

Oxide	**Single bond strength kJ/mole**	**Oxide**	**Single bond strength kJ/mole**	**Oxide**	**Single bond strength kJ/mole**
Formers		**Modifiers**		**Intermediates**	
SiO_2	443	MgO	154	ZnO	301
V_2O_5	330	Li_2O	150	BeO	261
GeO_2	450	CaO	134	PbO	303
B_2O_3	372	K_2O	53	ZrO_2	253
P_2O_5	462-370	Na_2O	36	Y_2O_3	248
-	-	-	-	Al_2O_3	280-221

Apart from this, if color of the glasses is necessary for their further optical and fibre applications then added a colorant with a very small quantity. There are different transition elements added for different colors. However, *3d* transition metals or *4f* rare-earth elements are mostly used for color change. Uranium oxide is the best colorant but it degrades overall properties due to its radioactive behavior, so, this is not much use as the colorant. Finally, there are some elements added in a small amount such as NaCl, CaF_2, arsenic and antimony oxides into the glass forming process, which reduced the formed voids and bubbles in it, which are called the fining agent.

Recently, some reports have appeared in literature according to properly selected agro-food waste ashes could produce most of the above-mentioned glasses, ceramics, and glass-ceramics. Since, common agro-food waste ashes contain almost all the desirable oxides, which are required to synthesize silicate-based glasses and glass-ceramics.[60,108]

1.6 Silicate based glasses and its application

Most of the commercially available glasses are silica-based ternary systems with adding the variable amount of oxides to achieve the specific properties. These additive oxides content could act as the modifiers and reduce the melting temperature with desirable applications such as containers, lamps and window glasses, substrate, microelectronic, applications, etc. The addition of soda-lime into silicate glasses produces large numbers of non-bridging oxygen (NBO) atoms or breaks the connectivity of the network. These NBOs atoms cause a huge reduction in the viscosity and glass transition temperature (T_g) of the glass relative to vitreous silica. T_g value of commercial available soda-lime-silica glass is in the temperature range of 550-580 °C.[19] CTE depends on the NBO atoms in the network system; it is about 8-9×10^{-6}/K for soda-lime glasses, which means that these glasses are much more susceptible to thermal shock failure than other glasses. The combination of a lower T_g and a higher CTE severely limits the applications of these glasses for products requiring good structural, thermal, optical performance and other various applications. Glasses derived from agro-food waste ashes are inexpensive and easily available as compared to mineral-derived glasses. The formation of glasses and glass-ceramics using proposed approaches of waste ashes having other advantages too. Firstly, it could be a better and effective way to manage huge amounts to produce efficient engineering materials. Additionally, the organic contents present in the waste materials exhaust some gases on burning, which provide in-situ foaming sites for the prepared materials. These byproduct gases can also be collected carefully for additional applications. Inherent spongy nature of the glasses and glass-ceramics is beneficial to produce low weight material with high surface area, which enhances its surface reactivity.[38] Glasses and glass-ceramics derived from agricultural waste and ESP, contain K_2O, Na_2O (5-20 wt%) and CaO (92-94 wt%), inherently, which decrease the melting temperature as well as increase the performance as a bioactive material in biomedical applications.[19,109] Therefore, it is worthwhile to form the glasses and glass-ceramics from agro-food wastes and study their suitability for different applications.

The most common fluxes are the alkali oxides, especially Na_2O (soda) and PbO to produce the glasses. Most commercial glasses contain soda, including those used for containers and window glasses. Window glasses can be produced using many types of ashes, even at a lower price than available in the market through melt-quench, sol-gel method, which can also reduce the overall dumped ashes quantity. Cornejo *et al.*[17] reported that a typical window glass composition (soda lime) that was made from RH and ES with a small amount of table salt and alumina from non-waste sources.

Thus, the careful selection of wastes and processing techniques can result in the generation of multiple value-added materials. However, extensive research is required for large scale use of these renewable and sustainable resources to convert into valuable materials. So, based on the application, these can be selected, extracted and converted into applications based materials, to make engineering materials like bioactive glasses, dielectric and optical materials. Utilization of these agro-food waste ashes provides a practical and environment-friendly way to convert them for further uses. Further, these by-product materials could replace conventionally synthesized mineral-based products. This approach could also provide an effective solution to the agro-food waste management problems.

Therefore, agro-food waste ashes could be used to make glasses and glass-ceramics for different fields of engineering and medical such as substrate, slides absorbers, reflectors. Therefore, this research work will provide alternative ways for better use to them into effective and inexpensive byproducts.

Chapter 2 Literature review

2.1 Recycling and utilization of the agro-food wastes

The ever-growing amount of agro-food waste materials increases the environmental pollution concerns, with the ensuing threat of intoxication to human-health, as well as the contamination of water. Regardless to the region, the consumption level is already having a substantial impact on the environment across the world. The main problem with agro-food waste materials is with their disposal or storage. To overcome the problem of acquired the area by wastes, most of the farmers are burnt these agro-food wastes in an open area. The burning of agro-food waste causes many harmful environmental threats. So, the huge amount of agro-food wastes is a concern for the scientific community, to search for viable solutions for them. Many research groups have been working on the recycling and utilization of the agro-food wastes like rice husk (RH), maize husk (MH), sugarcane leave (SCL), peanut shell (PS), and wheat straw (WS), eggshell (ES), etc. To utilize agro-food wastes as resource materials particularly to synthesize glasses and glass-ceramics and their optical and dielectric properties are reviewed in this chapter. Based on the available literature, the motivation for selecting the objective of the present work is given in the last of this chapter. Moreover, the work of other researchers and their merits and demerits, which led to the methodology adopted by our group have also been discussed.

Presently, agro wastes are being used for a number of applications *e.g.* animal feed,[110] as a fuel in power plants,[111] to form activated carbon,[112] rubber filler industries,[113] steel industries,[114] and partially replaced as a filler in cement and construction,[115] direct resource of silica, etc.[116] However, without any pretreatment, some of the wastes like palm shell (PS), coconut shell (CS) and RHA are chosen and performed as the lower dielectric resources materials at different frequencies in various applications. The dielectric constant of palm shell and palm biochar was calculated using a coaxial probe within the range 0.2-10 GHz frequency range. The obtained

dielectric constant (1.99-2.83) and loss (0.16-0.23) of PS and palm biochar is a promising material to use as the good microwave absorber into microwave heating applications. Similarly, dielectric constant (3.35-3.76) and loss (0.21-0.30) of the CS-based composite are also measured and used for microwave absorber application.[117] On the other hand, forsterite ($2MgOSiO_2$) phase has been developed using RHA, with 1% porosity, 2.9 g/cc density and low dielectric constant with minimum loss found as comparable a good insulator.[118] With good insulating and suitable dielectric properties of the RHA and RB were performed within the wide frequency range (4Hz-1MHz). Firstly, RHA and RB are sintered at 500 °C and determined the dielectric constant, loss and conductivity behavior with the above-mentioned frequency. The order of dielectric constant and conductivity are decreased after increasing the RB into the RH raw materials, which could be used as the renewable energy source for electric field applications.[119] RHA was processed at different temperatures and determined dielectric constant (7) and minimum loss (~1) could be a promising option for good absorption capacity.[120] As mentioned in chapter 1, the agricultural wastes are being used to generate heat in boilers, small scale industries. They generate the ashes of these wastes that could be used resource to synthesize new materials.

2.2 Silica extraction

These agro-food waste ashes have shown various potential applications in different fields. Due to inherently presented silica is an interesting and alternative source to reuse and convert them into value-added materials. So, many researchers have tried to extract the silica content using different chemical and physical methods. From all the existing agro-food waste ashes, RHA, SCLA, WSA, and PSA exhibit high content of silica, this silica has been attracted to the scientific community for finding new ways to use it commercially. Although silica occurs as a component of cells or cell walls in virtually all unused parts of the rice plant, it is most abundant in the husk. Owing to their small diameter, many technological applications such as thermal insulators, composite fillers, etc., is used for ultrafine silica powders.[121]

2.2.1 Rice husk ash (RHA) as silica source

Extensively work have been done on the waste minimization and exploiting green chemistry route to extract usable materials for engineering applications.[122] The lingo-cellulosic agricultural waste materials to prepare weak base anion-exchanger have been identified.[123] The anion exchange capacity of cellulose decreased with water content in the reaction mixture. The prepared materials are exhibited good nitrate removal capacity. The direct obtaining of the silicon materials from RH waste has been reported.[124] RH contains 17-20% silica in complex form and RHA contains 85-95% amorphous silica, obtained silica percentage (%) is also depending on processing temperature and adopted method.[125] Swatsitang *et al.*[126] investigated the possibility of producing high purity silicon from RH by purifying RH silica. This purified silica could be a possible alternate of the commercially available silica source for solar grade silicon production. The isothermal heating at 400 °C is enough to complete the destruction of organic content from bio-waste such as RH to release the silica. Cristobalite and tridymite phases are observed when RHA is heat-treated at a higher temperature.[118] In addition to this, RHA is used as resources materials and silica synthesized using sol-gel technique and cetyl-tri-methyl-ammonium bromide as the surfactant at RT.[127] This solution is calcined at 500 °C for 5h and found silica nanotube with specific length and diameters (2-4 mm) with good surface area 607 m^2/g. Burning of RH at higher temperature is directly formed silica (80-85%) for further uses at 700 °C, RHA shows the amorphous nature of silica. The percentage of silica is also depended on incineration temperature and time process of burning the wastes.[128] The different sintering temperature is the key factor to decide the amorphous or crystalline nature of the extracted silica from RHA. If RHA is sintered at 800 °C, silica is showing amorphous nature rather than 900 °C same silica content is showing the crystalline phase. Microcrystalline silicon has been produced from the RHA, which further can be used for metallothermal reduction process.[129] The same temperature is implemented for 6h and 95% blue silica was obtained. Due to sintering temperature, the cristobalite phase is changed into the

tridymite phase. The RHA based ceramics were formed using this RHA with sintering at 1000 °C. Silica (89-93%) is obtained from RHA after heat-treatment for better applications.[28] Nano silica is synthesized by a very simple method from RHA without adding any extra surfactant.

2.2.2 Sugarcane leave ash (SCLA) as silica source

SCL and SCB are also produced at a large scale, which may be alternative sources of the silica after some further chemical and thermal treatment. So, amorphous silica is found during harvesting time when sugarcane plant brunt. Blond *et al.*[130] also have investigated the physicochemical properties of the cultivated SCLA and they tried to quantify the presence of crystalline silica. (SiO_2NPs) nanoparticles (<20 nm) with a specific surface area of 131 m^2/g are formed, which is normally about 23 times higher than the raw SCLA. The presented silica content (65.35-69.01%) is also dependent on SCLA. It was higher when the initial particle size of SCLA was 0.85-2.00 mm. Arumugam[131] has employed SCLA as the inexpensive precursor of silica (~80%) to synthesis SBA-15.

2.2.3 Wheat straw ash (WSA) as silica source

WS and WH are being used also as fuel due to their high calorific value. On the other hand, the morphological properties like cellulose content 49.78%, lignin (19.64%), ash (5.28%) and extractives (4.93%) of the WS are determined and it can be used as nonwood papermaking.[132] WS has a calorific value of about 3500 kcal/kg. Thus, burning WS as a fuel in boilers could be one of the suitable ways to reuse this waste in an efficient and controlled manner. After burning, WS generates valuable silica as the residue. WSA contains 55% silica with a small amount of trace elements.[133] Wheat plant ash contains the silica or quartz (58.88%), which proposed that the efficient and economical extracted Si can be used for various engineering applications.[134] WSA contains 10-12% silica in complex form and 80-90% silica in amorphous form.

2.2.4 Peanut shell ash (PSA) as silica source

Peanut shell (PS), a residue after separation of the pod, is available in copious amounts in the world. PS is already used for developing roof sheet materials, concrete blocks, as a cement and construction.[135] The lignocellulosic PS could be utilized for producing bioethanol. It is well-reported that PSA has a higher content of sodium with calcium, potassium and alumina oxides. When PSA added into standard glasses (SLG) the overall color has been changed due to presented content of sodium oxides in PSA.[108]

2.2.5 Eggshell powder (ESP)

The ES weighs approximately 10% of the total mass (ca. 60 g) of hen egg, and ES is the significant solid waste produced from food processing and manufacturing plants. Most of the ES waste is commonly disposed of in landfills without any pretreatment, because, it was traditionally useless. Enrichment of CaO with a small amount of the trace elements of the ES waste is getting the attention of the scientific community, in recent times. ES from a pasteurized liquid egg is perhaps the most difficult waste to manage. However, this waste management system is not a desirable practice in view of the environmental odor from biodegradation. In recent years, a great deal of effort has been conducted for the application of ES to make them valuable products. The role of presented trace ions in ESP derived cement can enhance the setting time, compressive strength and biologic properties.[136] Bahrami *et al.*[137] studies have proved that hen ES is an aviculture byproduct that has been listed worldwide as one of the worst environmental problems, especially in those countries, where the egg product industry is well developed. ES also has a relatively lower density compared to mineral calcium. Qureshi *et al.*[138] suggested that ES is generally thrown away as waste. The ES also creates some allergies when kept for a longer time in the garbage. They found 93.70% $CaCO_3$ with some other trace elements for using better mechanical and physical properties. Brun *et al.*[139] optimized that the ESP produced near about 45000 tons, globally, which can be directly consumed as the calcium source after dissolved in vinegar, lemon and orange juice.

Guru *et al.*[140] reviewed that ESP can be used as the new novel calcium dietary supplement, directly. Since, the material is abundant, low-cost, biodegradable, and has valuable applications in chemistry and chemical technology, further detailed studies on this material may propel its classification as excellent utility material in the areas of research. Interest is forcing the industry to change its approach to recyclability, reusability, and new materials. At present, there is very limited information in the literature discussing the industrial scale utilization of food wastes at the local, national, or international level. However, food wastes produced and their utilization in aquaculture, livestock, poultry, and dairy industries are rarely reported and need further research. Tsai *et al.*[141] reported that the median size and surface area of ESP were determined to be approximately 15µm and 21m^2/g respectively, which can be an effective adsorbent for the removal of anionic dye from aqueous solution. Vasan *et al.*[142] purposed that ES waste (natural $CaCO_3$) was used as an inducer for the cellulose enzyme system.

2.3 Optical properties of the agro-food wastes derived glasses

Interestingly, a few groups have been prepared glasses and glass-ceramics from different types of agricultural waste ashes. Basically, all the existing waste ashes have major content of silica with other required chemical components to form the general glasses like window glasses. Among them, RHA has maximum silica content with a small amount of trace elements. This silica can be an alternative source of commercially available silica. The traditional kaolin clay ceramics replaced by RHA with various percentage ceramic blocks have been designed using alternative raw materials such as RHA (16–32%) to produce thermal insulating buildings.[143] It is a well-known fact that gamma radiation has higher penetration power, which is directly harming human health, so it is required to synthesize the gamma radiation shielding glasses. Such types of glasses are technologically important because they are transparent to the visible radiation and hinder the gamma rays. Tuscharoen *et al.*[144] studied the structural, optical and radiation shielding properties of barium-borate-RHA glasses. It was indicated that such systems could have potential applications in

gamma-ray shielding. Ruengsri *et al.*[145] used RHA to produce barium borosilicate glasses and studied their radiation shielding capabilities. It was found that these glasses possess good optical transparency and can be used as radiation shielding materials. Mustafa *et al.*[146] fabricated glasses with the following composition: $x$$Bi_2O_3$-*(1-x)*ZnO-0.2$B_2O_3-0.3SiO_2$RHA and studied their potential for radiation shielding. It was found that the mass attenuation coefficient increased with the increase in the Bi_2O_3 content and can act as good transparent radiation shielding material. Recently, Sudiana *et al.*[147] used RHA to synthesize silica xerogels, which was mixed with SnO_2. It was found from the microstructural and optical properties of the material that these can be a potential candidate for ceramic waveguide materials. Agro-food waste ashes could be used to synthesize silicate-based glasses and glass-ceramics for optical devices, windows, and some other applications.[80] Cornejo *et al.*[60] reported that typical window glass (soda-lime) could be synthesized from RH and ES with a small amount of table salt and alumina. Further, it found that the silicate matrix acted as a suitable host for producing phosphors. Devi *et al.*[148] used ES and RH to synthesize monoclinic Ca_2SiO_4 doped with Dy^{3+} and Eu^{3+}. The photoluminescence data showed white and red light emissions, respectively, hence, they can find application in producing LEDs. Punj and Singh[61] used CHA, SCLA and ESP to synthesize silica phosphor glasses. Due to the presence of an inherent trace element, these glasses emit blue-green light. The same group has also synthesized glasses using ES along with CHA and SCLA and observed photoluminescence in the UV-Visible region. Kaewakhao *et al.*[149] used RH to produce glasses doped with Cu, Mn, Zn, Er, Co and concluded that RH can be used for the production of color and colorless glass production. Apart from these, researchers have studied the effect of MnO_2 and ZnO concentration on the optical properties of zinc silicate and borotellurite glasses derived from RHA.[150–152] Berkin *et al.*[153] have synthesized soda-lime glass by taking 69% of RHA as a substitute for silica. They studied that the transmission percentage of the UV-Visible-NIR light through the as-synthesized glass samples and found the transmission of light from the samples is very low, and absorbance is high especially

in the IR region. Thus, RHA-lime glass suitable as heat-absorber in buildings, to minimize the use of air conditioners, and to avoid the use of sand as a source of silica.[153] RHA is heat-treated at high different temperature and converted into 90-98% silica with small particle size. Due to the small particle size of RHA is suitable as the filler in the rubber and ink industries.[154] Optical and radiation shielding based barium borate glasses have been formed using the melt-quench process with RHA as silica source. The optimized density and optical properties are found for gamma-ray shielding materials. Glasses with 3 wt% Eu^{3+} doped Zn_2SiO_4 have been synthesized using the solid-state method. Silica is taken from the RHA as a silica resource. The optical band gap (4.23-2.22 eV) and photoluminescence $^5D_0 \rightarrow {}^7F_2$ electron configuration at 612nm (red peak emission) properties have been discussed. These agro-wastes inorganic phosphors are shown great interest in optical devices such as storage, communication lasers, display panels, and upconverting optical based devices.[155,156] Wasanpiarnpong *et al.*[157] performed a comparative study of glass prepared via RHA and RRH (raw rice husk), after sintering the samples using 25 and 50% of spodumene ($LiAl(SiO_3)_2$). They observed the thermal expansion variation of glass and found that the coefficient of thermal expansion (CTE) decreases with the increase in the percentage of spodumene in RHA content. Naskar *et al.*[158] studied the synthesis of silica-based ceramics (cordierite powder) from the RHA and compared it with the ceramics prepared from other sources also. Nayak *et al.*[159] have synthesized bioglass-ceramics using RHA as a source of silica via sol-gel technique. Biomass ashes such as SCBA adding with some boric oxide alumina and phosphorus have been used to prepare the glasses. The σ_{dc} conductivity of these glasses is found of the order of 10^{-10} $\Omega^{-1}cm^{-1}$, which shows the insulating behavior of the glasses. Tchakoute *et al.*[160] demonstrated that sodium water glasses made by mixing of waste glass with rice husk is showing better mechanical properties, which further could be used for a fire-resistant application. Andreola *et al.*[161] used RHA as a silica precursor for making glass frits, whose microhardness, water absorption capacity was found to be superior as compare to glass-ceramics such as neoparies. Essien *et al.*[162] prepared the

bioactive glasses using RHA and ESP as the silica and calcium sources via sol-gel techniques and they have checked the possible uses of these glasses as the bioactive products.

R-SBgC composite 3D scaffold with high porosity and compressive strength has been prepared using RHA to use as a bone substitute in medical applications.[96] Agricultural waste like RHA is used as a silica precursor for making 45$5 bioactive glasses.[23] Different silica content extracted from RHA using controlled heat-treatment (600 and 750 ^{o}C) and technique. This extract silica from this process after mixing with some additives is effectively used in making silicate glasses, which further could be used for economic and technological important bioproducts with reducing the disposable problem.[163] Excellent and highly pure silica are obtained from RHA, which acted as the cheaper reagent as compared to the commercially available reagent. The SiO_2-CaO-P_2O_5 ternary bioactive glass was formed using silica derived from RHA via sol-gel route. To check the suitability of silicate glass in the SBF solution dipped for 7 days and concluded that the apatite layer was formed with better mechanical for required tissue engineering applications.[164] Silica aerogel micro particles were synthesized from RHA, using water-in-mineral oil emulsion for sol-gel, followed by aging in ethanol to strengthen gel network and drying with $ScCO_2$. The as-prepared silica micro particle surface area was found 640 m^2/g and pore volume of 1.38 cm^3/g, which could be acted like the better drug delivery vehicles.[165] Glasses derived from agro-food wastes like RHA, SCLA and other bio-wastes are required high melting temperature, so, these glasses are suitable for high-temperature applications. PL-g pigment glasses are formed using RHA for potential and better photoluminescence properties.[166] Controlled porous silicate glass (CPG) was obtained using acid treatment of the RH. RHS-supported Pd-CeO_2 with separated CeO_2 clusters and Pd nanoparticles was fabricated via subsequent impregnation/calcination of molten cerium nitrate and different amounts of palladium nitrate solution. Porous silica prepared from RH is an effective catalyst support for separating the Pd-CeO_2 system yielding a highly reactive catalyst for complete catalytic methane oxidation at low temperatures even under wet conditions.

2.4 Dielectric properties of the wastes and their byproducts

Dielectric properties exhibit insulating capabilities of a material that could be made to exhibit an electric dipole structure (displace the positive and negative charge so that their center of gravity is different) and thus are used within electrical circuits to separate conductive elements. A dielectric material also exhibits the ability of a capacitor to store a charge. A major use of dielectrics is in fabricating capacitors. Another major application of dielectric materials is in semiconductor chips to insulate transistors from each other. Dielectric materials are, as well, utilized for dielectric resonator antenna applications. The dielectric constant of a material is attributed to the material's ability to retain energy when exposed to electric fields, whereas the dissipation factor is attributed to the capability for absorbing energy from the applied field. The dissipation factor is an index of the materials energy dissipation characteristics in the applied electric fields. The tan d value is a material characteristic in the dissipation of energy. The dielectric constant is a sensitive parameter in sophisticated electronic equipment such as semiconductors, transducers, and amplifiers and in material processing, electronics, and biomedical engineering. Porous mullite and cristobalite-corundum ceramic composite were prepared for better properties (low thermal conductivity, good creep resistance excellent thermal stability and high oxidation resistance) using commercial available RHA as the major constituents with pore-forming agent alumina. RHA based silica aerogel has been prepared to make lightweight mesoporous materials and their common properties such as density, porosity, surface area, and pore volume are calculated 0.38g/cc, 98.3%, 597.7m^2/g, and 8.65cm^3/g, respectively.[167] Dielectric permittivity, dielectric loss factor and conductivity with different rice bran (RB) content have been measured.[119] It was found that dielectric permittivity, dielectric loss factor and conductivity decreases with an increase in RB content. Such behavior may be attributed to the reduced number of mobile carriers. Inherent porosity of the glasses and glass-ceramics synthesized from the ashes of agro-food waste decreases the thermal conductivity, dielectric permittivity and density of the glasses as compared to the conventionally synthesized

glasses. On the other hand, it enhances the sensing and absorption of sound waves. So, these glasses and glass-ceramics can readily find applications in microelectronic devices, such as band-pass filters, dielectric resonant antennas and oscillators, etc. For these applications, the material should have dielectric permittivity ~10 or above at room temperature with good thermal and mechanical stability. It also must have temperature and frequency independent behavior in the microwave frequency region. Inegbenebor *et al.*[168] investigate dielectrically insulation properties of seven selected agro-waste materials (CH, mango, palm kernel, and PS, and corncob and RH) bound with gum Arabic. The dielectric constant of different waste-based materials like coconut, palm kernel and peanut shell, are reported ~3.5-5.5.[117,169,170] These waste materials could be used in high voltage applications. White RHA and SLG based glasses have shown the dielectric constant from 11-102 with minimum losses (0.26-0.72) in the frequency range of (10 Hz-1MHz), which is promising just as commercial material for electronic applications.[171] Danewalia *et al.*[10] concluded that the dielectric constant (9-40) and losses (~1) of the glasses and glass-ceramics synthesized using RHA and SCLA are obtained at the temperature (350 °C). So, it is worthwhile that RHA, SCLA and ESP are taken according to weight percentage (wt%) to synthesize these glasses. Mango shell, corncob, RH and bean shell, exhibit low dielectric constant less than 3.0 that fall into the low voltage application category. Low-density polyethylene (LDPE/RHA) silica composites have been synthesized by melt mixing and due to low dielectric constant (3.6) can be used as dielectrics.[172] On the other hand, RHA microwave absorber has been synthesized and reported by Shu-Ting *et al.*[120] Very low value of bulk density has been reported for these materials, i.e., 0.4 g/cm^2 due to high porosity with advantages such as high electromagnetic (EM) wave absorption, low density, low cost, and environmental friendliness, these waste ashes are the promising light-weight EM wave absorber.

On the other hand, ES waste has found tremendous applications in biomedical industries, composite and nano-material related application. ES is directly used as the source of calcium and

used to make different types of glasses.[110,173,174] Further, these glasses/glass-ceramics can be used as bio-glasses, scaffold glasses, etc.[175] The major advantages of adding the ES into composite foams are to increase thermal and mechanical properties, to reduce the cost for sponge rubber products, and to decrease ES waste problem reported by the authors. ESP has contained 95% calcium carbonate crystals ($CaCO_3$) and the remaining 5% is composed of calcium phosphate, magnesium carbonate, soluble and insoluble proteins, which is a great source of calcium (Ca) for human nutrition. Ibrahim *et al.*[38] also reported that the spongy-like mesoporous hydroxyapatite from raw waste ES for enhanced dissolution of ibuprofen loaded via supercritical CO_2. They purposed that the hydroxyapatite nanoparticles (HApNP) with a large pore volume (1.4 cm^3/g) and surface area (284.1m^2/g) were produced. Balazsi *et al.*[78] reported that the film of HAp and calcium phosphate bio-ceramic were prepared using ESP at the higher temperatures (900 °C), which can be good adherence of films to the HAp substrate with higher strength.

Table 2.1 The concluded literature survey of the recent work on agro-food waste and their ashes

Authors	System	Chemical composition	Result and conclusions
Ashworth and Pablo[176]	Agricultural wastes	Wastes as resource materials to recycling and utilization in different basic uses	Most of the farmers used agricultural wastes to make animal feed, fuel, compost, vermin compost, mulching material, biogas, and animal shelter
Cornejo *et al.*[60]	Agro-food wastes	Different wastes have been considered as the resource materials to various applications	Many valuable potential applications are found in agro-food wastes to make them with cost-effective value-added materials and reuse these wastes into the proper manner
Ajila *et al.***.**[177]	Agro-food wastes	Most of the agro-food waste are reviewed	RHA, SCLA, WSA, Vegetable wastes, fruit wastes, juice wastes, and many more wastes are used as the animal feed with better supplements resources to animals

Kumar *et al.*[114]	RHA	All the possible uses of the RHA is discussed in the review article	RH and RHA could be used as animal feed, home shelter, mud house and steel making, silicon chip, extraction pure silica
Naghizadeh *et al.*[175]	PCL/RHA	PCL/Rice husk derived bioactive glass-ceramic composite scaffolds	highly porous composite scaffolds based on R-SBgC/PCL is fabricated and used as the bioactive materials
Nayak *et al.*[159]	RHA	Silica extracted from RHA and prepared ceramics	Three varieties of silica powders, namely brown ash, white ash and silica gel containing 96.0, 99.8 and 99.9% silica respectively.
Nayak *et al.*[89]	RHA	Amorphous silica-based porous bioactive ceramics have prepared using gel casting	Gel-casted SG-body can be used as a bio-ceramics for different clinical applications
Qureshi *et al.*[138]	ESP and RHA	Get 93.70% $CaCO_3$ and rest are minerals	Added into the cement with RHA for better mechanical properties
Ghosh *et al.*[125]	RH and RHA	Silica content determined from RH and RHA	RH contains 17-20% silica in complex form and RHA contains 85-95% amorphous silica, obtained silica% from RH is also depending on processing temperature and adopted method
Pode[28]	RHA	RHA converted into silica	RHA based ceramics were formed using this RHA with sintering at 1000 °C. Silica (89-93%) is obtained from RHA after heat-treated to propose for better applications.
Tuscharoen *et al.*[144]	Barium-borate-RHA glasses	Studied the structural, optical and radiation shielding properties	RHA derived glass systems could have potential applications in gamma-ray shielding.
Mustafa *et al.*[146]	xBi_2O_3-(1-x)ZnO-	He fabricated glasses using RHA as the silica	He studied of these glasses as the potential candidate for radiation shielding

	$0.2B_2O_3$-$0.3SiO_2$ RHA glasses	resource in borate glasses	Increasing of the Bi_2O_3 content can act as a good transparent radiation shielding material
Devi *et al.*[178]	ES and RHA	Used ES and RHA to synthesize monoclinic Ca_2SiO_4 doped with $Dy^{3+}$and Eu^{3+}.	White and red light emissions can find the application in producing LEDs
Andreola *et al*.[161]	RHA	SiO_2-Al_2O_3-MgO composition was synthesized using solid-state reaction	RHA as silica precursor to making glass frits, whose microhardness, water absorption capacity was found to be superior as compare to glass-ceramics such as neoparies
Lee *et al*.[179]	RHA	Photoluminescent glass derived from rice husk	Potential and various applications of the PL rice husk glass are used for building decorations, highway markings, exit signs, accessories, and glassware
Bateni *et al.*[171]	RHA	Glasses were prepared using RHA and SLG system	Dielectric constant is found from 11-102 with minimum losses (0.26-0.72) in the frequency range of (10 Hz-100 kHz), which could be used for microelectronic applications
Danewalia *et al.*[180]	RHA and SCLA	glasses and glass-ceramics were prepared using RHA and SCLA	Dielectric constant (9-40) and losses (~1) of the glasses and glass-ceramics at the temperature (350 °C) for microelectronic applications
Blond *et al.*[130]	SCLA	Silica is extracted from SCLA wastes	Investigated the physicochemical properties of the cultivated SCLA and they tried to quantify the presence of crystalline silica
Kaur and Singh[181]	RHA+Rare-earth	Silica is taken from RHA	Optical and photoluminescence properties of the RHA derived glasses have

			discussed
Punj and Singh[61]	RHA+ESP +CS	Silica extracted from RHA	Optical and structural properties are reported for blue-green LEDs
Arumugam[131]	SCLA	SCLA is used as a silica precursor	An inexpensive precursor of silica (~80%) is formed from using SCLA to synthesis SBA-1
Norsuraya *et al.*[133]	WS	Burning effect of the WS is observed	Burnt WS generate valuable silica as the residue. The silica content of WSA has also calculated 55% silica with trace elements
Trivedi *et al.*[134]	WS	Silica content is also found from WSA	It contains the silica or quartz (58.88%), which proposed that the efficient and economical extracted Si can be used for various engineering applications
Patel *et al.*[182]	WSA	WSA has both forms of the silica	He determined the 10-12% silica in complex form and 80-90% silica in amorphous form
Aktus *et al.*[108]	PSA	Higher content of sodium with calcium, potassium and alumina oxides is obtained from PSA	When PSA added into SLG standard glass the overall color has been changed due to higher content of sodium oxides presented in PSA
Baláž *et al.*[183]	Eggshell powder	50000 tons ES wastes produced, globally	Ball milling of ESP can enhance various mechanical and physical properties, which, further make better composite, bio-ceramics, HA layers
Yasothai *et al.*[184]	Eggshell powder	India is third largest producer eggshell powder due to production of 47 billion eggs per annum	The large production of eggs and ESP is considered as a waste which has a disposable problem
Bahrami *et al.*[185]	Eggshell powder	Get 95% $CaCO_3$ and 5% inorganic Materials	Lower density as compared to mineral calcium
Murakami *et*	Eggshell	It contents calcium	Calcium carbonate can be used as an

al.[186]	powder	carbonate (94%), calcium phosphate (1%), magnesium carbonate (1%) and organic substances (4%).	alternative pharmaceutical excipient.
Oliveira *et al.*[110]	Eggshell powder	Reuse ESP for making HA layer	It can reduce the production cost as well as disposable problem and better uses in bioactive applications
Ibrahim *et al.*[187]	Eggshell powder	Spongy-like mesoporous hydroxyapatite from raw waste ES	HApNP with a large pore volume (1.4 cm^3/g) and surface area (284.1 m^2/g) was produced for enhanced dissolution of ibuprofen loaded via supercritical CO_2
Balazsi *et al.*[78]	Eggshell powder	Calcium phosphate-based bio-ceramics were prepared at a higher temperature (900 °C)	The good adherence of films to the HAp substrate assured a higher strength for these samples.

The literature review suggests that although a few research groups pursue preparation and characterization of agro-waste derived glasses, some important issues must be addressed to exploit their full potential for various applications.

Most of the studies are limited to the extraction of silica and its properties. Direct use of agro-food wastes ashes to synthesize glasses and glass-ceramics and their optical and dielectric properties have not been reported as far as our knowledge. So, still, there is a lot of scope of research to encompass more properties. Apart from the use of agro-waste derived materials in the aforementioned applications, there is a worth possibility to generate value-added materials for microelectronic and energy conversion devices. To best of our knowledge, not much attempts have been done to RHA, SCLA, WSA, PSA and ESP wastes synthesize glasses and study their properties to suitability for different applications.

Objective

1 **To synthesize glasses/glass-ceramics derived from waste material ashes by melt-quench technique.**

2 **The formed materials will be characterized by various techniques for their structural, thermal, optical and dielectric properties.**

Chapter 3 Materials and Methods

Selected agro-food waste ashes were used as the resource materials to synthesize glasses and glass-ceramics. The chemical composition of selected raw materials i.e. different agro-food waste ashes, glasses, and glass-ceramics composition are given in this chapter. Glasses are synthesized via melt-quench technique followed by controlled heat-treatment to convert them into glass-ceramics. These as-prepared and heat-treated samples were characterized using various experimental techniques to study their structural, thermal, optical and dielectric properties. The details of the sample preparation and characterization techniques are discussed in this chapter.

3.1 Raw materials

Ashes of the agro-food waste i.e. RHA, SCLA, WSA, and PSA were taken from rice mills, sugarcane mills and wheat farming fields of north India, respectively. The ashes of these wastes were further heat-treated at 1000 ^{o}C for 2 h to remove only remaining organics substances before taking in different weight percentage (wt%) to synthesize glasses and glass-ceramics. On the other hand, the shell of hen eggs was collected from the poultry farm. Eggshell washed with distilled water followed by acid-treatment in a dilute solution of hydrochloric (HCl) and nitric acid (HNO_3) in the ratio of 1:1 to remove the adhering albumin and impurities. Further, eggshell dried in an oven at 110 ^{o}C for 3 h and ground in an agate mortar-pestle to make the fine powder of the shells i.e. ESP. The chemical compositions of these heat-treated waste ashes along with their sample labels are given in table 3.1. Ashes of the wastes and ESP were taken as stoichiometric formula, mixed and ground in an agate mortar-pestle to obtain a homogenized powder. The homogenized mixture was kept at the programmable furnace for melting at 1550 ^{o}C in the air. The melted samples were quenched on the solid copper plates at room temperature (RT) in the air. These samples were crushed using an agate mortar-pestle to get a fine powder. The ground powder was used to make pellets applying 10 $kNcm^{-1}$ pressures using a hydraulic press. The pellets were heat-treated at 1000 °C for 10 h in an electric muffle furnace to convert them into glass-ceramics.

3.2 Chemical analysis of raw materials

The chemical compositions of the ashes such as RHA, SCLA, PSA, ESP, and WSA, are calculated using energy dispersive spectroscopy (EDS). The elemental analysis of the raw materials is shown in Fig. 3.1. RHA, SCLA, WSA exhibit silica as major constituents with some minor and traced elements oxides as given in table 3.1.

Table 3.1 Chemical constituents (wt%) of the ashes of the agro-food waste

Wastes → / constituents ↓	RHA	SCLA	WSA	PSA	ESP
SiO_2	96.87	77.58	72.65	0.25	0.54
CaO	1.12	6.75	3.67	0.34	98.03
MgO	0.06	5.37	2.62	3.02	0.41
Na_2O	0.08	0.44	0.87	2.40	0.41
K_2O	1.62	6.78	14.33	1.61	-
Al_2O_3	0.24	1.93	5.87	0.25	0.46
FeO	-	1.16	-	-	0.15
C	-	-	-	87.25	-
P_2O_5	-	-	-	0.63	-

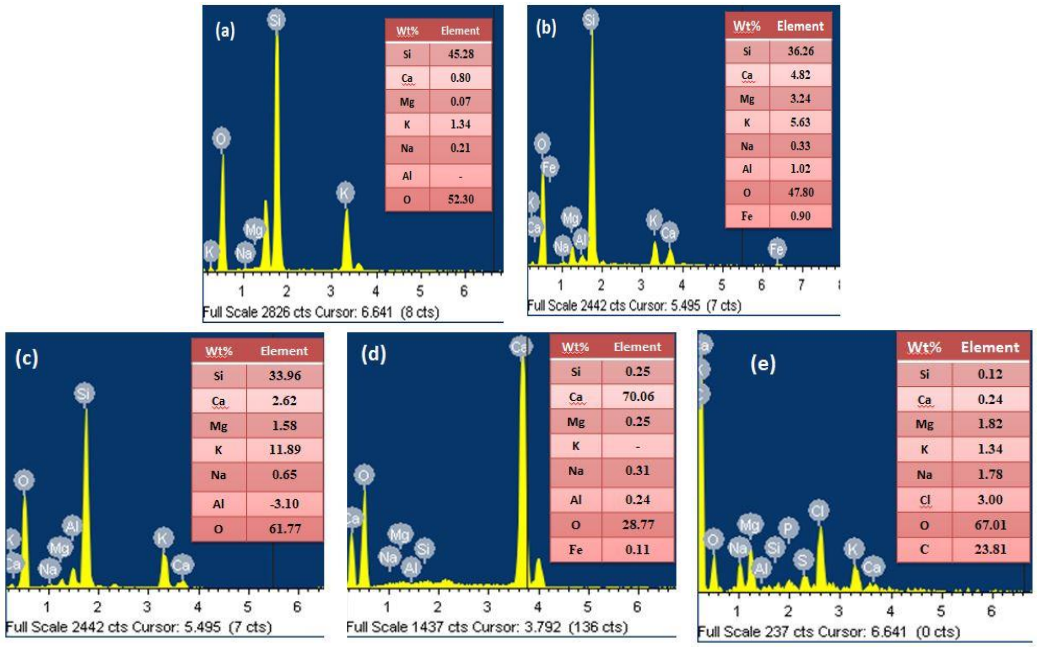

Fig. 3.1 Chemical analysis of **(a)** RHA, **(b)** SCLA, **(c)** WSA, **(d)** ESP and PSA using EDS

On the other hand, PSA (without any heat-treatment) exhibits mainly carbon as major constituents. Usually, EDS provided the wt% or at% values of the elements in the specimen. The measured wt%

of elements presented in the waste ashes are converted into oxides using the EDS inbuilt software. ESP has CaO ~98 (wt%) with a small amount of trace elements.

3.3 Samples preparation

For the present study, we have selected thirteen different samples composition as mentioned in table 3.2. the composition selection is based on the avaiablity of agro food wastes, locally their constituents to form the glasses and glass-ceramics. All the compositions are taken according to weight%. All compositions were prepared from agricultural-food wastes using melt-quench technique.

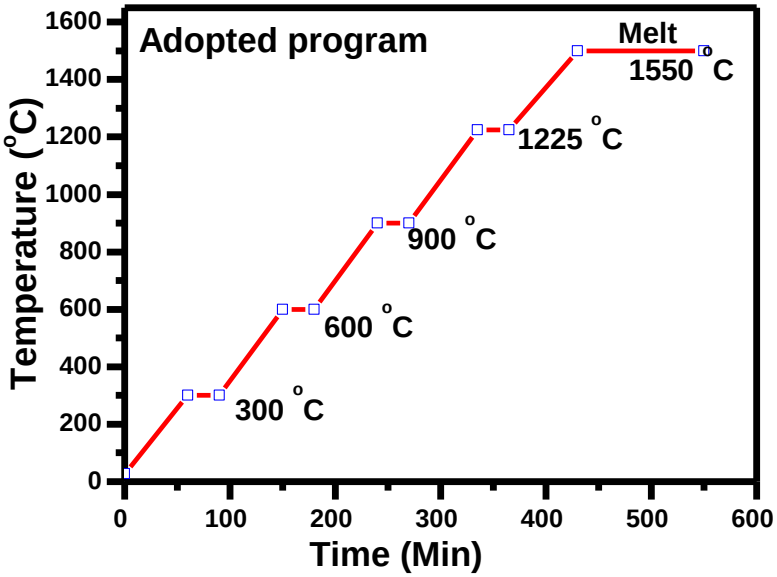

Fig. 3.2 Furnace program followed during melting process of the glasses

Table 3.2 Samples compositions of glasses and glass-ceramics (wt%) along with their labels

Sr. no.	Samples Id	RHA	SCLA	ESP	PSA	WSA
1	**AF-1**	70	-	30	-	-
2	**AF-2**	60	-	40	-	-
3	**AF-3**	50	-	50	-	-
4	**AF-4**	40	-	60	-	-
5	**SRE-1**	45	45	10	-	-
6	**SRE-2**	45	40	15	-	-
7	**SRE-3**	45	35	20	-	-
8	**SRE-4**	45	30	25	-	-
9	**SE-1**	-	90	10	-	-
10	**SE-2**	-	75	15	10	-

11	**SE-3**	-	70	20	10	-
12	**SE-4**	-	65	25	10	-
13	**WSA**	-	-	-	-	100

Before melting, pellets of the different waste ashes have prepared and placed into the programmable electric muffle furnace in recrystallized alumina crucible for melting at 1550 °C, a considerable amount of the holding time 2 h had been given to ensure the homogenized of the mixture. To enhancing the fusibility of the ingredients with each other, the furnace was held for 30 minutes at intermediate temperatures (i.e. 300, 600, 900, 1225 °C). The adopted program is followed to melt the samples in the muffle furnace as shown in Fig. 3.2. Flow chart of the sample preparation and their characterizations are shown in Fig. 3.3.

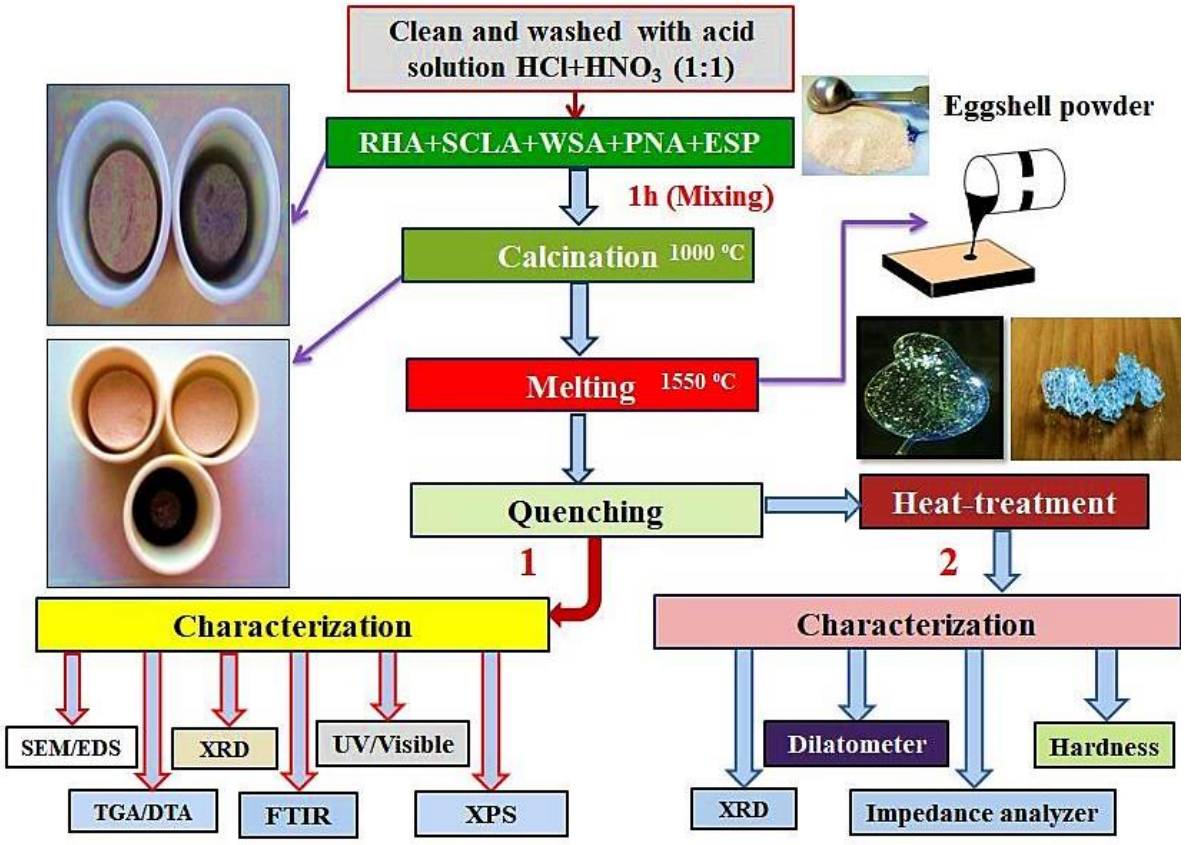

Fig. 3.3 Flow chart to prepare the samples, using agro-food waste ashes and characterization techniques

3.4 Characterizations techniques

After making all the samples followed above preparation methods. To check their suitability for various applications, these as-prepared and heat-treated samples have characterized using different techniques. Physical parameters like density, molar volume have been calculated using Archimede's principle. The hardness of the samples is also calculated using Vicker's hardness instruments for checking better for mechanical properties in storage devices. The optical, thermal and dielectric properties of the samples are discussed (next chapter) using various techniques.

3.4.1 Density measurement

The density of the samples was calculated using Archimedes' principle. Xylene was used as a bouncy fluid. Samples weight was taken by microbalance. The least count of the balance was 0.01 mg. The density of the samples was calculated as follows:[188]

$$\rho_{sample} = \frac{w_a}{w_a - \mathrm{w_x}} \times \rho_{\mathrm{x}} \tag{3.1}$$

where, ρ_{sample} is the density within the sample, w_a and $\mathrm{w_x}$ are the weight of the sample in air and in xylene. ρ_{x} is the density (0.863 g/cc) of xylene at room temperature (RT).[189]

3.4.2 Scanning electron microscopy/energy dispersive spectroscopy (SEM/EDS)

SEM is a very useful technique for the surface analysis of solid samples by taking high magnification resolution images; SEM uses a focused beam of electrons. Magnification up to ~3,00000 times can be achieved by advanced SEM. SEM has better resolving power as compared to an optical microscope due to a very small wavelength of incident electrons than the photons. SEM has a depth of field up to 100 times greater than optical microscopes. The common SEM/EDS instrument is shown in Fig. 3.4. In addition to this, SEM equipped with energy dispersive spectroscopy (EDS) gives valuable information about the semi quantitative elements presented in samples. Scanning electron micrographs of all the samples were taken using SEM JEOL/EO (version 1.0). The samples are coated with platinum (Pt) on an auto fine coater-JEOL

(JEC-3000 FC) under an operating current of 20 mA for 120 s (seconds). EDS analysis is carried out using an attached INCA x-act (Oxford instruments). At the same time, lower atomic number elements below boron cannot be detected using EDS. Moreover, the detection limits of EDS ±1%. EDS spectra of all the samples were recorded at appropriate acceleration voltages up to 10 keV. The chemical analysis of the some samples has been identified with better quantification limit better than 1 ppm using ICP-MS spectroscopy with model (Thermo Fisher Scientific, Element XR).

Fig. 3.4 Scanning electron microscopy/energy dispersive spectroscopy instruments

3.4.3 X-ray photoelectron spectroscopy (XPS)

XPS is a very sophisticated elemental analysis technique. It is used to identify and quantify the presented chemical elements on the surface of the samples. The detection capability of trace elements of the XPS is in parts per million of the samples. It was performed on some selected samples to confirm and compare the obtained results by EDS. An XPS spectrum is plotted between the numbers of photoelectron ejected and detected the binding energy of the elements. A characteristic set of the peaks at different binding energies are corresponding to each element present in the specimen or samples by obtaining upon X-ray irradiation and photoelectrons. The significant number of electrons is directly related to the amount of elements in the sample. The

lighter elements like helium cannot detect by XPS technique. X-ray photoelectron spectroscopy (XPS) was performed to confirm the presence of different elements in as-quenched glasses. XPS was done on (Oxford Instruments) using AlK_{α} (1486.7 eV) radiation with a pass energy of 20 eV. This instrument was operated at about 340 W with base pressure ~1.0×10^{-10} mbar in the analysis chamber. The binding energy range was 0-1100 eV at the duration of the recording of survey scan of the as-prepared samples.[190]

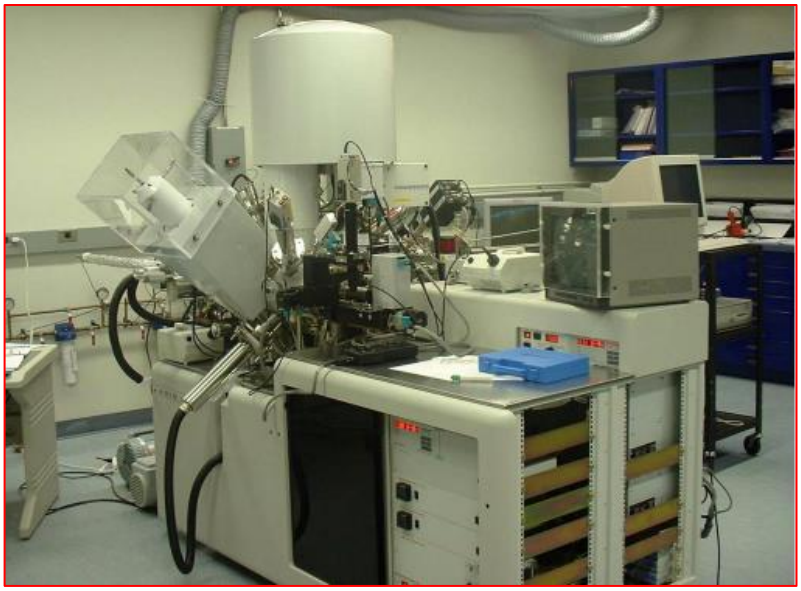

Fig. 3.5 Photo of X-ray photoelectron spectroscopy (XPS) instruments

3.4.4 X-ray diffraction (XRD)

XRD is the sophisticated technique to confirm the nature of the as-prepared samples weather amorphous or crystalline.[105] Furthermore, crystalline phases presented in heat-treated or as-quenched samples were identified using XRD. Basically, cathode ray tube (CRT) produces x-rays, which is filtered to generate monochromatic radiation, collimated to concentrate, and directed toward the sample. XRD is based on constructive/distractive interference of monochromatic x-rays, which diffracted from the crystalline sample. The interaction between sample incident rays produces constructive interference of the diffracted rays when the Bragg's low condition ($2d\sin\theta=n\lambda$) is satisfied. The wavelength (λ) of x-rays lies between 0.1-100 Å, which is exactly the

same order as of the inter-planar spacing (d) of the crystals. Therefore, the interaction between x-rays and crystals would cause diffraction patterns as per Bragg's law. The details of the structure along with the volume of crystalline phases, crystallite size, and strain, etc. can be calculated by XRD.[1] Glass being amorphous materials does not possess diffraction peaks. Instead of diffraction peaks, a broad halo or more is observed. The position of the centre of the broad halo depends on the composition of the glasses. More than one broad halo is directly related to a separate phase in glasses. The phase-separated glasses are the consequence of compositions containing immiscible phases in the melt. The phenomenon of phase separation is governed by the overall lowering of energy. If the separation of the mixture of two components favors the lowering of free energy, then glass becomes phase-separated, sometimes homogeneous melt without any phase separation leads to the lowering of free energy. Glass-ceramics possess some crystalline peaks, which are embedded in the base glass matrix. The volume fraction of different phases, crystallite size, and type of strain such as compressive and tensile in the samples of the crystalline phases could be obtained. In the present study, the XRD patterns of the as-quenched and heat-treated samples were recorded using a PANalytical'sX'Pert Pro X-ray diffractometer with CuK_{α} radiation having wavelength λ=1.54Å.[189] Measurements were done in the air between the 2θ ranges of 10-90°. The scanning speed and step size were kept ~3° min^{-1} and 0.017°, respectively. The crystalline phases and their peaks were matched by the standard international center of diffraction data (ICDD) card using inbuilt X-pert high score software.

3.4.5 Fourier transforms infrared spectroscopy (FTIR)

This method uniquely characterizes the chemical bonds present in the glass or any substance. It is worked on the interaction between IR radiations and the samples. Two covalently bonded atoms can be visualized to be similar to a mass containing spring, which attached with two heavy balls at both ends vibrating with some unique frequency. When the frequency of incident radiation becomes equal to the frequency of vibration of a bond it gets absorbed which produced an IR-band.

The molecule can be vibrated with different modes such as stretching, bending, rocking, etc. depending on its available degrees of freedom.[127] Same bond can also be given more than one IR bands at different wavenumbers. Shifting of IR-bands is very useful to know about the weakening or strengthening of the bonds of the materials. The broadness of the FTIR bands is due to close continuum vibrational frequencies, which are difficult to resolve. It shows the range of bond lengths, bond strength of the functional groups available in the materials. Also, it is a decent tool to examine the functional group of glasses and glass-ceramics. FTIR spectra of the as-prepared samples were recorded at an ambient temperature range of 450-4000 cm^{-1} on the Perkin Elmer-Spectrum-RX-IFTIR spectrometer. The spectral resolution was kept 0.8 cm^{-1}. Only 5 mg powder sample was mixed with 20 mg KBr and then pelletized using a hydraulic press at a pressure ($0.63kNmm^{-2}$). These pellets were used to check the functional group of glasses and glass-ceramics by FTIR.

3.4.6 Differential thermal analysis

Differential thermal analysis (DTA) technique is basically useful to check about the thermal stability and phase transition of the samples. It is mandatory to analyze the samples using this technique to have an account of the characteristics temperature of the glasses. As already discussed in the previous chapter, the basic properties of glass are their characteristics temperatures, T_g, T_c, and T_m. Many potentially required processing like coating; enameling etc. requires subjecting glass to high crystallization temperature (T_c) zone. Hence, it is worthwhile to understand the thermal stability of the glass using DTA/TG. In this technique, the material is under study with an inert reference is made to undergo the same thermal cycles, whereas recording temperature difference between reference and sample. This temperature difference (ΔT) is then plotted with time, or temperature (DTA curve or thermogram) resulting changes in the sample with references to the inert reference can be detected in the form of either endothermic or exothermic peaks. Therefore, DTA graph gives data on the transformations that have occurred, such as glass transitions

temperature (T_g) crystallization temperature (T_c), melting temperature **(**T_m), sublimation temperature and phase transition, etc. DTA has a sample holder comprising thermocouples, sample containers, furnace, and recording systems as depicted in Fig. 3.6. Two thermocouples are joined in a differential arrangement and connected to the differential amplifier.

Fig. 3.6 Perkin Elmer (Model: Diamond Pyris) TGA/DTA equipment[191]

One thermocouple is positioned in an inert material (Al_2O_3) and the other one is positioned into the test sample. With increasing temperature, a deflection in voltage can be seen due to the phase transition of the samples. This happens due to the given heat is raised inert substance temperature. But be incorporated as latent heat is responsible to change the phase in materials.

Thermal analysis was carried out on Perkin Elmer (Model: Diamond Pyris) TG/DTA equipment.

The (T_g) and (T_c) were obtained from the DTA curves in the temperature range 100-1000 °C at 10 °$Cmin^{-1}$.

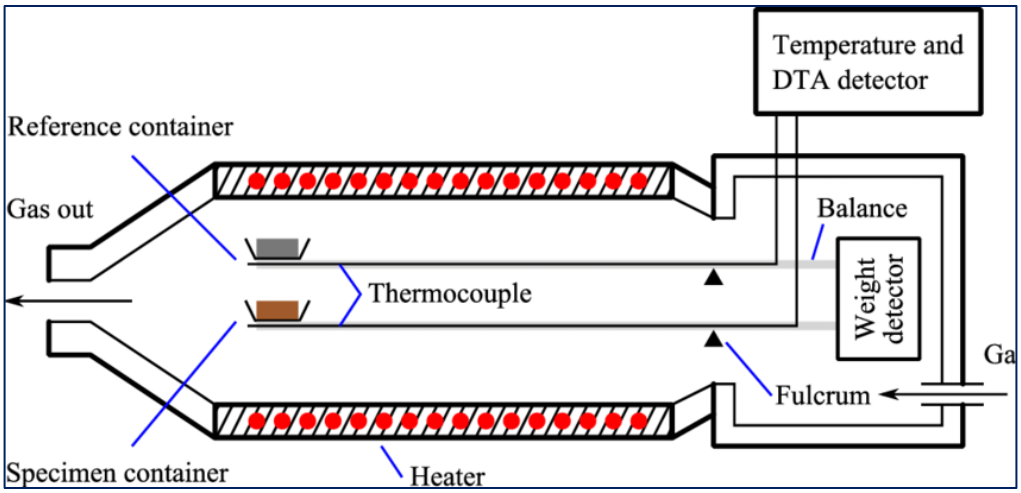

Fig. 3.7 The basic assembly of differential thermal analyzer

Approximately 10 mg of each glass powder was taken in a platinum (Pt) crucible for the measurements. Al_2O_3 (99.9% pure) was taken as reference material. The temperature of the samples and reference material was measured with the temperature accuracy of ±1°C.

3.4.7 Dilatometry analysis

Dilatometry is a thermo-analytical technique for the measurement of expansion or shrinkage of the material. Every material expands or contracts in response to heating or cooling. This response to temperature change is expressed as its coefficient of thermal expansion.

The coefficient of linear thermal expansion (CTE) is defined as:[192]

$$\alpha = \frac{\left(\frac{dL}{L_o}\right)}{dT} \tag{3.2}$$

Here, L_o is the initial length of the material, dL is the change in length and dT is the change in temperature. When a material is heated, we are giving energy to it. Atoms of the material start vibrating about their mean positions. As a net result, the material expands. Its expansion is dependent on the types of bonding involved, the strength of the material, etc. In a dilatometer, thermal expansion of the material is measured as a function of temperature or time. A pushrod is connected to an inductive displacement transducer on one side. Another end of pushrod is in close contact with a sample in order to register any length change in sample materials during heating or

cooling. Since the sample holder and the anterior part of the pushrod are exposed to the same temperature program just as the sample, they also undergo expansion. The resulting dilatometer signal is, therefore, the sum of lengths changes of the sample, sample holder and pushrod. To obtain the true sample behavior, it is thus necessary to correct the raw dilatometer data. There are two possible correction methods: to use tabulated expansion data for the sample holder material or to use a correction curve. The dilatometer is a very important tool to know the coefficient of thermal expansion (CTE). Apart from this, we can also determine the glass transition temperature (T_g), phase transition and change in the density of the samples.

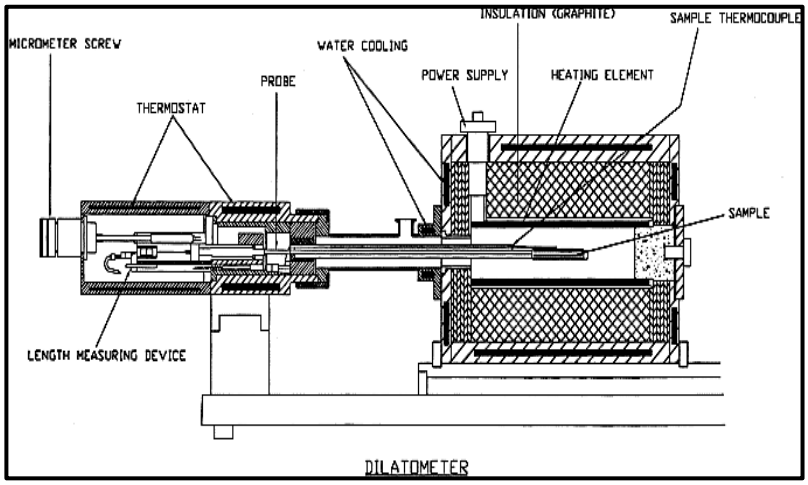

Fig. 3.8 Schematic diagram of dilatometer to calculate the CTE of glasses and glass-ceramics

Moreover, it can also be very useful techniques to find out the shrinkage and porosity of the samples. The coefficient of thermal expansion of heat-treated glasses was determined using the dilatometer DIL 402C (NETZSCH, Germany) from the 100-900 °C at the heating rate of 10°/min in the normal atmospheric conditions. The pellets of the glass-ceramics with the thickness (2mm) and diameter (10mm) were used for dilatometer measurements.

3.4.8 Optical analysis

When incident UV-Visible light is passed through sample dissolved in an appropriated solvent the following relation between optical band gap energy (E_g) and absorption coefficient (α) for small values of absorption coefficients ($\alpha \leq 10^{-4}$) are given:[188]

$$\alpha hv = B(hv - Eg)^n \quad (3.3)$$

Here, *hv* denotes the energy photon. *n* can be having different values such as 2 for indirect allowed, 3 for indirect forbidden, ½ for direct allowed and 3/2 for direct forbidden transitions. Band tailing parameter (B) is known as constant. Optical spectra of the materials are characterized by an exponential increase of the absorbance coefficient with an increase in energy of incident photons. The difference in the absorption coefficient in the Urbach tail region is given as follows:

Diffused reflectance spectra of the as-quenched samples are taken. From diffused reflectance spectra, the optical band gaps of the as-quenched samples were calculated using the Kubelka-Munk function.[193] For the infinite length for the sample, the absorption coefficient (α) can be related to the reflectance (r) by the following relation:

$$F(r) = (\alpha/s) = (1 - r)^2/2r \quad (3.4)$$

Where, F(r) is the Kubelka-Munk function. 'r' is the reflectance and 's' is the scattering coefficient. $(F(r)hv)^2$ versus energy (hv) plots were extrapolated to cut the energy axis (x-axis) corresponding to $(F(r)hv)^2=0$. The intercept gives the value of the optical band gap of the sample. UV-Visible spectra of all the samples are recorded on a double beam spectrophotometer (HITACHI U-3900 H) between spectral range 200-800 nm.[194] The scattered speed 120 $nmmin^{-1}$ and resolution 0.20 nm are used. The spectra are recorded in the reflectance mode of the powder samples.

3.4.9 Photoluminescence analysis

The luminescence behavior of the samples was analyzed by photoluminescence (PL). The room-temperature, PL excitation and emission spectra were recorded in the fluorescence mode with a fluorescence spectrophotometer (Model-Agilent Carry Eclipse G9800A, Mulgrave Melbourne, Australia) equipped with a xenon flash lamp. The wavelength corresponding to the maximum PL intensity of the excitation spectrum was observed from 235-265 nm. In this region, it exhibits strong, medium and weak intensity peaks. These peaks lie in the blue to the green spectral region. All the prepared glasses show the high refractive index (n~2.31) and good transparency (T-80%) in

the UV-Visible (λ-235nm) and near-infrared range. In more complex silicate glasses, luminescence can be promoted by the incorporation of several alkalines and rare-earth ions, but the concentrations usually effective due to heavy elements in these glasses. Impurities have been identified in silicate glasses by luminescent effects atomic concentration levels, which produce undetectable optical absorption.

3.4.10 Impedance analysis

Dielectric measurement was done to get an account of ion mobility and other transport phenomena. These parameters are ultimately related to the structural forming unit in the glass and glass-ceramics. So, this technique would add valuable information to understand the nature of glasses and glass-ceramics, which is directly linked to the local structure of the materials. For this, glass ingots were cut using Buehler diamond cutter (Iso Met low speed saw) to get uniformly thick glass slices.

Fig. 3.9 Impedance analyzer instrument (SOLATRON SI-1260) with furnace

These slices were washed ultrasonically prior to Pt coating on both sides by JEOL auto fine coater (JEC-3000FC). On the other hand, few pellets of the samples are heat-treated at 900 ºC for 10 h to make the appropriate samples for dielectric measurements. Operative current and time were 20 mA and 160 sec, respectively. Dielectric measurements were carried out on SOLATRON impedance

analyzer (SI-1260) within the temperature and frequency ranges 100-600 °C and 100Hz-1MHz, respectively.[195] Error of temperature measurement was ±2°C during performing the samples. Bias voltage 2V (V_{AC}**)** and 2V (V_{DC}) were applied during perform the samples.

3.4.11 Vickers's microhardness

For the measurement of microhardness, micro-indentations were done on the surfaces of both bare and immersed pellets using a diamond Vickers indenter on a microhardness testing machine (Mitutoyo MVK-HO, Japan). Additionally, representative four glass slices cut from the as-quenched cuboidal block of glass sample to measure microhardness in the bulk form. The indentations using applied load 200 g for 15 s were made at three different points on the samples.

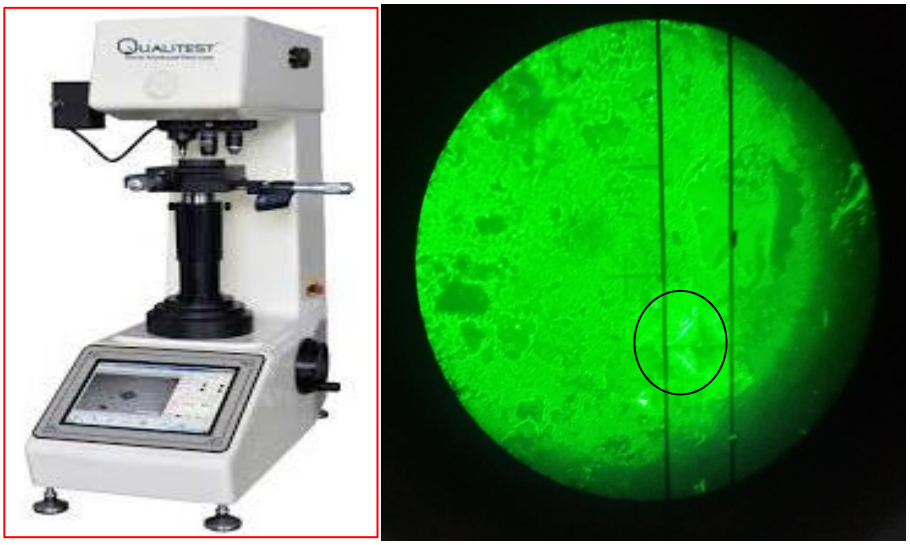

Fig. 3.10 Vicker hardness testing machine and indentation on the samples

The mean of diagonal of the pyramidal shape indentations was taken. The microhardness was calculated using the following equation:[196]

$$H = 1.854\ F/d^2 \qquad (3.5)$$

Where F is the applied load (kilograms-force) and *d* is the average length (mm) of the diagonal of pyramidal indentation.

As mentioned in the previous chapter that thirteen samples were synthesized from agro-food wastes ashes using melt-quench technique. Where, RHA, SCLA and WSA are the major sources of silica. On the other hand, ESP exhibits CaO as a major constituent along with some trace elements (table 3.1). These waste ashes are used to prepare the glasses and glass-ceramics. Four glass series have been synthesized and characterized by various experimental techniques as discussed in chapter 3. Obtained results and their discussion are given in four subsections of this chapter. In the last section, an interaction study between Crofer 22 APU (solid-state interconnect) and glasses have been given. In this study, two different glasses were synthesized using different sources i.e. wheat straw ash (WSA) and mineral oxides. However, the chemical composition of both glasses was similar. Conclusively, the WSA sample is suitable and better sealing glass as compared to similar glasses synthesized from mineral oxides. Different steps are taken to synthesize the glasses and glass-ceramics as shown in Fig. 4.1.

Fig. 4.1 Agro-food waste ashes grounded in agate mortar-pestle, heat-treated ashes, and as-quenched glasses

4.1 XRD of raw materials

XRD of the heat-treated raw materials is given in Fig 4.2. All the raw materials exhibit different silica-based crystalline phases. These observed peaks in RHA, SCLA, WSA and PSA have also indexed of SiO_2 based phases (ICDD card no. 01-075-0923, 01-076-0894, 01-085-0794 and carbon oxide phase with ICDD card no. 01-07602378). Moreover, the volume fraction of the cristobalite phase as compared to the tridymite phase is higher in RHA as calculated from the direct comparison method. In this method, the area of high intense peaks of different phases are taken and equated as 100%. Area of the individual phase provides the idea of its volume fraction of the phases. PSA sample has a silica-based phase with the presence of carbon. The ESP has the calcium oxide-based phase with ICDD card no. 01-076-0937.

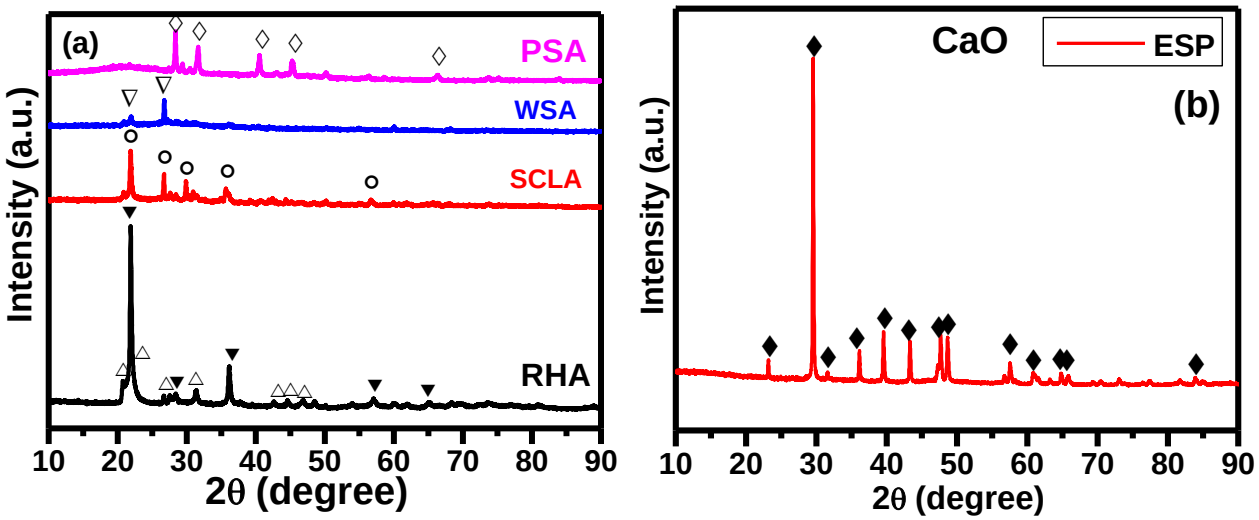

Fig. 4.2 (a) XRD pattern of RHA, SCLA, WSA, PSA and **(b)** ESP raw materials

4.2 (100-x)RHA-(x)ESP (x=30, 40, 50, 60) series

In this series, four samples have been synthesized using RHA and ESP as the raw materials. These four samples were prepared with varying (wt%) of RHA and ESP**.** Composition (100-*x*)RHA-(*x*)ESP, where *x*=30 (AF-1), *x*=40 (AF-2), *x*=50 (AF-3) and *x*=60 (AF-4) were used to form the glasses as given in table 4.1. These compositions were thoroughly mixed and ground in an agate-mortar pestle to get a fine powder. The homogenized mixtures were heat-treated at 1000 °C for 1 h in an electric muffle furnace followed by grinding.

Table 4.1 Four samples prepared using RHA and ESP in weight%

Samples	**AF-1**	**AF-2**	**AF-3**	**AF-4**
RHA	70	60	50	40
ESP	30	40	50	60

The ground powder was used to make pellets by applying 10 $kNcm^{-1}$ pressure using a hydraulic press. These pellets were placed into the programmable electric muffle furnace at 1550 °C in re-crystallized alumina crucible for melting, a considerable amount of the holding time 2 h had been given to ensure the homogenization of the mixture. These four AF-samples have been melted at 1550 °C and directly poured on a copper plate in the air, but due to high viscosity, AF-1 sample could not quench on the copper plate properly. However, the other three samples are poured on the copper plate for rapid quenching. The as-quenched samples were greenish in color with higher viscosity and lighter weight in comparison to mineral-based glasses and glass-ceramics. Moreover, as ESP concentration increases, color of the glass changes from greenish to light whitish to some extent. It indicates the presence of transition metals in RHA. As ESP content increases on the cost of RHA, the color of the quenched samples became whitish.

4.2.1 Density

The density of the as-prepared glasses is measured using the Archimedes' principle. Based on density measurement, the calculated molecular weight (M) of the glasses is presented in table 4.2. The replacement of RHA by ESP in the glass compositions increases the density as shown in Fig. 4.2. The error is (±0.01) in density measurement. It is related to SiO_2 and CaO present in RHA and ESP, respectively. The density of SiO_2 (2.65 g/cc) is less than CaO (3.34 g/cc). Moreover, the replacement of RHA by ESP in glass composition modified the glass network.

Table 4.2 Density, molecular weight and Vicker's microhardness of the heat-treated samples

Sample ID	Density (g/cc) ±0.01	Molecular wt	Hardness (HV)
AF-1	1.78	59.86	586 ±0.06
AF-2	2.35	63.44	590 ±0.07
AF-3	2.61	62.32	630 ±0.04
AF-4	2.76	62.92	609 ±0.06

Modifier ions normally occupy the interstitial sites in glass-network, which leads to an increased packing of glass structural units; it decreases the overall volume of the glasses.

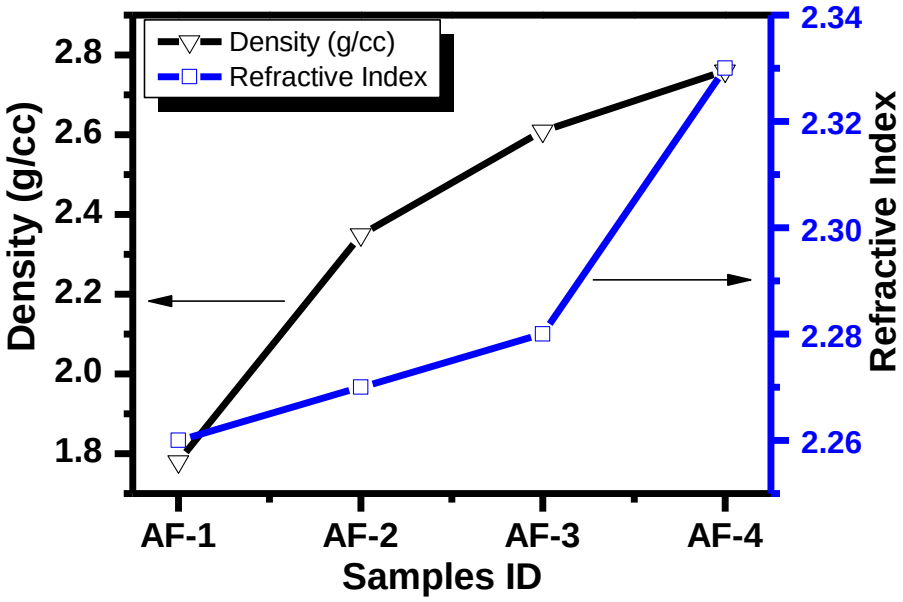

Fig. 4.3 Density and refractive index of as-quenched AF-1, AF-2, AF-3 and AF-4 samples

Interestingly, the calculated density of the present glasses is lower than the similar glasses derived from minerals oxides. It may be associated with the presence of higher porosity in agro-food waste ashes derived glasses than mineral-derived glasses.[197]

4.2.2 SEM/EDS analysis

The elemental analysis of the as-quenched samples was done by EDS as shown in Fig. 4.4. AF-1 sample contains a higher amount of SiO_2 with a small amount of alkali and alkaline-earth metals oxide like Na_2O, MgO, CaO along with some trace transition elements. The presence of trace elements oxides like TiO_2, Fe_2O_3, etc. is also reported earlier in agro-food waste ashes.[60] Further, increasing the amount of ESP (wt%), SiO_2 MgO, Na_2O and Al_2O_3 content decrease and CaO increases, as shown in table 4.3. In addition to this, the alumina content increases in AF-2, AF-3, and AF-4 glasses. Probably, this Al_2O_3 diffuses in glass composition from recrystallized alumina crucible during the melting process of the glasses. This tendency increases with increasing of ESP content in the glass composition. However, a small amount of alumina (Al_2O_3) is present inherently in raw ashes of agro-food wastes as confirmed by EDS of raw materials as given in table 3.1.

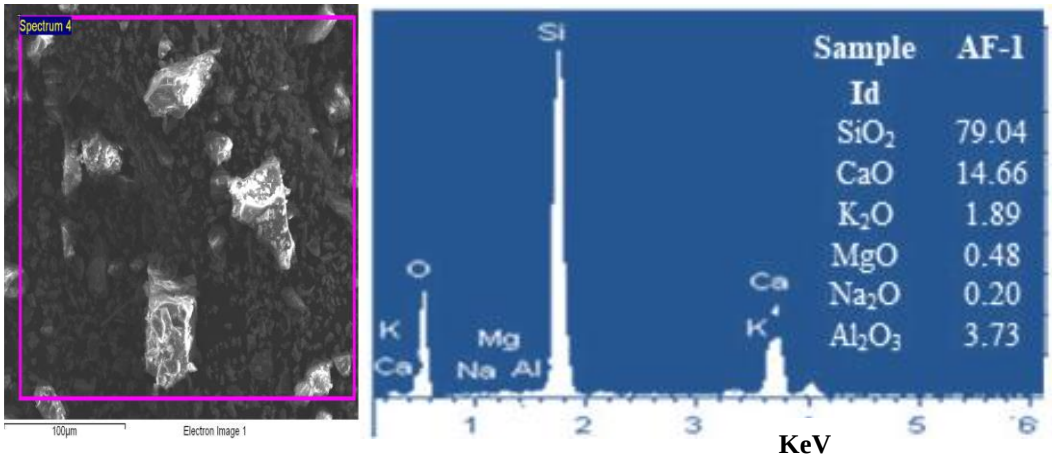

Fig. 4.4 Representative SEM image and EDS analysis of as-quenched AF-1 sample

It seems that during the melting process at 1550 ºC, Al^{3+} diffused in the melt, particularly in AF-2, AF-3 and AF-4 glasses, where ESP content is higher in the glass composition. It is observed that the tendency of Al^{3+} diffusion increases from the alumina crucible as ESP content increases in

composition. It means that alkaline and alkaline-earth metal cations contain a higher affinity towards Al^{3+} as compared to Si^{4+}. Higher content of K_2O, CaO, and Na_2O, are responsible for creating more NBOs due to their role as the modifiers, which may provide good sites for Al^{3+} diffusion from the crucible in the glasses. This effect clearly confirmed by decreasing the glass transition temperature (T_g) with increasing ESP in the present glasses as given and discussed in section 4.8.

Table 4.3 Chemical compositions (wt%) of the as-quenched AF-samples determined by EDS

Sample Id → / constituents ↓	**AF-1**	**AF-2**	**AF-3**	**AF-4**
SiO_2	79.04	65.34	61.30	52.12
CaO	14.66	22.86	29.67	35.61
K_2O	1.89	1.33	1.11	1.28
MgO	0.48	0.66	1.06	1.07
Na_2O	0.20	0.27	1.06	0.32
Al_2O_3	3.73	9.51	6.59	9.61

4.2.3 XPS analysis

EDS analysis confirmed that some trace elements are present in the as-quenched glasses. Thus, to confirm the presence of these elements, XPS survey scans of some selected samples are done and represented in Fig. 4.5 and Fig. 4.6 (a)-(d). The significant peaks of all the elements present in the glasses like Si, Ca, Mg, Na, Al, Ti, Fe, and O are also confirmed using XPS spectra. XPS scan also consists C1s peak, which is not part of the initial composition.[181] Oxygen peaks show some shifting towards the lower binding energy with ESP content. The intensity of these peaks also increases with ESP. It means that with the addition of ESP, increases the non-bridging oxygen (NBOs) in the glasses. XPS survey also confirms the presence of titanium as trace elements in these glasses, which is shown in Fig. 4.5. It is well-reported in the literature that agro-food wastes derived glasses exhibit some trace elements depending on region to region and fertilizers used during crop growth.[48]

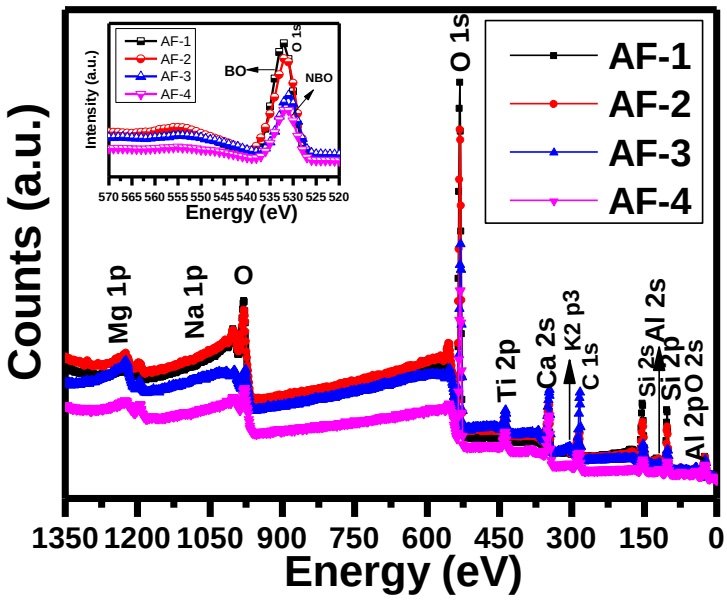

Fig. 4.5 XPS spectra of as-quenched samples along with oxygen dependency of these samples in an inset

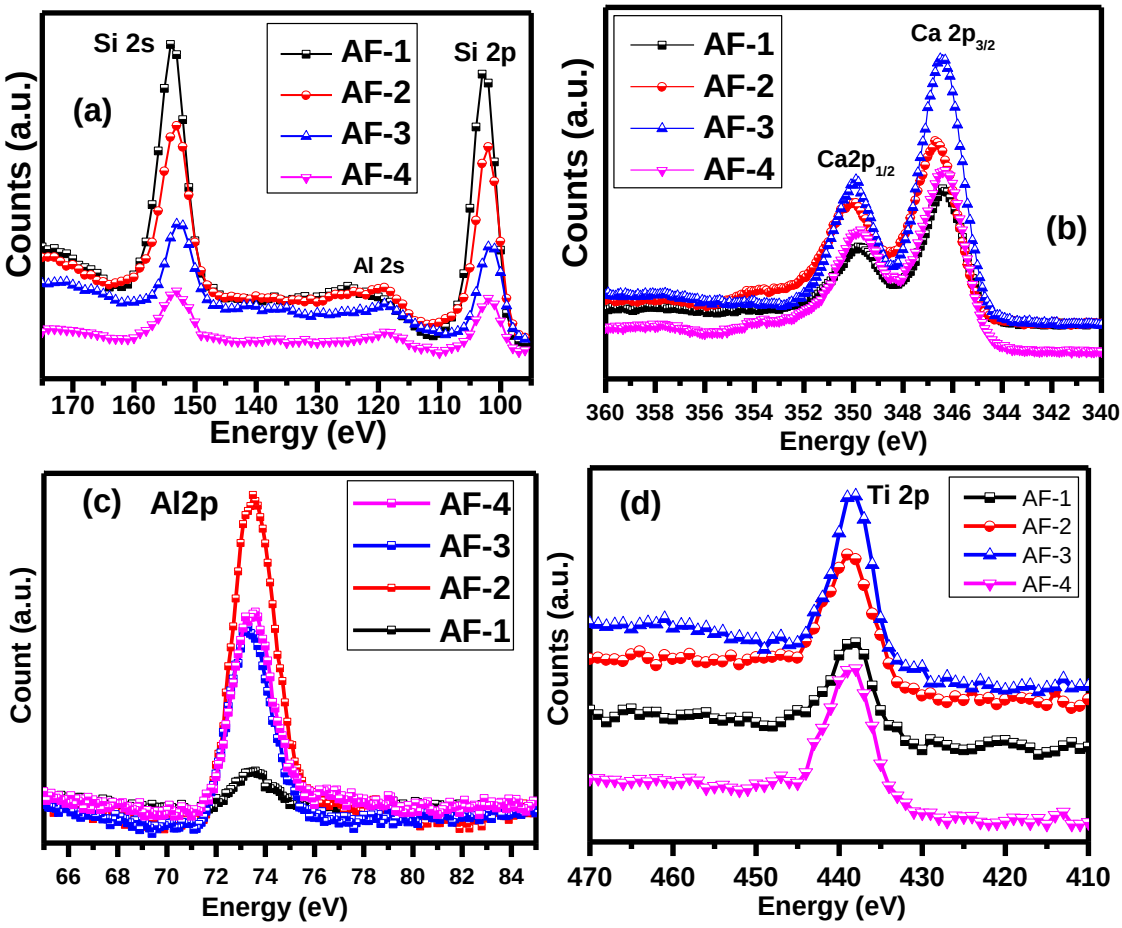

Fig. 4.6 XPS spectra for individual elements **(a)** Si **(b),** Ca **(c),** Al and **(d)** Ti of as-quenched AF- sample

4.2.4 X-ray diffraction analysis

The as-quenched samples are transparent with a blue tint as shown in Fig. 4.1. The blue color may arise due to the presence of some transition trace elements like Ti and Fe as observed in EDS and XPS analysis. AF-1 has not formed the glass due to the high amount of RHA in this sample, which contains high silica (required high melting temperature for melting). It exhibits two different crystalline forms of SiO_2 i-e., cristoballite (ICDD no.- 01-017-785) and wollastonite (ICDD no.01-075-1396). These are well-known crystalline phases, observed in high silicate containing glass-ceramics. On the other hand, XRD of the as-quenched AF-2, AF-3, and AF-4 samples show broad hump at 20-35°, and it confirms the amorphous nature of these samples. A high amount of ESP acts as a modifier, which decreases the melting point of the glass compositions and formed glasses at 1550 °C. Moreover, modifier ions like Ca^{2+}, Mg^{2+}, Na^{+}, K^{+}, etc. also increase the number of NBOs that influence the different properties of the glasses. Based on differential scanning calorimetry (DSC) results (as discussed in section 4.2.8), the as-prepared glasses are heat-treated at 900 °C (above to the crystallization temperature (T_c)) for 10 h to study the crystallization kinetics of the as-quenched glasses. The XRD patterns of the as-quenched, as well as heat-treated samples are shown in Fig. 4.7 (a) and (b), respectively. All the glass-ceramics exhibit different silicate and aluminate based crystalline phases. These crystalline phases are indexed with standard ICDD cards (as mentioned in Fig.4.7 (b)). During heat-treatment, initially, SiO_2 may nucleate in the glass-matrix later stage modifier ions diffused and formed the metastable or stable crystalline phases depending on the local affinity of different ions as presented in the glassy matrix. Surprisingly, $CaSiO_3$ phase is not formed in the present glasses. This phase is very common in calcium silicate glass-ceramics. It may be possible, that this phase is formed initially in the present glasses and converted to a more stable Ca_2SiO_4 phase with heat-treatment duration (10 h). The mechanism of the formation of crystalline phases in glasses could be proposed as follows:

$$SiO_2 + MgO = MgSiO_3 \quad (4.1)$$

$$SiO_2 + 2CaO = Ca_2SiO_4 \quad (4.2)$$

$$MgO + 2SiO_2 + CaO = CaMgSi_2O_6 \quad (4.3)$$

It seems that the presence of intermetallic oxides like Al_2O_3 is also provided nucleating site in the present glasses and leads to form the aluminate based crystalline phase such as $Ca_5(Al_3O_7)_2$.

$$5CaO + 3Al_2O_3 = Ca_5(Al_3O_7)_2 \quad (4.4)$$

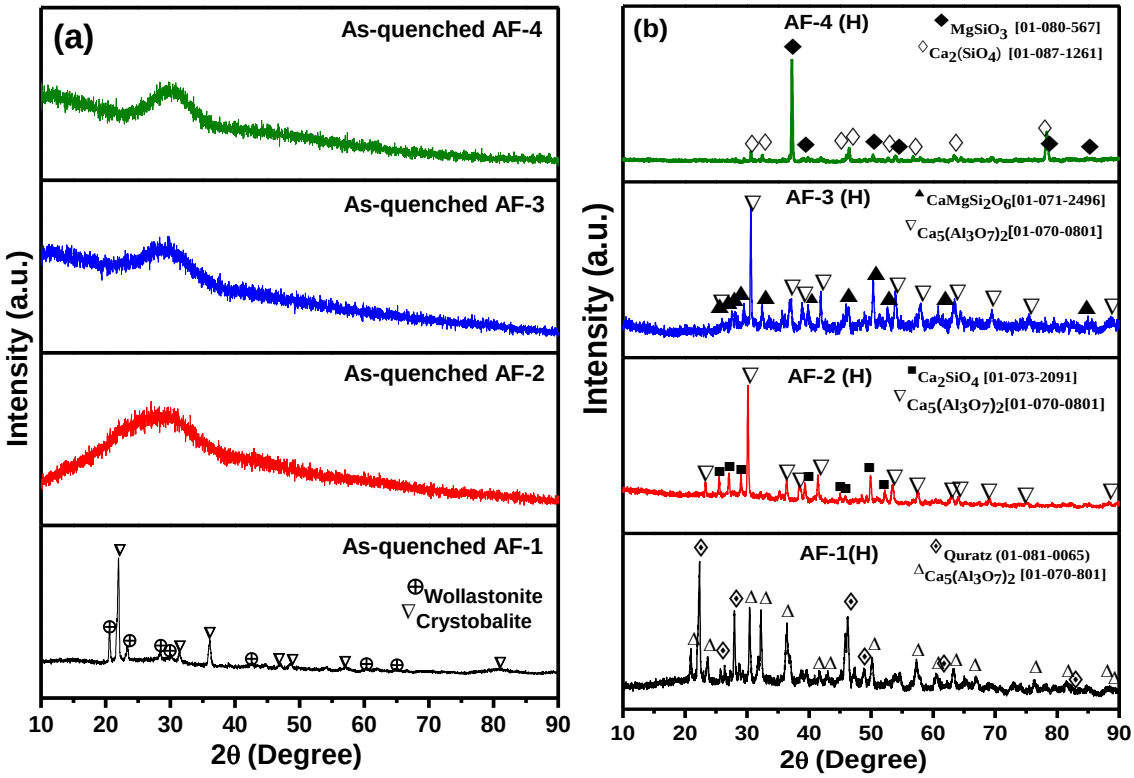

Fig. 4.7 XRD patterns of **(a)** as-quenched and **(b)** heat-treated AF(H)-samples at 900 ºC for 10 h

Interestingly, these glasses also contain some trace elements like Ti as confirmed by EDS and XPS analysis of the glasses. Usually, in mineral-derived glasses, the small amount of titanium acts as the nucleating agent.[192,198] However, in the present glasses, any crystalline phase related to titanium is not formed. Formation and presence of $MgSiO_3$ and Ca_2SiO_4 phases in these glass-ceramics can be explored their uses in light-emitting diode (LEDs) applications since some Ti^{4+} are inherently present as the trace elements in these glasses, which may act as optically active species.

4.2.5 FTIR analysis

Infrared transmittance spectra of the as-quenched samples are shown in Fig. 4.8 (a). Different FTIR bands are observed around 1877, 1624, 1462, 1103, 786, 622 and 482 cm^{-1} as given in table 4.4. The observed transmittance spectra of the as-quenched samples could be explained based on different structural units presented in the glasses. The band at 1877 and 1624 cm^{-1} is observed in AF-1 sample. It is associated with Si-OH water molecules and -OH bending vibration of molecular water. The relative intensity of both the bands become diffuse in AF-2, AF-3 and AF-4 samples as ESP increases in the glass composition. Shifting of the bands from higher to lower wavenumber also depend on bond length and bond angle among different structural units present in the glasses. However, besides of AF-1 sample, rest of the samples is completely glassy in nature. The maximum phonon energy of the present glasses is associated with ~1100 cm^{-1}. As ESP increases in the glasses, it shifts towards lower wavenumber ~1072 cm^{-1} for AF-2, AF-3, and AF-4, respectively. A similar result has been reported for silicate glasses derived from mineral oxides.[99] The silicate bands are shifted towards the lower wavenumber. It is associated with increased reduce mass and enhancement of NBOs with ESP content, as shown in Fig. 4.8 (b)-(e). The bands around at 786 and 482 cm^{-1} is mainly due to Si-O-Si bending vibration and Si-O-Al stretching mode.[199,200] An intense band around at 622 cm^{-1} is observed in AF-1.

Table 4.4 FTIR bands observed in the AF-samples.[96,163,201]

Wavenumbers	**Attributed bands**
1877 cm^{-1}	Si-OH Water molecules
1624 cm^{-1}	Si-O bending vibration
1462 cm^{-1}	Related to CO group and molecules of water
1103 cm^{-1}	Si-O-Si symmetric stretching
786 cm^{-1}	Si–O–Si bending vibration and Si–O–Al stretching mode
622 cm^{-1}	Bending vibrations of Al-O bands
482 cm^{-1}	O-Si-O bending vibrations

The bending vibrations of Al-O bonds also occur within this wavenumber region. However, the intensity of this band is reduced drastically after increasing the ESP content from AF-1 to AF-4 samples. The changes in band intensity and their peak positions are related to change in the amount of Q^4, Q^3, Q^2, Q^1, and Q^0 units. The change in band position and intensity with increasing ESP is well related to the optical and other properties of the samples.

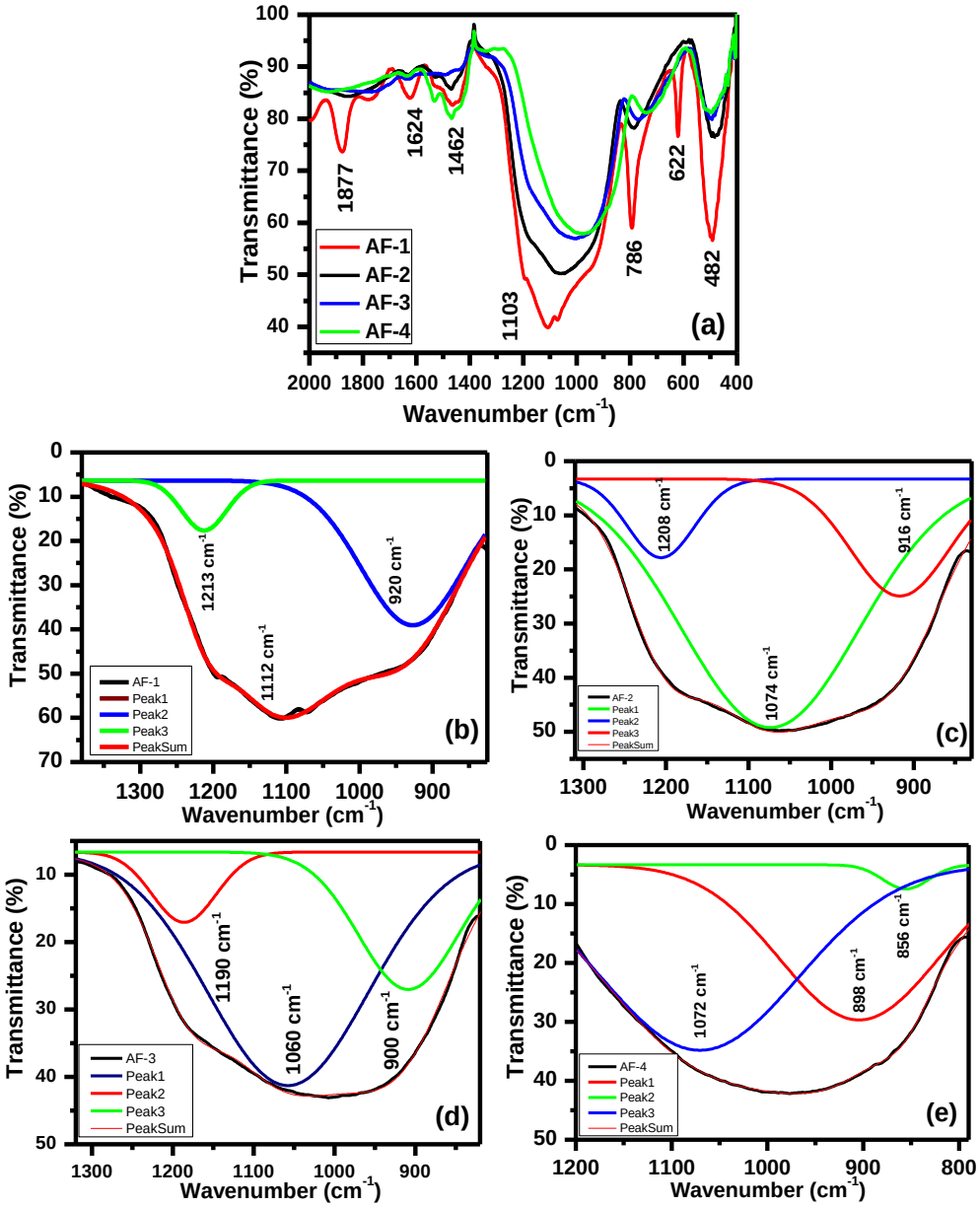

Fig. 4.8 FTIR spectra **(a)** as-quenched AF-samples and de-convolution of fingerprint region **(b)** AF-1 **(c)** AF-2 **(d)** AF-3 **(e)** AF-4 samples

4.2.6 Vicker's microhardness

Vicker's microhardness of the heat-treated samples is shown in table 4.2. The hardness of heat-treated samples is 590-630 HV. Basically, hardness is related to the compactness of the samples. In other words, the well-connected topography of the glasses is responsible for the good hardness. Vicker's microhardness in the present samples shows an increasing trend after replacing RHA by ESP. The hardness is slightly higher than the similar type of glass-ceramics synthesized from commercially available oxides.[2] Hardness also depends on the volume fraction of the different crystalline phases and its chemical nature.[81,202]

4.2.7 Optical properties

4.2.7.1 Optical band gap

The optical absorption spectra and optical band gap of the as-quenched samples are given in Fig. 4.9 (a) and (b). It is clear that the fundamental edge of absorption is not sharp. It is a common feature of the glasses. From diffused reflectance spectra, the optical band gap of the as-quenched samples was calculated using the Kubelka-Munk function.[203,204] Curve $[F(r)hv]^2$ versus energy (hv) is plotted to calculate the optical band gap of the present samples. The optical band gap is also given in table 4.5. All the glasses exhibit an optical band gap above 3.25 eV. It lies in the wide-semiconductor range. The optical band gap also lies in the range of earlier report glasses derived from mineral oxides of similar composition.[99] Urbach energy (E_u) of the as-quenched glasses was calculated using the following equation:

$$F(r)hv = \beta \exp(^{hv}/_{E_u}) \quad (4.5)$$

Urbach energy can be obtained from ln F(r) versus photon energy plot, by taking the reciprocal of the slope of the linear portion. Urbach energy is governed due to short-range structural disordering, imperfection like non-bridging oxygens (NBOs) in the glasses. It is always below the absorption band edge of the sample and having lower values than optical band gap. Urbach energy is

increased by adding the ESP in the glass composition. It manifested the higher defects as presented in AF-4 than other glasses. It is well-reported in the literature, the increased amount of modifiers, in general, decreases the optical band gap due to breaking the glass-network and created more NBOs and other defects in the glass network.[205,206]

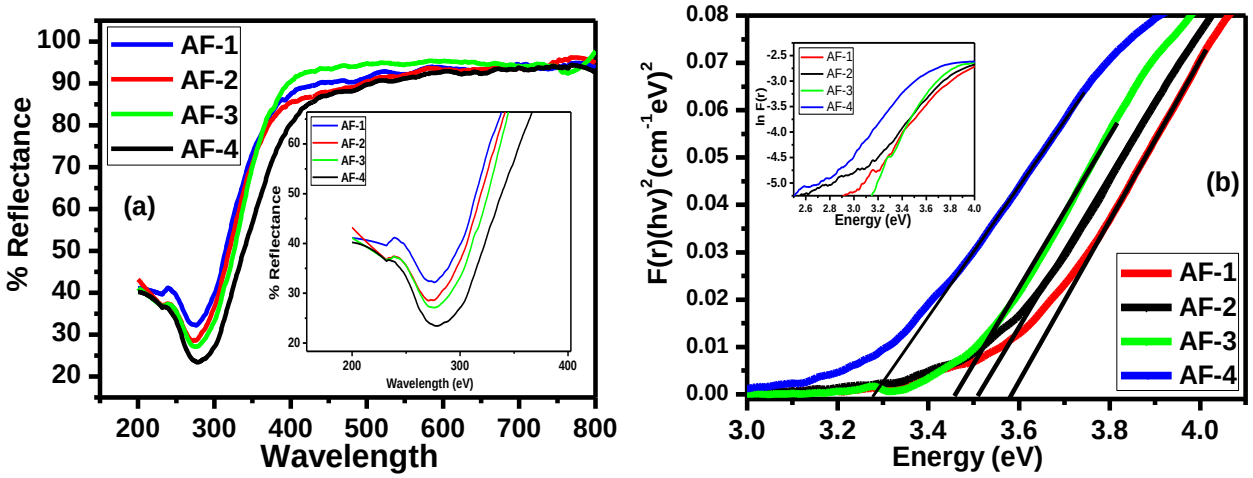

Fig. 4.9 (a) Reflectance spectra **(b)** optical band gap, and Urbach energy (given inset) of the AF-1, AF-2, AF-3 and AF-4 samples

4.2.7.2 Refractive index

Using the optical band gap, the refractive index of the samples is calculated using Dimitrov and Sakka equation[207] and given in table 4.5 and Fig. 4.9 (b). The refractive index is calculated using the following equation.

$$\frac{(n^2-1)}{(n^2+2)} = 1 - \sqrt{\frac{E_{opt}}{20}} \qquad (4.6)$$

The refractive index values are increased up to AF-3 glass almost linearly with increasing ESP. Refractive index increases with decreasing optical band gap values, which is well-reported in the literature.[1] Normally, reflective index depends on polarizing power of the first nearest neighbor ions coordinated with the anion, field strength of the cations, coordination number, NBOs, electronic polarizability of the oxide ion and crystallization, etc.

Table 4.5 Optical band gap, refractive index, Urbach energy and CTE of the AF-samples

Sample Id ⟶ Properties ↓	**AF-1**	**AF-2**	**AF-3**	**AF-4**
Optical band gap (eV)	3.57	3.51	3.49	3.26
Refractive index (n)	2.26	2.27	2.28	2.33
Urbach energy (eV)	0.308	0.309	0.310	0.313
(CTE)×10^{-6}/K	15.06	14.05	14.14	16.17

Refractive index increases with an increasing covalent character of the bonds, which further depends on the difference in the electro negativities of the bond-forming atoms of the glass constituents. The percentage covalent character of the bonds is increased in the following sequence SiO_2>CaO>K_2O, etc. The variation of the refractive index is a good agreement with the variation in the covalent character of the bonds in the glasses.

So, the refractive index also depends upon the concentration of the NBOs. Although, formation of partial crystalline phases maybe also affect the refractive index. Mostly, the covalent character and polarizability have been the dominating factors to determine the refractive index of the as-quenched samples. Actually, RHA is having maximum SiO_2 with a small amount of the trace elements. This silica acts as a glass-former with trace elements like alkali and alkaline-earth metals, these trace elements can act as the modifiers. Conclusively, the optical band gap and refractive index may also depend on the other factors than NBOs.

4.2.8 Thermal properties

4.2.8.1 Thermo gravimetric analysis

The DSC thermographs of the as-quenched samples are shown in Fig. 4.10. In the present samples, the one endothermic and two exothermic peaks are observed in the temperature range 500-900 ºC for AF-2, AF-3, and AF-4 glasses. First endothermic peak corresponds to the T_g of these glasses. The thermal stability of the glasses and glass-ceramics are associated with difference between (T_g) and (T_c). Larger the difference between (T_g) and (T_c) indicates higher the thermal stability of

glasses. Glass-ceramics contain some crystalline phase embedded in glass-matrix, so, they are always having higher thermal and mechanical stability than glasses. Other two exothermic peaks are associated with two crystallization temperatures in these glasses. On the other hand, AF-1 sample could not form the glasses. Two crystalline phases are observed in this sample as shown in Fig. 4.7 (a). In this particular sample (AF-1), peaks in DSC are related to the phase transition of different polymorphous of crystalline phases. In these samples, the substitution of RHA by ESP, promote to disrupt the polymerization of SiO_2 networks, which should be responsible for decreasing the glass-transition temperature (T_g) as well as crystallization temperature (T_c).

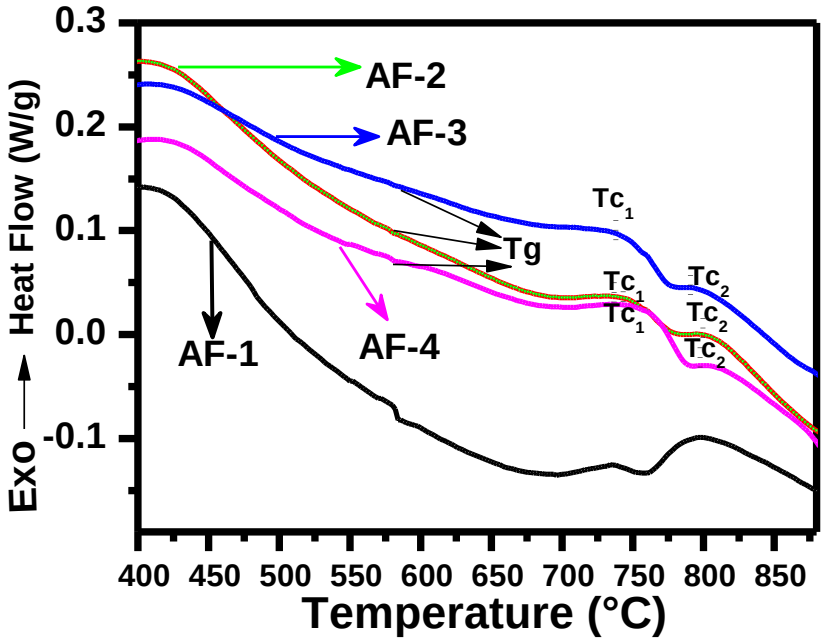

Fig. 4.10 DSC curves of the as-prepared AF-1, AF-2, AF-3 and AF-4 samples

However, T_g and T_c of the present glasses do not follow any trend. The presence of two (T_c) is related to phase separation in the present glasses. Phase separated is well-reported in the silicate glasses, in general, where two formers/modifiers are presented.[208] The melting point of the present glasses is not noticed up to 900 ºC. TGA curve of the as-quenched samples is shown in Fig. 4.11. All the as-quenched samples show weight loss ~1-3 wt% in the temperature range from 30-300 ºC. This weight loss is associated with the water absorbed and organic solution of the samples.[209] AF-3

and AF-4 sample shown lesser weight loss than the other two samples. Lesser weight loss in the glasses is related to thermal stability. The present glasses show very stable behavior above 350 ºC particularly, AF-3 glasses.

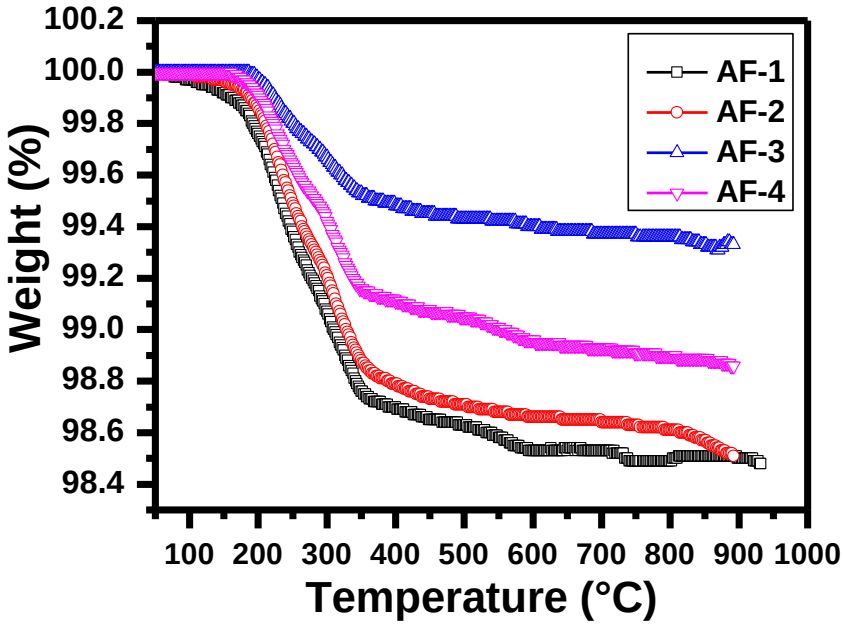

Fig. 4.11 Weight loss of the as-quenched AF-1, AF-2, AF-3 and AF-4 samples

4.2.8.2 Dilatometry analysis

CTE plays a significant role to decide the efficiency and working life of any device that used in variable high-temperature applications. CTE measurement was done on the heat-treated samples (900 ºC for 10 h) as given in Fig. 4.12. As XRD indicated, all the heat-treated samples exhibit at least two crystalline phases. All the CTE curves show the non-linear behavior with respect to temperature. This non-linearity is more pronounced in AF-1 followed by AF-3 and AF-2. Whereas, AF-4 is exhibit more or less linear behavior above 350 ºC. As shown in Fig. 4.7 (b), a particular sample is formed the only silicate-based crystalline phases i-e., $MgSiO_3$ and Ca_2SiO_4. On the other hand, heat-treated AF-1, AF-2, and AF-3 samples contain $Ca_5(Al_3O_7)_2$ crystalline phases apart from silicate phases. Calcium aluminate crystalline phases may be responsible for the non-linearity in CTE curve due to some phase transition related to this particular phase. CTE is calculated in the temperature range from 300-700 ºC. The CTE value is found $14\text{-}16\times10^{-6}$/K. This range of CTE is

on a little higher side as required for sealing glasses for solid oxide fuel cells (SOFC's). So, these glasses and glass-ceramics after some compositional modification may find application as the sealants in SOFCs.[104]

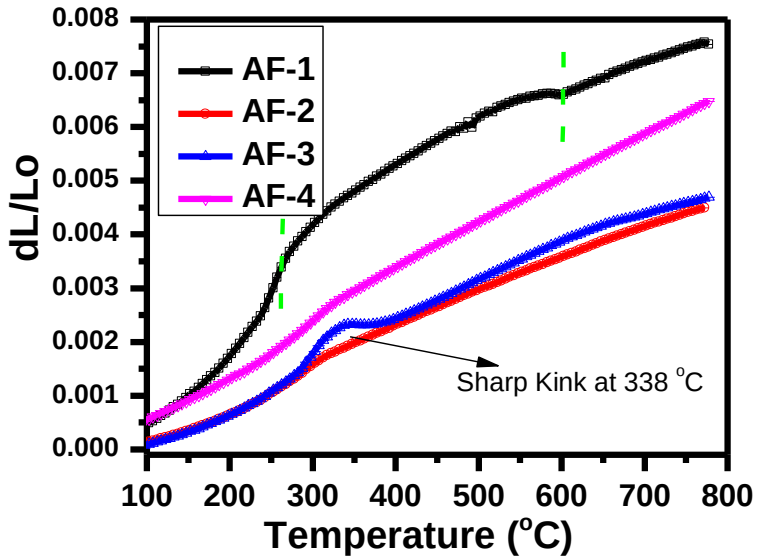

Fig. 4.12 CTE curve of heat-treated AF-1, AF-2, AF-3 and AF-4 samples

4.2.9 Dielectric properties

In this section, the impedance analyzer is used to define the contributions of various processes such as bulk, grain boundaries, and electrode interface effects in the frequency domain. Generally, complex permittivity, complex impedance ($Z^{\prime}$), is having three basic formalisms, which are related to each other and represented here.[210,211]

$$E^* = \epsilon' - j\epsilon'' \tag{4.7}$$

$$Z^* = Z' - jZ'' = 1/jwC_o\epsilon' \tag{4.8}$$

$$\tan d = \epsilon''/\epsilon' = Z'/Z'' \tag{4.9}$$

where (ϵ', Z') and ϵ'', Z'') are real and imaginary permittivity and impedance, respectively. The imaginary factor is represented $j=\sqrt{-1}$ and angular frequency is $w= 2\pi f$.

The frequency response of dielectric permittivity to the applied electric field can be expressed by dielectric permittivity as follows:

$$\in (w) = \in' (w) - i \in'' (w) \qquad (4.10)$$

and $\in' = {}^{C}/_{C_o}$ is free space permittivity and w is angular frequency; $\in'$ is the real component. Basically, relative permeability (also dielectric constant k) is the ratio of the permittivity of a substance and free space. Dielectric measurement was done on glass-ceramics (heat-treated samples). The dielectric constant of all the samples is varying from 18-32, which is almost independent with frequency from (100Hz-1MHz) at room temperature, however, at low frequency, the tangent loss is minimum up to 10^3 Hz, beyond this frequency, it exponentially increases.

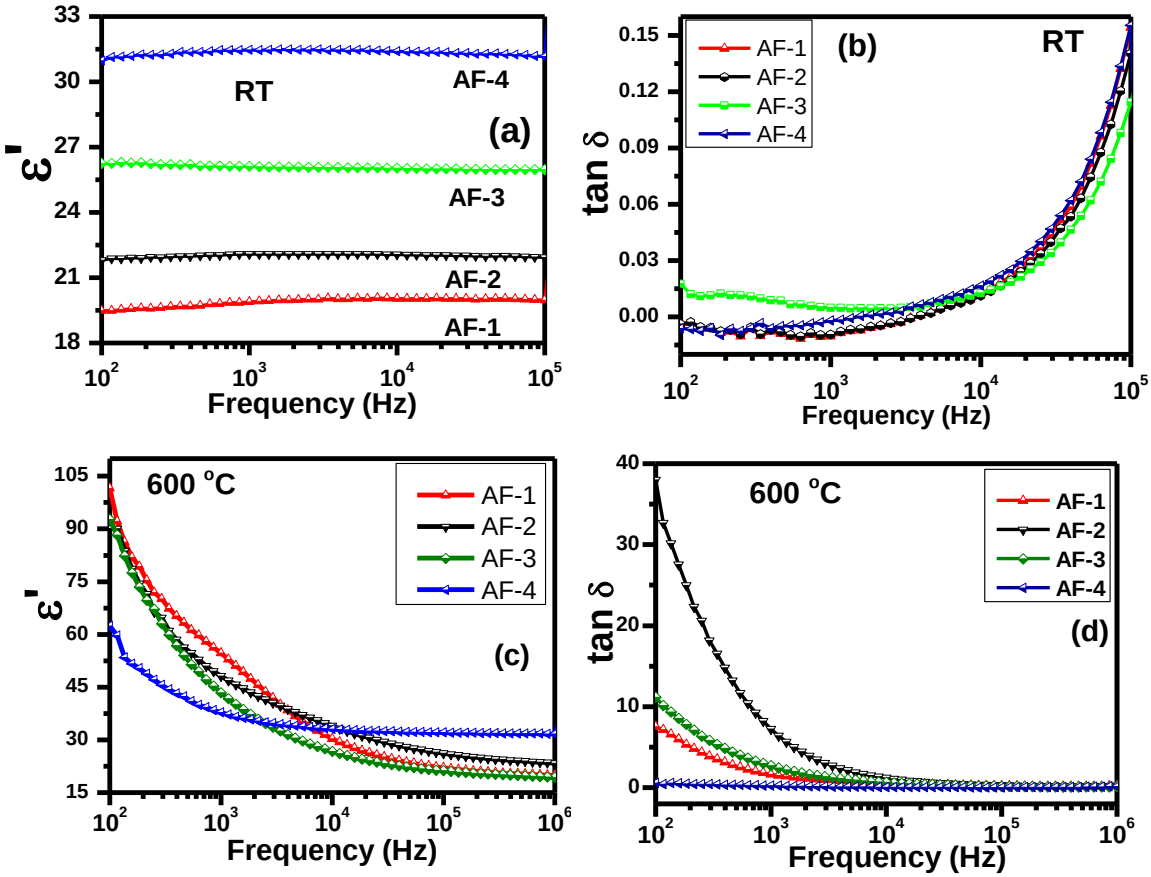

Fig. 4.13 (a)-(d) Dielectric constant and tan d of the heat-treated AF-samples with frequency at room temperature (RT) and 600 °C

Materials with lower polarizability have lower dielectric constant. The AF-4 sample is expected to have a high dielectric constant due to the higher polarizability of Ca^{2+} (3.16Å^3) ion as compared to Si^{4+} (0.87Å^3) ions at room temperature.[209] The dielectric constant and tangent losses of all glass-ceramics firstly decrease exponentially with frequency up to 10^4 Hz, after that, dielectric constant

and tan d become almost constant particularly, in AF-4 sample as shown in Fig. 4.13 (c) and (d). Space charge polarization plays a vital role to influence the dielectric permittivity at the lower frequency.[10] The accumulation of charge carriers at the grain boundaries is responsible for high dielectric constant at the lower frequency. At the same time, different modifiers and their concentration-effect are also leading the dielectric properties with the temperature and frequency. The highest dielectric constant with minimum loss is observed for AF-4 sample. This particular sample exhibits two crystalline phases. Both the phases are silicate-based phases. Moreover, AF-4 sample shows more stable behavior with respect to temperature and frequency.

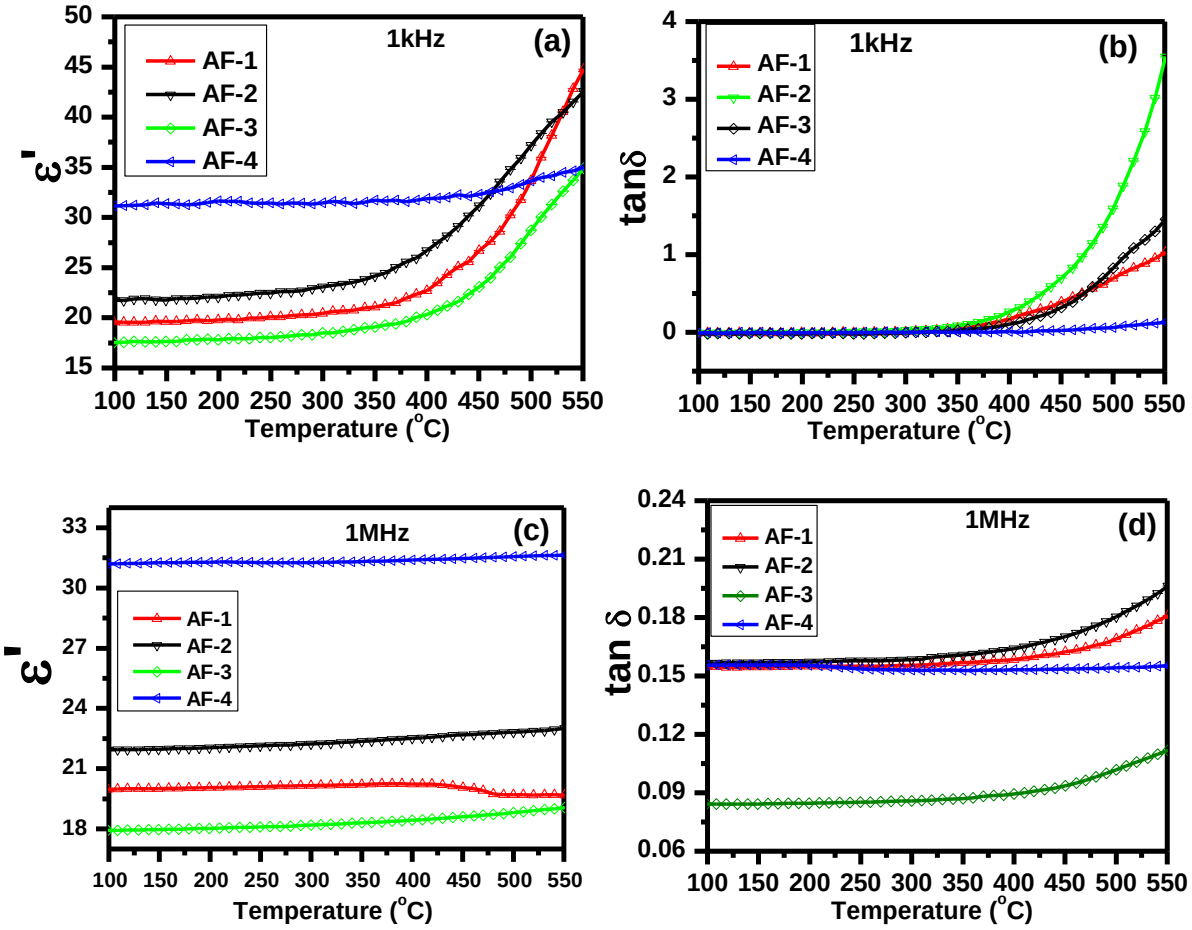

Fig. 4.14 (a) (c) Dielectric constant and **(b) (d)** tan d of the AF-samples at (1kHz) and (1MHz) with 550 °C

The variation of the dielectric constant and tangent loss with respect to temperature and two frequencies (1kHz and 1MHz) is presented in Fig. 4.14 (a)-(d). It can be seen that the dielectric

constant and losses are almost constant up to 400 ℃ after that dielectric constant increases up to 550 ℃ at 1kHz, whereas, dielectric constant of the samples exhibit independent behavior with respect to the temperature and frequency at 1MHz. In AF-1, AF-2 and AF-3, the tangent loss is gradually increased at a higher temperature in the higher frequency region may be due to the large glass content and the high mobility of alkali ions. These glasses and glass-ceramics may find applications in energy conversion devices and microelectronics.

4.3 45SCLA-(55-x)RHA-(x)ESP (x=0, 10, 15, 20, 25) series

In this series, four samples have been synthesized using RHA, SCLA, and ESP as initial constituents. Raw materials were taken in wt% as given in table 4.6. All the samples were melted in recrystallized alumina at 1550 ^{o}C via melt-quench technique. The as-prepared samples are characterized using various techniques.

Table 4.6 Ashes of the SCLA, RHA and ESP in (wt%) along with their labels

Samples ID	SRE-1	SRE-2	SRE-3	SRE-4
SCLA	45	45	45	45
RHA	45	40	35	30
ESP	10	15	20	25

4.3.1 Density

Density of the as-prepared glasses increases with increasing ESP due to ESP has a higher content of CaO than RHA. Since, CaO (3.34 g/cc) has a higher density as compared to SiO_2 (2.65 g/cc). However, density of the glasses follows the increasing trend with increasing ESP content in the main composition. The density of the present glasses is comparable or lower than the other synthesized glasses using minerals oxides. The molecular weight of constituent oxides in the present compositions follows the following trend; $Na_2O<K_2O<SiO_2<MgO<CaO<Al_2O_3$. The modifier breaks the glass network led to the compactness of the glassy system. It is also reported by many researchers when glasses were synthesized using the minerals. Molar volume for the glasses and glass-ceramics was calculated using following equation:[194]

$$V_m = M / \rho_{sample} \quad (4.11)$$

Where, M denotes the molecular weight of the sample.

At high temperature, where the melt is fluid, the melt consists of a eutectic mixture of modifier ions and various structural units of the network. They may be as small as the basic building block of the network or it may consist of a few of these building blocks connected to form small discrete

ions of modifiers. When the melt is cooled rapidly, the network begins to form as the local structural units and become connected.

Table 4.7 Molecular weight, density, and molar volume of as-quenched samples

Sample ID	Molecular weight (g/mole)	Density (g/cc)	Molar volume (V_M)
SRE-1	61.38	2.27	27.04
SRE-2	61.36	2.44	25.14
SRE-3	61.69	2.48	24.80
SRE-4	62.31	2.54	24.53

The alkaline-earth metal or other modifiers ions could break the connectivity of the glass-network. A certain amount of alkali and alkaline-earth metals like K_2O, Na_2O, and CaO always increase the density within the silicate glass system due to their molecular size and modifying behavior. In addition to this, SiO_2 and alkali/alkaline-earth elements like MgO, K_2O replacing by CaO result reduced the electrostatic forces between the kinds of non-bridging oxygen (NBOs) considerably and hence, decreases the characteristic temperature such as T_g, and T_c of the as-prepared glasses. These modifiers have broken the network and increased the compactness of the system, which leads to decrease the molar volume of the glasses as observed in table 4.7.

4.3.2 EDS analysis

The chemical composition of the as-quenched samples was evaluated by SEM/EDS as presented in table 4.8. The EDS analysis shows the systematic variation of SiO_2 and CaO content in the samples. However, K_2O, MgO and Na_2O could not show any trend.

Table 4.8 Chemical compositions of the as-quenched samples calculated by EDS

Samples ID	SiO_2	CaO	K_2O	MgO	Na_2O	Al_2O_3
SRE-1	81.85	8.02	4.77	3.59	0.45	1.32
SRE-2	78.37	12.76	4.38	2.66	0.09	1.74
SRE-3	74.98	15.05	3.68	2.90	0.00	2.22
SRE-4	69.91	18.36	4.34	2.51	0.35	4.52

4.3.3 X-ray diffraction analysis

The X-ray diffraction patterns of the as-prepared and heat-treated samples are presented in Fig. 4.15 (a) and (b), respectively. A very broad hump is observed between 2θ=17-35°, which associated with the amorphous characteristic of the as-quenched samples. The broad halo shifts towards the higher diffraction angle as SiO_2 content decrease after adding of the ESP, which acted as a modifier.

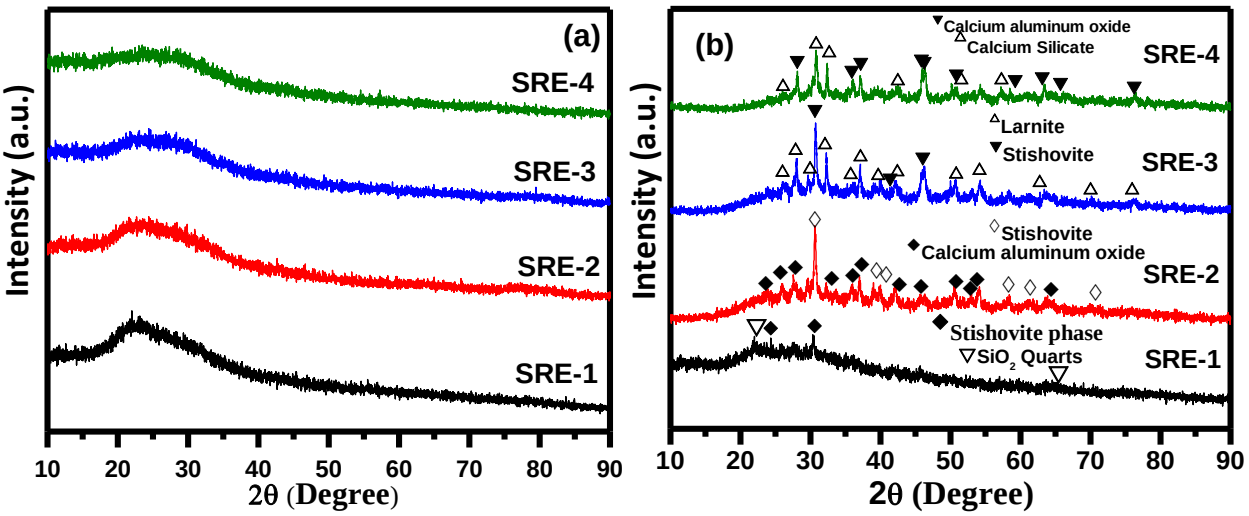

Fig. 4.15 XRD patterns of the SRE samples **(a)** as-quenched **(b)** heat-treated at 900 ºC for 10 h

It may be associated with the higher number of NBOs and glass network connectivity with the packing of the local glass structural unit. It is well-reported that the modifiers break the network units and modify the structural units packing of the different glass network, which influences the density of glasses. The higher amount of K_2O, CaO, Al_2O_3, and other trace elements promote to disturb the connectivity of the glass networks. SRE-4 has more modifying cation, hence, the viscosity is lower as compared to SRE-1. So, as ESP increases, the glass formation tendency also increases in the present samples. All the samples are heat-treated at 900 ºC for 10 h to study the crystalline behavior of the glasses. SRE-1 sample exhibits two crystalline phases. These phases are formed accordingly to the given equation (4.12) (4.13) and (4.14).

$$2CaO + SiO_2 = Ca_2SiO_4 \quad (4.12)$$

$$3Al_2O_3 + 5CaO = Ca_5(Al_3O_7)_2 \quad (4.13)$$

$$CaO + Al_2O_3 = CaAl_2O_4 \quad (4.14)$$

This sample is formed the polymorphous phase of the silicate i-e. stishovite phase SiO_2 (ICDD no-010-80-0371) and SiO_2 phase (ICDD no.-010-82-1554). Whereas, SRE-2 sample exhibits stishovite SiO_2 (ICDD no.- 01-081-1666) and calcium aluminum oxide $CaAl_2O_4$ (ICDD no.-010-88-2477) with a monoclinic structure. On the other hand, SRE-3 samples also shown the two crystalline phase i-e larnite Ca_2SiO_4, (ICDD no.- 01-073-2091) with the monoclinic crystal structure and stishovite SiO_2 (ICDD no.- 010-80-0373) Ca_2SiO_4 phase shows the phase transition at the different temperatures. SRE-4 sample shows higher crystallization tendency due to higher CaO and Al_2O_3 content. In this sample, calcium silicate Ca_2SiO_4 and calcium aluminum oxide $Ca_5(Al_3O_7)_2$ (ICDD No.- 01-087-1261 and 01-070-0801) crystalline phases are formed. The crystallization tendency of the heat-treated SRE-4 sample could be clearly seen in Fig. 4.15 (b). At the same time, the SRE-1 sample shows a lower tendency of crystallization. All the samples are formed from the silicate-based crystalline phases. Additionally, SRE-2 and SRE-4 samples formed aluminates based phases. It is also reported by many researchers in the literature that in case of silicate-based glasses, during heat-treatment, initially, SiO_2 is nucleate followed the diffusion of the modifier cations leads to form the different crystalline phases.[212] In addition to this, it seems that intermediate oxides (Al_2O_3) are also acted as nucleating species to form the aluminates related to crystalline phases. In all the four samples, $Ca_5(Al_3O_7)_2$ is a very good ionic conductor as well as it exhibits excellent oxygen storage within nanocages in a wide concentration range.[213] So, this ceramic sample can be useful for electrolytes in fuel cell applications.

4.3.4 FTIR analysis

FTIR spectra of the quenched samples are shown in Fig. 4.16. The FTIR result indicates that the intensity of bands is increased after adding ESP in initial constituents of the glasses. The small kink is also observed at-3688 cm^{-1}, particularly in the SRE-4 sample. This band may belong to H-OH group. Both the bands are prominent only in the SRE-4 sample. The prominent and broad band is observed at~1081 cm^{-1}, which corresponds to various silicate units like Q^0, Q^1, Q^2, Q^3, and Q^4. As CaO increases in initial composition at a certain level, this band becomes diffuse up to SRE-3 clearly indicates the disturbance in the silicate glass network. Moreover, this band shifts towards lower wavenumber. It means the addition of ESP leads to some modifications in silicate units. The band becomes sharp in SRE-4 sample. It may be associated with some ordering is taken place at the local level in this particular glass. It is possible even an amorphous sample may have some crystalline or nanocrystalline phases in short-range regions or sand-witch between two amorphous matrix.[214]

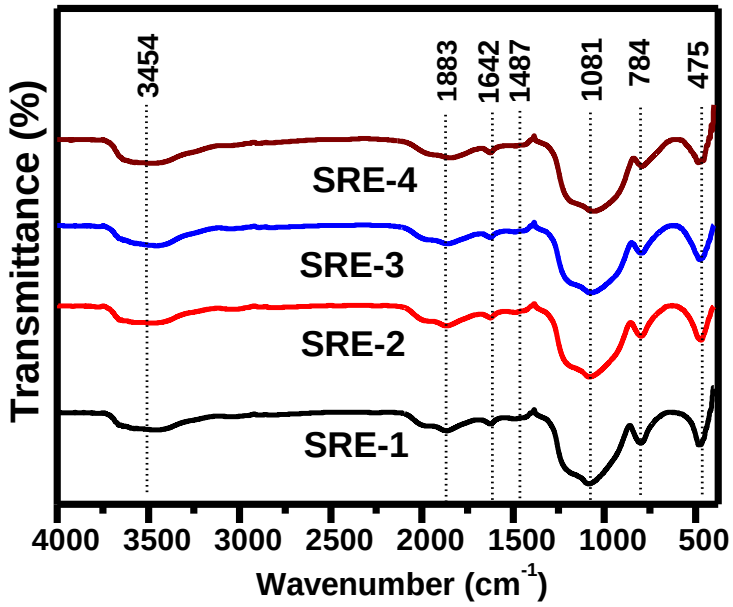

Fig. 4.16 FTIR spectra of the as-quenched SRE-1, SRE-2, SRE-3 and SRE-4 samples

The broadness of the band is due to the superposition of the IR-bands of the asymmetric vibrations of different types of Q-units of silica network. All molecules containing tetrahedral coordinate

silicon are presented because this band becomes more intense and sharp in SRE-4 as compared to other samples. So, it could be related to the crystalline silicate network presented at the local level in this sample.[215] The band at ~790 cm^{-1} corresponds to the stretching vibrations of the silicate network, i-e., Si-O-Si bond vibrations.[216]

4.3.5 Thermal properties

4.3.5.1 Thermogravimetric analysis

TGA curve of the as-quenched samples is shown in Fig. 4.17. All the as-quenched samples show weight loss with minima at 350 ºC except SRE-3 sample. SRE-3 sample shows continuous weight loss up to 900 ºC. However, initial weight loss is very steep up to 350 ºC followed by 0.5% weight loss. All samples show the weight loss up to 350 ºC due to the evaporation of crystalline water or trapped water in closed pores in the glasses. After 350 ºC, SRE-1, SRE-2, and SRE-4, glasses exhibit the weight gain continuously. SRE-2 sample shows the highest weight gain ~1% followed by SRE-1 and SRE-4 sample, respectively. In general, the weight gain is related to the oxidation of the transition metals presented in the glasses. In the present samples, the transition metal oxides are not found as shown in table 4.7.

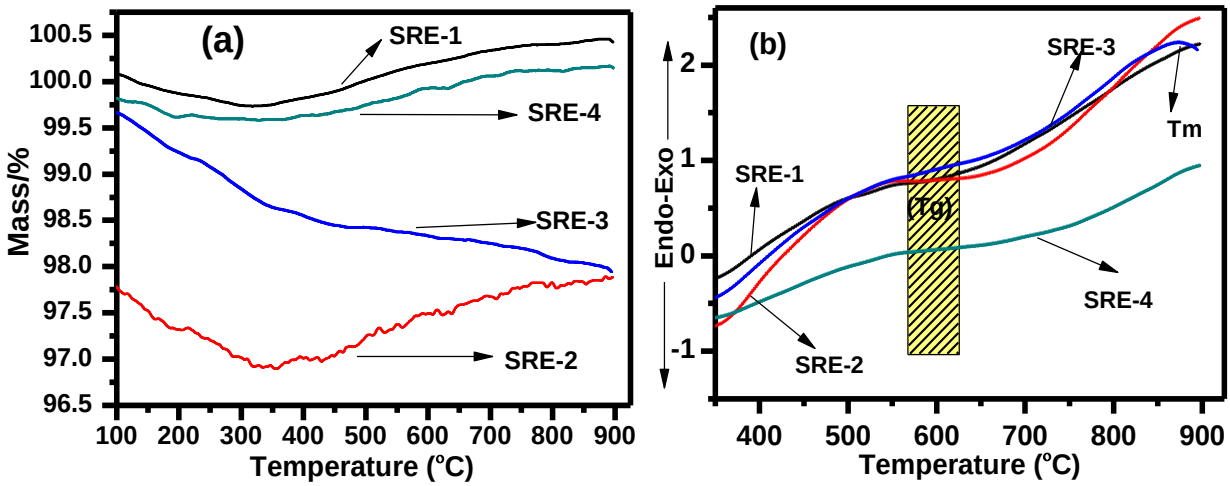

Fig. 4.17 (a) TGA and **(b)** DTA analysis of the SRE samples heated at 10ºC/min in the air

However, some trace transition metals are reported in the agricultural or food wastes, when these wastes analyzed by more sophisticated analysis techniques like MP-AES, ICP or XPS.[34] In contrast

to other samples, SRE-3 shows the different behavior i.e. continuous weight loss in this particular sample is observed, either it is related to some trace elements are reduced. However, further and more sophisticated measurements are required to confirm the above interesting results. For the thermal stability point of view, SRE-4 sample is more stable than the other samples. Moreover, the thermal stability of the present samples (derived from wastes) is comparable with those glasses synthesized by normal chemicals (minerals) for the similar compositions.[217]

4.3.5.2 Dilatometry analysis

CTE is calculated on the heat-treated samples at 900 ºC for 10 h. The thermal expansion curves of heat-treated samples are shown in Fig 4.18. The addition of ESP (CaO) acts as a modifier and then, it creates more non-bridging oxygen (NBO) in the samples, which affect the stabilization of glass-network to decrease the characteristic glass-transition temperatures. The heat-treated SRE-4 sample shows the deviation at 260 °C. It may be related to the phase transition of SiO_2 (quartz). The crystalline phase $Ca_5Al_6O_{14}$ exhibits the phase transition as reported by Lahl *et al.*[212]

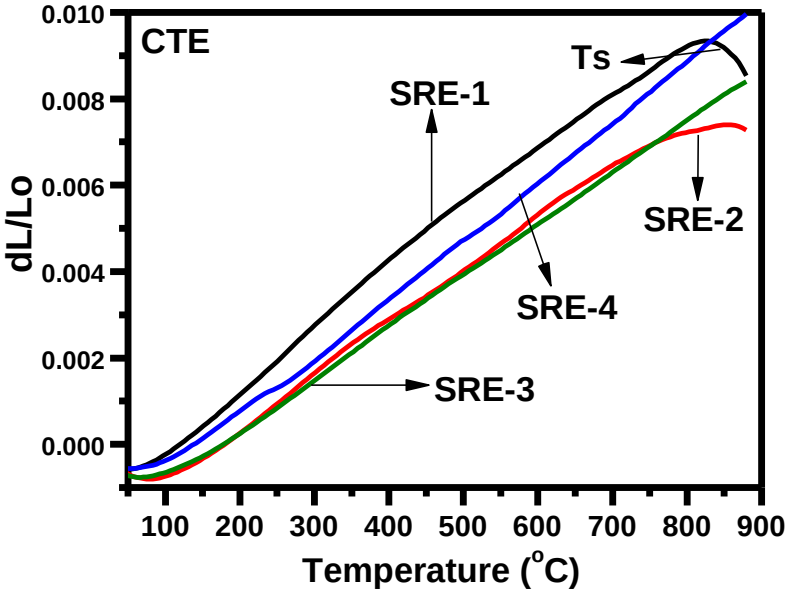

Fig. 4.18 CTE of glass-ceramic samples after sintering the pellets at 900 °C for 10 h

The SRE-1 and SRE-2 show the softening temperature at ~ 800 °C, which clearly indicates that some glassy matrix still present in these samples, even after heat-treatment. SRE-3 and SRE-4,

glasses show the higher tendency to grow the crystalline phase become glass-ceramics as compared to SRE-1 and SRE-2, samples. SRE-1 sample also shows higher slop that indicates higher CTE of this sample as compared to the other samples. The replacement of RHA by ESP, at a particular level in the samples is support to enhance the crystallization tendency of the glasses as also observed in XRD (Fig. 4.7 (b)). The properties of the glasses and glass-ceramics could be tailored to select proper agro-food wastes. SRE-3 and SRE-4 samples show the remarkable thermal stability up to 900 ºC as shown in Fig. 4.18. It is comparable with glasses, which are synthesized using minerals.

4.3.6 Optical properties

4.3.6.1 Optical band gap and Urbach energy

Diffused reflectance spectra of the as-quenched glasses are shown in Fig. 4.19 (a). The signature of phase separation phenomena in the glasses could be established by the UV-Visible spectra. A kink at ~262 nm is clearly seen in all the glasses. This kink might be originated due to the presence of a different glass matrix within the glass matrix, i-e. phase-separated glass. From spectra, optical band gap of the as-quenched glasses was calculated using the Kubelka-Munk function.[204] Tauc's plot shown in Fig. 4.19 (b) ensures optical band gap decreases with increasing ESP content. Maximum optical band gap (3.72 eV) is shown in SRE-1 sample. The minimum value of band gap is measured in SRE-4 sample due to the RHA is replaced by ESP (wt%). These values are comparable to conventional mineral-based silicate glasses. Band gap of all the samples lies in the insulator region. Usually, NBOs are responsible to vary the band gap in the glasses. After increasing the modifiers content, band gap decreases, this expected trend is also followed in the present samples. A kink is observed in agro-food wastes, which become diffuse due to a higher amount of CaO. In addition to this, phase separation tendency decreased by the addition of ESP in the present glasses. It clearly indicates that the phase separation tendency decreases and Urbach energy increases by addition of ESP in initial composition.

Table 4.9 Optical band gap, refractive index and Urbach energy along with their samples labels

Samples ID → Properties ↓	SRE-1	SRE-2	SRE-3	SRE-4
Optical band gap (eV)	3.72	3.60	3.51	3.34
Refractive index (n)	2.23	2.25	2.27	2.31
Urbach energy(E_u) eV	0.29	0.30	0.32	0.34

4.3.6.2 Refractive index

The refractive indexes of the glasses are determined by the interaction of light with the electrons of its glass constituents. Normally, the covalent character of the bonds and difference in the electro-negativities of the bond-forming influenced the refractive index. Additionally, it also depends on the NBOs created by adding different modifiers. The increasing trends of the percentage of the covalent character of the bonds are following this sequence SiO_2>CaO>K_2O, etc, whereas, in K_2O bond, refractive index also decreases with decreasing covalent bond character. The variation of the covalent character of the bonds is responsible to vary the refractive index. However, the refractive index is shown an increasing trend in all the samples after increasing the ESP (CaO). ESP rich modifier creates NBOs, which is more polarizable than bridging oxygen. So, the formation of the non-bridging oxygen increases the refractive index of the glasses. Therefore, refractive index (n) is higher in SRE-4 with maximum ESP containing glass in comparison to other samples. Although, the formation of partial crystalline phases maybe affects the refractive index of the samples. However, the covalent character and polarizability have been the dominating factors to influence the refractive index of the as-quenched samples. For calculating the Urbach energy (E_u) of all samples details are given in chapter 3. All the values like optical band gap and Urbach energy are shown in table 4.9. The Urbach energy increases with increasing ESP in the agro-wastes based samples. Actually, RHA is having maximum SiO_2, which acts as a glass matrix with a small

amount of alkali and alkaline earth metals and these trace elements can act as the modifiers as well as the network former.[218]

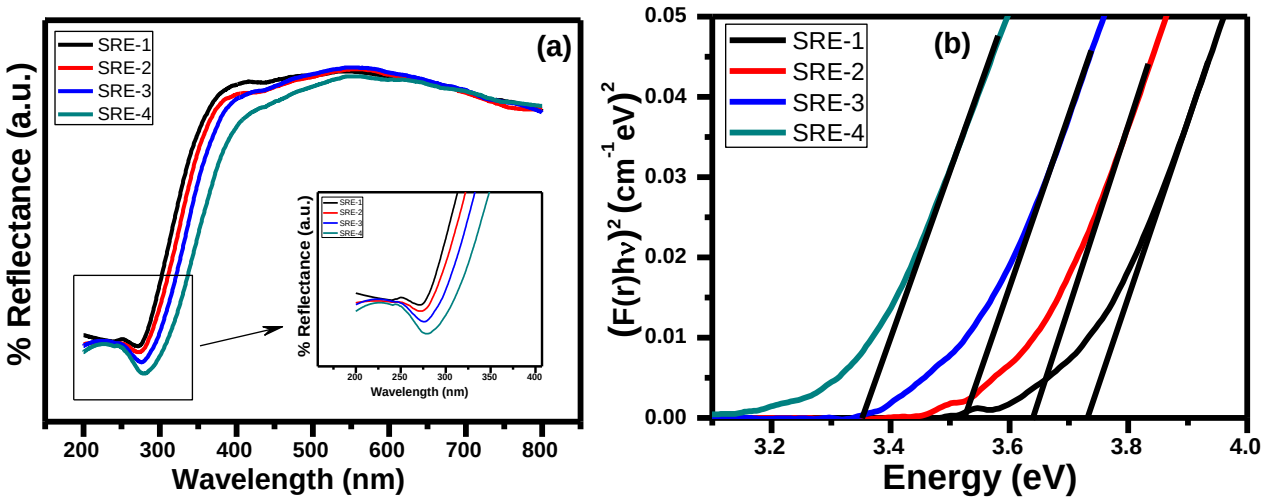

Fig. 4.19 (a) Diffused reflectance and **(b)** Tauc's plot of the as-quenched SRE-samples

However, in the given samples, modifier contents are higher in the SRE-4 sample due to the higher ESP amount. Conclusively, covalent character, Polarizability, and NBOs play an important role to decide the values of band gap and Urbach energy in these samples.

4.3.7 Photoluminescence analysis

In the present study, the as-quenched glasses are heat-treated at 900 °C for 10 h then photoluminescence (PL) spectra recorded in the region of 300-500 nm. In this region, it exhibits strong, medium and weak intensity peaks. These peaks lie in the blue to the green spectral region. All the prepared glasses show the high refractive index (n~2.31) and good transparency (80%) in the UV-Visible (λ-235nm) and near-infrared range. In more complex silicate glasses, luminescence can be promoted by the incorporation of several alkaline and rare-earth ions, but the concentrations usually effective due to heavy elements in these glasses. Impurities have been identified in silicate glasses by luminescent effects atomic concentration levels, which produce undetectable optical absorption.[61,148] PL spectra of the sintered pellets (900 °C for 10 h) of the four samples are shown in Fig. 4.20. The UV-Vis-NIR absorption spectrum reveals several peaks centered at excitation of

electron from ground state $^4I_{9/2}$ to $^4D_{3/2}$ + $^4D_{5/2}$ (360 nm), $^2G_{9/2}$ + $^2D_{3/2}$ + $^2P_{3/2}$ (485 nm). It is clearly observed that emission consists apparently of the many broad-bands at 360-364 nm, 369-373 nm, 408 nm, 421-423 nm, 446 nm, and 484-485 nm also shifted to the right side for all the samples. At 360-373 nm peaks observed in the UV-Visible region due to the exceeding defects of Si- and oxygen defect center (ODC), the singlet-singlet transition of Si-divalent of Ca^{2+}.[219] Consequently, an investigation of the source of this luminescence was undertaken. Weak luminescence is observed in many glasses, but in the present samples, the PL sources are not understood. A blue luminescence in silicate glasses has been ascribed due to trace elements. Emission band at 421 nm shows the blue shift due to self-trapped exciton (STE) associated with Al^{3+} and creation of =O-O= bond and ODC. It is also affected by enhancing intrinsic defects, which found due to the presence of dopants or impurity in the glass. The green region also observed at 485 nm, which is directly influenced by Na^+, K^+, Al^{3+}, and Ca^{2+} implantations ODC or Al^{3+}-centre impurity corporation during growth or Ca-O valance-related defects attached with the triplet-singlet emission of CaO valency.[220,221]

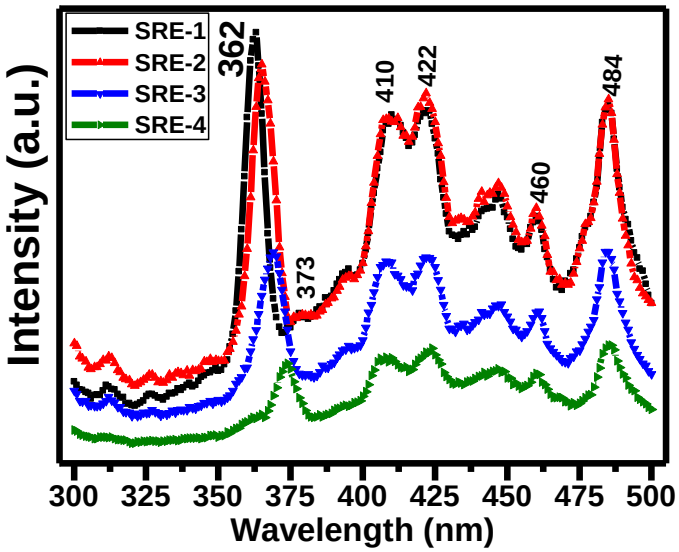

Fig. 4.20 Luminescent behaviors of the heat-treated SRE-1, SRE-2, SRE-3 and SRE-4 samples

In the present samples, as crystallization increases from SRE-1 to SRE-4 as discussed in XRD section, the intensity of PL emission spectra increases as ESP content increases and shift towards

the lower wavelength i.e. blue shift, particularly, bands at 300-380 nm. Conclusively, higher wavelength PL peaks are not shifted with respect to ESP content except peaks at 375-362 nm. The PL of the silicon clusters has potential applications in Si-based optoelectronic devices, especially in, green-blue and UV luminescence devices. Moreover, these glasses and glass-ceramics could be used in the continuous as well as pulsed laser applications. As-prepared glasses are shown an increasing trend with increasing the ESP content in the samples. The volume percentage of the sintered pellets of samples is different. ESP replaces RHA in increasing order, and its density increased, because CaO has a higher density as compared to SiO_2. When pellets sintered at 900 ^oC for 10 h, then density trend of the samples is not shown an increasing order. It may be that due to the sintering behavior of the samples, there may have been observed some shrinkage and expansion in it and volume has changed. During the heating process, some volatile content may come out of it. That why, the SRE-1 sample has been shown lower density as compared to other glasses.

4.3.8 Dielectric properties

Figure 4.21 (a) and (b) show the change in relative dielectric constant (ε´) and dielectric loss of SRE samples. Dielectric constant of SRE samples is found ~16-24 with minimum loss (~1) at a higher frequency and since slow polarization such as space and orientation is required large and enough time.

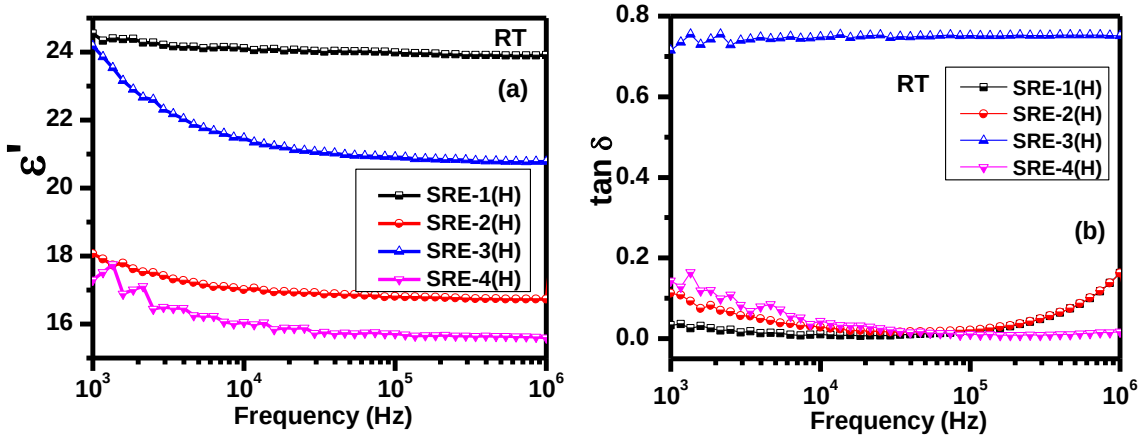

Fig. 4.21 (a) Dielectric constant and **(b)** tangent loss with frequency of the SRE-1(H), SRE-2(H), SRE-3(H) and SRE-4(H) glass-ceramics at RT

At low frequency, it is higher due to the higher contribution of space charge or interfacial polarization. Dielectric constant is decreased after replacing RHA (SiO_2) by ESP (CaO) in the samples; CaO creates more NBOs with disturbing the glass-network of SiO_2.

Table 4.10 Dielectric constant, tangent losses, σ_{dc} conductivity and activation energy (E_a) of the SRE-samples with different frequencies (100 Hz, 1MHz) at RT and 600 °C

Sample ID	**Dielectric constant (RT)**	**Tangent loss (RT)**	**Dielectric constant (100 Hz)**	**Tangent loss (100 Hz)**	**Dielectric constant (1MHz)**	**Tangent loss (1MHz)**	**σ_{dc}conductivity (S/cm) at 600 °C**	**E_a (eV)**
SRE-1 (H)	24	0.05	124	35	24	0.22	2.44×10^{-5}	0.42
SRE-2 (H)	17	0.11	125	20	22	0.26	2.34×10^{-5}	0.38
SRE-3 (H)	20	0.70	130	23	21	1.85	1.42×10^{-6}	0.34
SRE-4 (H)	16	0.15	80	5	12	0.35	1.05×10^{-5}	0.32

Dielectric behavior of the SRE glass-ceramics is measured at a discrete temperature from 100-600 °C within the frequency range (100Hz-1MHz) as presented in Fig. 4.22 (a)-(d) and also given in table 4.10. Reduced porosity is responsible to minimize the dielectric constant (12-24). The minimum loss (~1) is observed at 1MHz. At this frequency, the presented dipole of the samples may not have enough time to realign itself, so, dielectric constant is decreased. At low frequency, the charge gets enough time to accumulate, which is responsible for the high dielectric constant in the temperature range 100-600 ^{o}C.[10,222] Dielectric constant is increased after adding ESP in composition. It is also indexed with increasing temperature as presented in Fig. 4.22 (a)-(d). On the other hand, the variation of the tangent loss of SRE-samples are indicating normal behavior of dielectric materials having mobile charge carriers, (i.e., ions and electrons).[223]

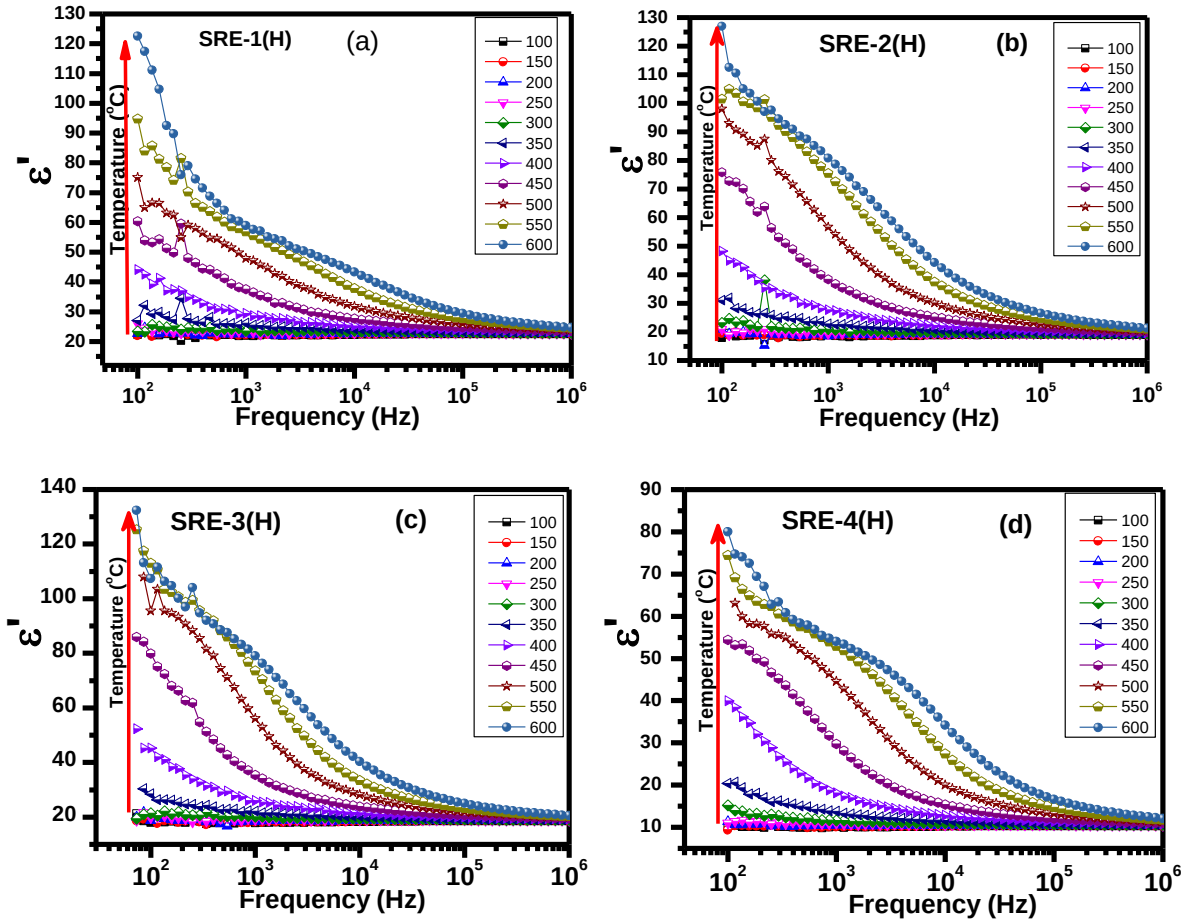

Fig. 4.22 Dielectric constant of the **(a)** SRE-1(H), **(b)** SRE-2(H), **(c)** SRE-3(H) and **(d)** SRE-4(H) glass-ceramics at discrete temperature 100-600 °C with 100Hz-1MHz frequency range

It is observed that dielectric constant with minimum loss is found in SRE-3(H) sample, which is most likely due to the least hopping of charge carriers in this glass-ceramics as shown in Fig. 4.23.

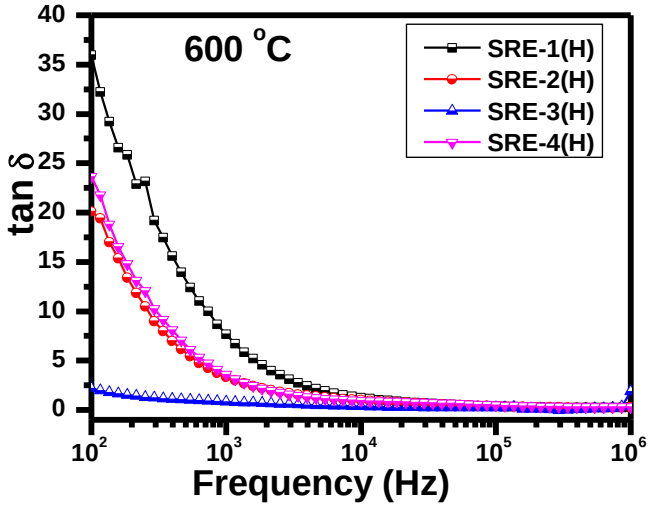

Fig. 4.23 Tangent loss of the given glass-ceramics at 600 °C from (10^2-10^6 Hz) frequency range

Moreover, the change carriers of these glass-ceramics could be alkali metal or alkaline-earth metal ions. It may depend on many factors like non-stoichiometric, structural homogeneity, the presence of modifiers content like Ca^{2+}, K^{+}, etc., in the composition. Present glass-ceramics exhibit lower dielectric losses than mineral-derived glass-ceramics of similar composition.

4.3.8.1 σ_{dc} conductivity

Arrhenius plot is used to evaluate the conductivity (σ_{dc}) and activation energy of the glass-ceramics.[58] Minimum σ_{dc} conductivity of the samples is confirmed the insulating nature of the glass-ceramics, as shown in Fig. 4.24. SRE-1(H) sample shows low σ_{dc} conductivity (9.1×10^{-9} S/m) at 250 °C due to the presence of the low number of non-bridging oxygen (NBOs) as compared to other samples.

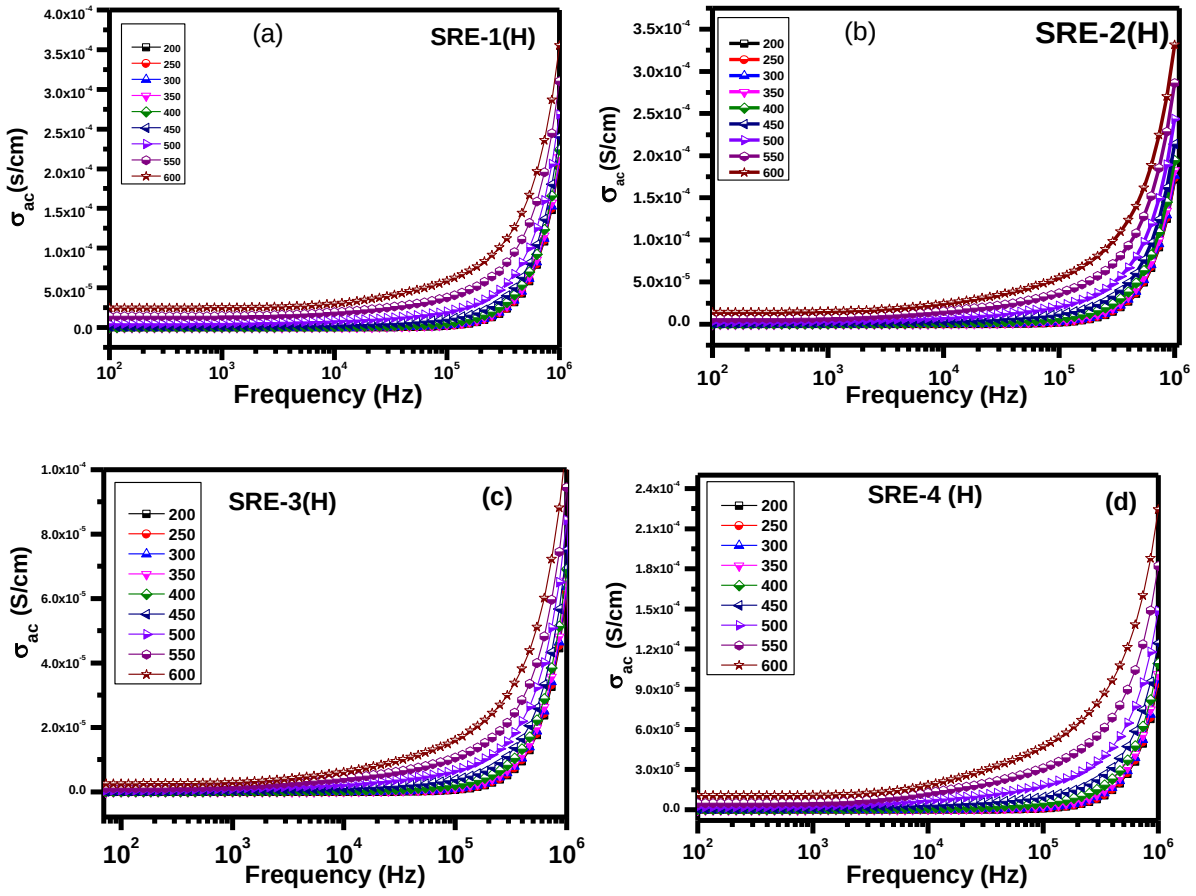

Fig. 4.24 σ_{dc} conductivity of **(a)** SRE-1(H), **(b)** SRE-2(H), **(c)** SRE-3(H) and **(d)** SRE-4(H) glass-ceramics

Secondly due to higher content of SiO_2 and low content of ESP (CaO) having higher glass-network connectivity. When the temperature is raised up to 600 °C, conductivity is increased up to 2.44×10^{-5} S/m. Maximum σ_{dc} conductivity is observed in SRE-4(H) sample. The conductivity of SRE-4(H) glass-ceramic is higher at the high frequencies, which may be due to the easy hooping between ions. Hooping frequency may increase with increasing frequency; as a result, the conductivity increases gradually with frequency and temperature.

However, the σ_{dc} conductivity is found to increase with increasing CaO concentration in the SiO_2 content with respect to temperature (100-600 °C), due to the thermal vibration of the mobile charge carriers. With the increasing frequency, dispersion is observed in σ_{dc} conductivity.

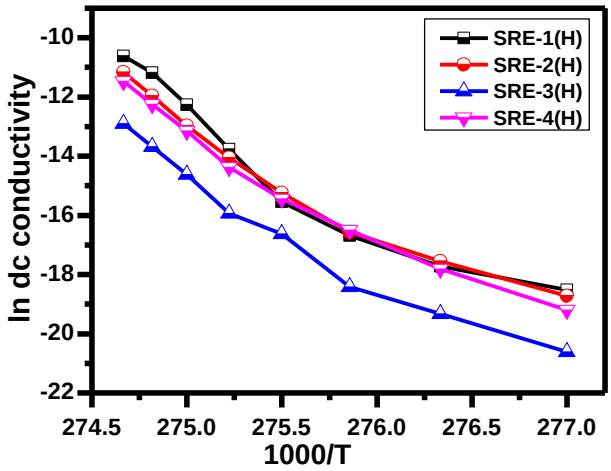

Fig. 4.25 Activation energy (E_a) of the SRE samples calculated using Arrhenius plot

This is a well-known conduction mechanism observed in glass-ceramics assisted by the polaron hopping between the available free state. Arrhenius relation is used to know the nature of the conduction in these samples.

$$\sigma_{dc} = \sigma_o \exp(-E_a/K_BT) \tag{4.15}$$

where σ_o is the pre-exponential factor. A linear fit of ln σ_{dc} versus (1000/T) plot has been used to evaluate the activation energy (E_a).

It found to be 0.42, 0.38, 0.34, 0.32 eV for SRE-1(H), SRE-2(H), SRE-3(H), and SRE-4(H) samples, respectively in the temperature region (250-600 ^oC). The variation of σ_{dc} (bulk) with the

inverse of absolute temperature (1000/T) of SRE-samples is shown in Fig. 4.25. E_a>1 eV is the predominance of ionic conduction, below to 0.2 eV, electronic conduction might be dominated. The decreasing trend of activation energy with increasing CaO content in SRE samples is similar to the activation energy calculated for mineral oxides glass-ceramics. Lower the activation energy, higher numbers of the charge carriers that would have the necessary energy to move and conduct electricity.

4.3.8.2 Electrical impedance analysis

The complex impedance behavior of the electrode/sample/electrode configuration can be explained as the sum of a single with a parallel combination of RC (R=resistance, C=capacitance) circuit. Thus, the result obtained using impedance analysis is unambiguous, and hence provide a true picture of the electrical behavior of the materials. In Fig. 4.26 (a), the variation of Z' as a function of frequency (100 Hz- 1MHz), SRE-glass-ceramics at 600 °C is observed. It found that the addition of ESP (CaO) in RHA and SCLA composition, magnitude of Z' (bulk-resistance) increases at low frequency (100 Hz) at 600 °C, and thereafter appears to merge in the high-frequency region. This is possible due to the release of space charge polarization with the rise in temperatures and frequencies.[195] This behavior shows that the conduction mechanism increases with increasing temperature and frequency (i.e., negative temperature coefficient of behavior like that of a semiconductor). The coincidence of the value of Z' at higher frequencies at this temperature indicates a possible release of space charge. The space charge polarization occurs maximum at the low-frequency side for SRE-3(H) as compared to all other samples. This may be due to the reduction in barrier properties of the materials with a rise in temperature which is responsible for the enhancement of conductivity of the materials. At the frequency range (10^5-10^6 Hz), Z' becomes independent of frequency. Fig. 4.26 (b) shows the frequency dependence of Z'' (usually called a loss spectrum) of samples at 600 °C. The magnitude of Z'' decreases with an increase in frequency as well as high-temperature region after addition of ESP in the composition.

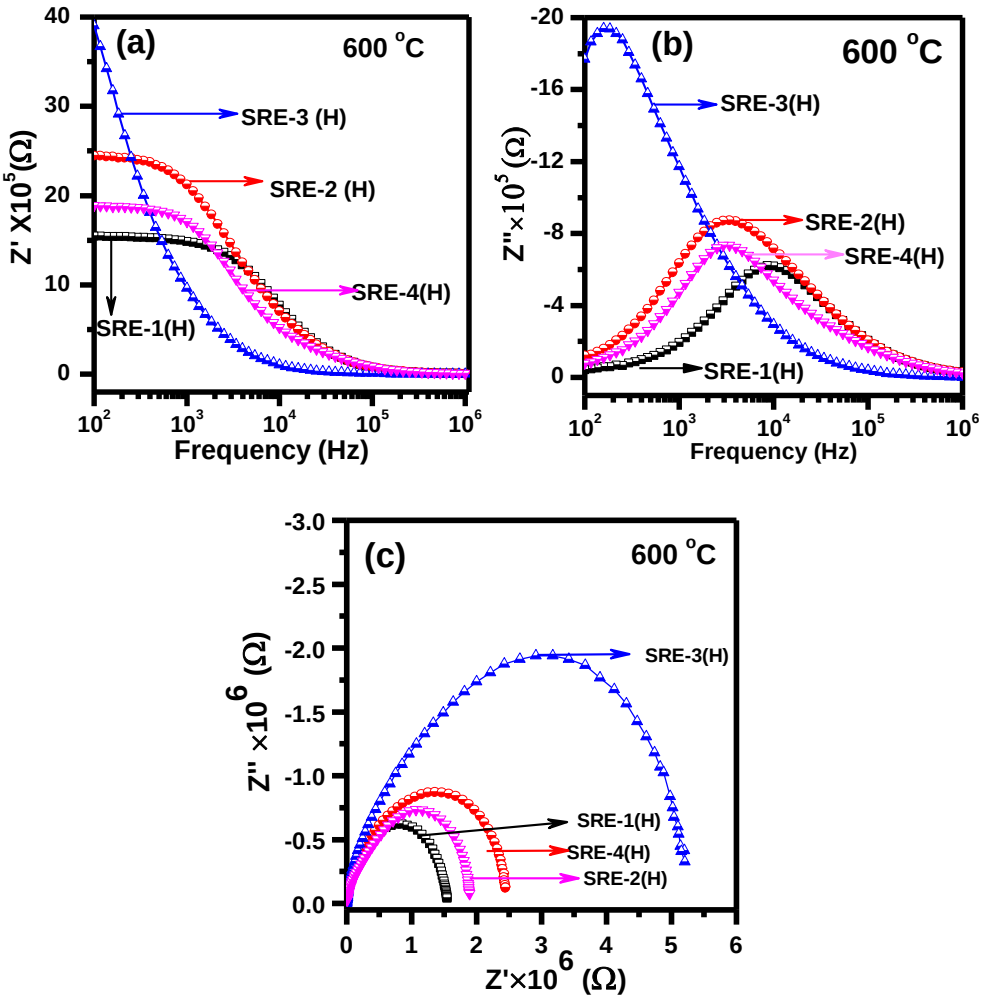

Fig. 4.26 (a) Real and **(b)** imaginary impedance plot with frequency and **(c)** Cole-Cole plot of heat-treated SRE samples

It shows that the magnitude of *Z´´* decreases and the entire peaks shift towards the lower frequency side. At higher frequencies, the contribution from the grain predominates owing to the absence of the space charge effects of the different heat-treated samples. The individual contribution from each of these entities can be represented by equivalent parallel RC circuits connected in series. Each RC element of the equivalent circuit gives rise to a semicircle with its center lying on the real axis, if there is a single value of relaxation time, τ given by $\tau = 1/\omega$, where ω is the angular frequency corresponding to maxima in Z´´versus frequency plot.[224]

The appearance of peaks in the loss spectrum at 600 °C temperature suggests the existence of the relaxation process of the different compositions. This may occur due to the immobile species at

low temperatures and defects or vacancies at high temperatures. The relaxation time of the samples is found from 1.96×10^{-6}-4.56×10^{-7}/s at a higher temperature, which is not showing any trend. SRE samples data have been plotted of real the complex impedance spectrum (*Z´ versus Z´´*) with imaginary impedance at 600 °C, as shown in Fig. 4.26 (c). Thus, obtained results are provided actual electrical behavior of the heat-treated samples. Single semicircle arcs are observed for all the samples with different radius at high temperature 600 °C, which confirms the presence of bulk effect of grain size in the system even after increasing the wt% of ESP in the initial glass. It is a well-known fact that if intercept point on the real axis shifts towards the origin indicates the decrease in the bulk resistance as the temperature increases. In this study, semicircle arcs also show the same trend that means bulk resistance of the materials is decreasing after increasing the temperature. The electrical process taking place within the glass-ceramics can be equated (as an RC circuit) on the basis of the brick-layer model. Generally, the impedance data were used to evaluate the relaxation time (τ) of the electrical phenomena in the different compositions using this relation.

4.4 (100-x)SCLA-10PSA-(x)ESP (x=00, 10, 15, 20, 25 wt%)

The raw materials SCLA, PSA and ESP are used to make the glasses and glass-ceramics. As discussed in the first section of this chapter, ESP is the main source of CaO with small trace elements and this CaO is acted as the modifier in these samples. So, with using of SCLA, PSA, and ESP as the basic constituents materials, four samples were synthesized; the nomenclature and selection of the materials according to the wt% are presented in table 4.11. The selected composition of the waste ashes has been melted at a higher temperature (1550 °C) to form the glasses using melt-quench technique.

Table 4.11 Nominations of the samples according to weight percentage (wt%)

Samples ID (wt%)	**SE-1**	**SE-2**	**SE-3**	**SE-4**
SCLA	90	75	70	65
ESP	10	15	20	25
PSA	00	10	10	10

4.4.1 Elemental analysis

The as-quenched glasses are crushed in an agate-mortar pestle and EDS analysis was done to quantify the chemical constituents in the as-quenched samples. The higher amount of silica is observed in SE-1 sample and this silica is decreasing with increasing ESP content.

Table 4.12 Chemical compositions of the SE-series determined using EDS

Samples Id → Composition ↓	**SE-1**	**SE-2**	**SE-3**	**SE-4**
SiO_2	71.81	63.56	57.32	53.41
CaO	10.86	13.39	14.53	22.63
K_2O	6.23	5.25	4.99	6.65
MgO	5.71	4.49	4.04	3.10
Na_2O	0.45	0.76	0.76	0.44
Al_2O_3	4.94	10.41	16.54	12.40
FeO	-	1.03	0.35	0.01
P_2O_5	-	1.12	1.47	1.36

Interestingly, during the melting process, these glasses are fused with recrystallized alumina crucible at higher melting temperature (i.e. 1550 ^{o}C) and glasses contained small amount of alumina (Al_2O_3) which comes from crucibles. The highest amount of alumina is observed in SE-3 samples. It may also possible that the agro-food waste ashes are more reactive as compared to similar mineral oxides glasses, which is associated with local structure and presence of miner trace elements in wastes ashes. It is also observed that the tendency of Al^{3+} diffusion is also increased from the crucible with increasing the ESP in the samples as shown in table 4.12. As discussed in the previous section, alkali and alkaline-earth metals cations may have an affinity towards Al^{3+} as compared to Si^{4+} cations.[225] However, the presented modifiers such as alkali and alkaline-earth metals in the samples are promoted to the more NBOs, which may provide the diffusion site for alumina. Other constituents like K_2O, Na_2O, etc. are not following any trend with increasing the ESP amount in the RHA samples, while PSA amount was added only 10 wt% in the samples. The motivation of adding PSA in the main composition was used to available a small amount of sodium oxide (Na_2O) in the PSA as the modifiers to reduce the melting temperature of the glasses.

4.4.2 Density

Physical parameters such as density, molecular weight, etc. are depending on the matrix of the glasses and used modifiers, intermediates for making the glasses and glass-ceramics. Normally, density of the glasses is increased by increasing the atomic weight of the used constituents. So, the increasing ESP in SCLA and PSA increase the density of the glasses as given in table 4.13. It is comparable with similar mineral oxides derived glasses.

The molecular weight of constituent oxides in the present compositions follows the following trend; $Na_2O<K_2O<SiO_2<MgO<CaO<Al_2O_3$. Many Modifiers break the glass-network that led to the compactness of the glasses. At very high temperature (1550 °C), where the melt is fluid, melt consists of a eutectic mixture of modifier ions and various structural units of the network. They may be as small as the basic building block of the network or it may consist of a few of these

building blocks connected to form small discrete ions of modifiers. During the rapid cooling of the melts, the network begins to form as the local structural units become connected. The alkaline-earth metal or other modifier ions could break the connectivity of the glass network. In addition to this, SiO_2 and alkali and alkaline-earth elements like MgO, K_2O replacing by CaO result reduced the electrostatic forces between the kinds of NBOs considerably and hence decreases the characteristic temperature such as T_g, and T_c of the as-prepared glasses. These modifiers have broken the network and increased the compactness of the system, which leads to decrease in the molar volume of the glasses.

4.4.3 X-ray diffraction

X-ray diffraction pattern of the as-quenched and heat-treated SE-samples (900 °C for 10 h) is performed from 10-90^o angle and presented in Fig. 4.27 (a) and (b). At 2θ=18-36°, A very broad hump is observed, which clearly indicates the amorphous nature of the samples. In other words, absence of sharp peaks in the diffraction pattern, confirms the amorphous nature of the glasses. The increments of the modifiers content at the cost of SiO_2 in glasses are completely responsible to shift the broad halo towards the higher diffraction angle; it basically signifies the more NBOs in the system. Most of the modifiers modify the original structure of the glass, which affects the density due to changes in compactness of the glass. Modifiers like K_2O, CaO, Al_2O_3 and some inherent trace elements disturb the connectivity of the glass former. In SE-3 sample, there is second hump that observed at 40^o, which may be related nanocrystalline/crystalline phase in the glasses.

The pellets of the as-prepared samples are heat-treated at 900 ^{o}C for 10 h. The crystalline phases were observed in all the samples. SE-1sample is shown the presence of $CaMg(SiO_3)_2$ phase with ICDD card no. 00-011-0654. After adding the ESP into the next three samples, formed glasses convert to glass-ceramics at this sintering temperature. SE-2 sample is shown the phase $CaMg(SiO_3)_2$ with ICDD card no 01-075-0945 crystalline phase. In SE-3 sample is formed two phases i.e. $CaMgSi_2O_6$ and $CaAl_2Si_2O_8$ with ICDD card no. 01-072-1497 and 00-041-1486. More

CaO and Al_2O_3 in SE-3 sample with other constituents are responsible for alumina related phases. SE-4 sample shows calcium magnesium silicate phases $CaMg(SiO_3)_2$ with another $CaAl_2O_4$ phase with ICDD card no 01-075-0945 and 01-088-2477. So, these modifiers play a very important role in the crystallization behavior of these glasses.

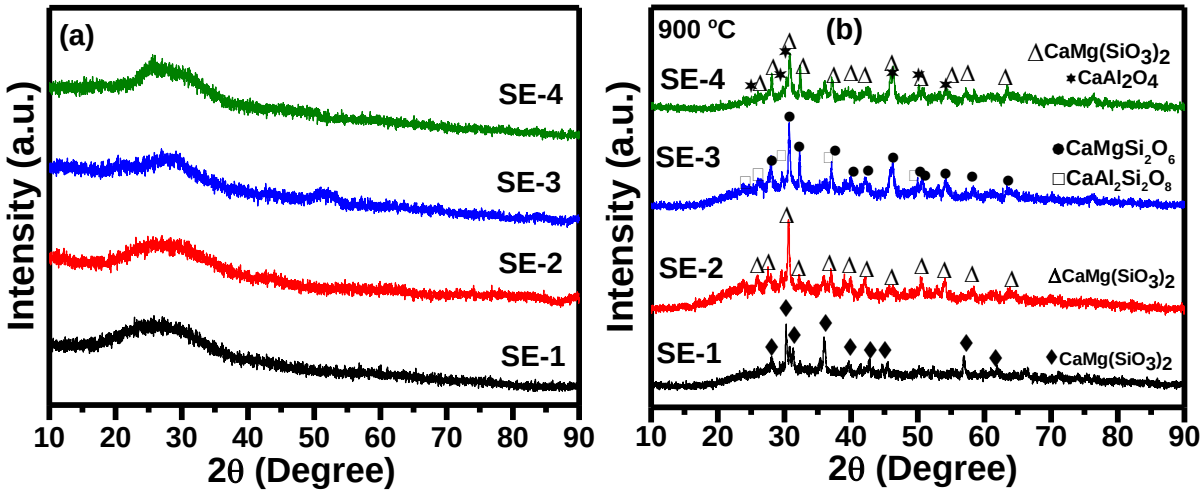

Fig. 4.27 X-ray diffraction pattern **(a)** as-quenched and **(b)** heat-treated SE-1, SE-2, SE-3 and SE-4 samples

4.4.4 FTIR analysis

FTIR spectra of the as-quenched samples are shown in Fig. 4.28. The observed peaks in FTIR spectra indicate that with increasing ESP content in the samples, broadening of the peak is reduced and shifted towards lower wavenumber. At 1630 and 1472 cm^{-1}, the band belongs to OH-group. A broad and prominent band is observed at 1052 cm^{-1}, which may correspond to various silicate units i.e. Si-O-Si symmetric stretching. As CaO is increased after adding ESP in the samples, the bands at wavenumber ~780 cm^{-1} and ~470 cm^{-1} slightly shift to lower wavenumber and broadening of the bands is reduced, which corresponds to the stretching vibrations of the silicate network, i.e., Si-O-Si bond vibrations. The shifting of the bands towards the lower wavenumber is directly related to the modification of the silicate structure. The sharp band in SE-4 samples at the fingerprint region belongs to some ordering at the local level in this particular glass. The broadness of the band is due to the superposition of the IR-bands of the asymmetric vibrations of different types of Q-units of

silica network. All molecules containing tetrahedral coordinated silicon are presented because this band becomes more intense and sharp in SE-1 as compared to other samples. So, it could be related to crystalline silicate network presented at the local level in this sample.

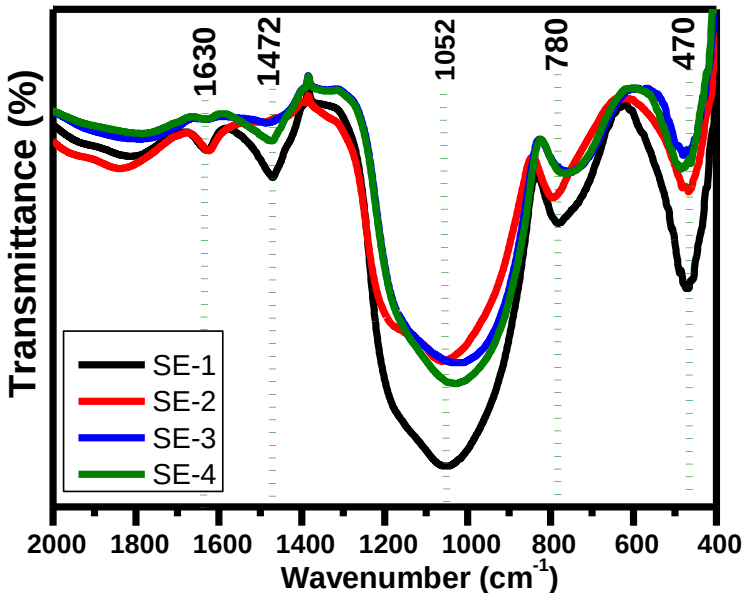

Fig. 4.28 FTIR spectra of the as-quenched SE-samples

4.4.5 Thermal properties

4.4.5.1 Thermo gravimetric analysis

The DTA curve of the as-quenched samples is performed from room temperature to 900 ^{o}C with the heating rate 10^{o}C/minutes. T_g of the as-quenched glasses is not clear in these samples.

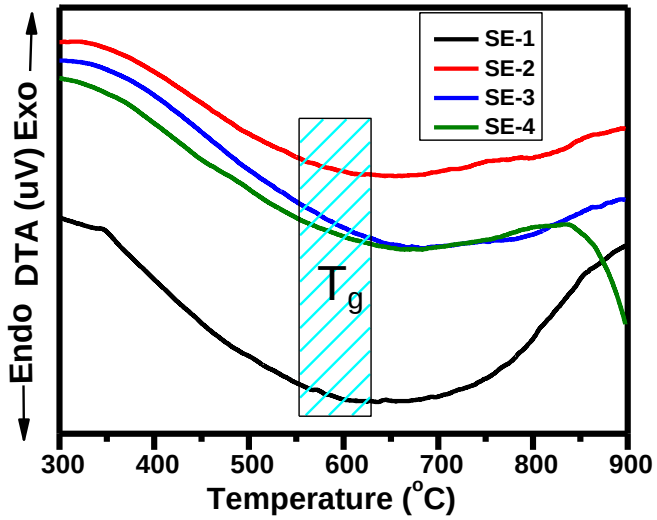

Fig. 4.29 DTA curve of the SE-1, SE-2, SE-3 and SE-4 samples

The range of the T_g is indicated from 570-610 ^oC as shown in Fig. 4.29. A broad peak is observed particularly SE-1and SE-4 glasses.

4.4.5.2 Dilatometry analysis

The coefficient of thermal expansion (CTE) is performed on the heat-treated samples at 900 ºC for 10 h. The thermal expansion curves of heat-treated samples are shown in Fig. 4.30. The replacing SCLA by ESP creates more non-bridging oxygens (NBOs) in the samples due to the present CaO in ESP as the main source, which acts as the modifiers. It also affects the stabilization of glass-network to decrease the characteristic glass-transition temperatures. SE-3 glass shows a peak ~600 ^oC, it may be associated with some phase transition. Since, SiO_2 may present in some nanocrystalline/crystalline form which is not observed in XRD. SE-2 sample also shows higher slop that indicates lower CTE of this sample as compared to the other samples. The maximum CTE is observed for SE-4 sample. It is 9.97×10^{-6}/K as given in table 4.13. The replacement of SCLA by ESP, at a particular level in the samples, is support to enhance the crystallization tendency of the glasses as also observed by XRD as shown in Fig 4.27 (b). The properties of the glasses and glass-ceramics could be tailored to select proper agro-food wastes.

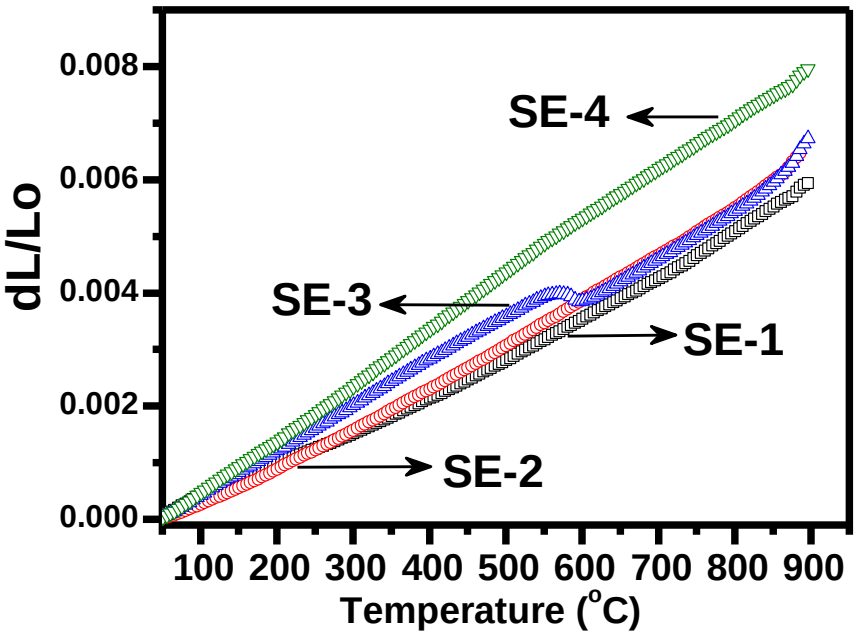

Fig. 4.30 CTE of the heat-treated SE-samples at 900 °C for 10 h

4.4.6 Optical properties

4.4.6.1 Optical band gap

Diffused reflectance spectra of the as-quenched glasses are shown in Fig. 4.31 (a). The signature of phase separation phenomena in the glasses could be established by the UV-Visible spectra also. A kink at ~262 nm is clearly seen in all the glasses. This kink might be originated due to the presence of a different glass matrix within the glass matrix, i-e. phase-separated glass. From spectra, the optical band gap of the as-quenched glasses was calculated using the Kubelka-Munk function.[204]

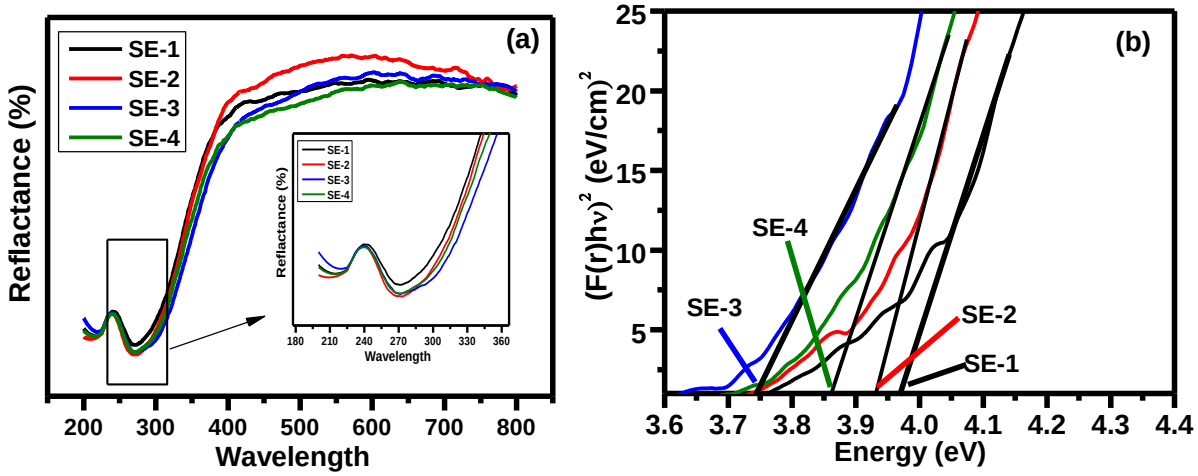

Fig. 4.31 (a) Reflectance and **(b)** optical band gap of as-quenched SE-1, SE-2, SE-3 and SE-4 samples

Tauc's plot manifests the optical band gap decreases trend with increasing ESP content as presented in Fig. 4.31 (b). From all the samples, SE-1 sample is showing a maximum optical band gap (3.96 eV). It is related to a higher amount of silica presented in the SE-1 sample (exhibited low content of NBOs). The observed optical band gap and Urbach energy of the samples are compared with the existing similar mineral-derived glasses. The optical band gap of the glasses lies in the insulator region. Usually, NBOs and other defects are responsible to vary the band gap in silicate glasses. Optical band gap is following the similar expected trend with adding the ESP in composition except for SE-3 sample as given in table 4.13, as discussed above, this particular sample exhibit a higher phase separation tendency than other glasses.

Table 4.13 Density, optical band gap, refractive index, Urbach energy and CTE of the SE samples

Samples ID	SE-1	SE-2	SE-3	SE-4
Density (g/cc)	2.21	2.52	2.56	2.68
Optical band gap (eV)	3.96	3.93	3.74	3.86
Refractive index (n)	2.17	2.18	2.22	2.19
(CTE)×10^{-6}/K	6.83	6.59	6.86	9.57

4.4.6.2 Refractive index

Refractive index of the glasses is determined by the interaction of light with the electrons of glass constituents. Normally, the covalent character of the bonds and difference in the electro-negativities of the bond-forming influenced the refractive index. Additionally, it also depends on the NBOs created by adding different modifiers. The increasing trends of the percentage of the covalent character of the bonds are following this sequence SiO_2>CaO>K_2O, etc, so, K_2O containing glass exhibits lower refractive index as shown in table 4.13. The variation of the covalent character of the bonds is responsible to vary the refractive index. However, the refractive index is shown an increasing trend in all the samples after increasing the ESP (CaO). ESP (CaO rich) creates NBOs, which is more polarizable than bridging oxygen. So, the formation of the NBOs increases the refractive index of the glasses. Therefore, refractive index (n) is higher in SE-4 with maximum ESP containing glass in comparison to other samples. Although, formation of partial crystalline phases maybe also affect the refractive index of the glasses. However, the covalent character and polarizability have been the dominating factors to influence the refractive index of the as-quenched samples.

4.4.7 Dielectric properties

Figure 4.32 (a) and (b) show the change in relative dielectric constant (ε΄) and dielectric loss of SE samples. Dielectric constant of SE samples is found ~16-40 with minimum loss (~1) at higher frequency at room temperature. As frequency increases, the materials net polarization drops as each

polarization mechanism ceases to contribute, and hence its dielectric constant drops. At low frequency, it is higher due to the higher contribution of space charge polarization. Dielectric constant is decreased after replacing SCLA (SiO_2) by ESP (CaO) in the samples. This CaO creates more NBOs with disturbing the glass-network of SiO_2.

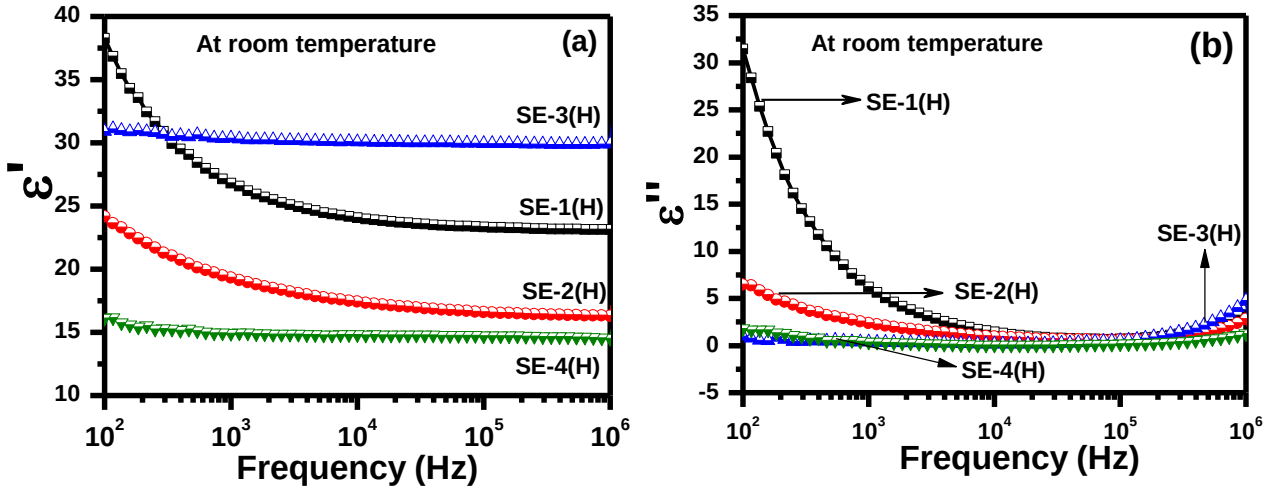

Fig. 4.32 (a) Dielectric constant and **(b)** losses of the as-quenched SE-samples at room temperature

Dielectric behavior of the SE glass-ceramics is measured at a discrete temperature at 300 °C and 600 °C within the frequency range (100Hz-1MHz) as shown in Fig. 4.33 (a)-(d) and presented in table 4.14. The observed porosity and voids are decreased due to heat-treatment of glasses,

Table 4.14 Dielectric constant, tangent losses, and σ_{dc} conductivity of the SE-1, SE-2, SE-3 and SE-4 sample with different frequencies (100 Hz, 1MHz) at RT, 300 °C and 600 °C

Sample ID	**Dielectric constant (RT)**	**Dielectric losses (RT)**	**Dielectric constant (1kHz) at 300 °C**	**Tangent loss (1kHz) at 300°C**	**Dielectric constant (1MHz) at 600 °C**	**Tangent loss (1MHz) at 600°C**	**σ_{dc} conductivity (S/cm) at 400 °C**
SE-1 (H)	38	32	39	63	67	4417	5.26×10^{-6}
SE-2 (H)	24	6.6	45	59	234	9289	9.58×10^{-6}
SE-3 (H)	31	1.95	58	17	164	146	5.29×10^{-7}
SE-4 (H)	16	0.6	108	443	597	25000	3.47×10^{-5}

Reduced porosity is responsible to minimize the dielectric constant (40-109) with minimum loss (~17-445) at 300 °C with frequency range (100Hz-1MHz) at low frequency. At this high

frequency, the presented dipole of the samples may not have enough time to realign itself, so, dielectric constant is decreased.

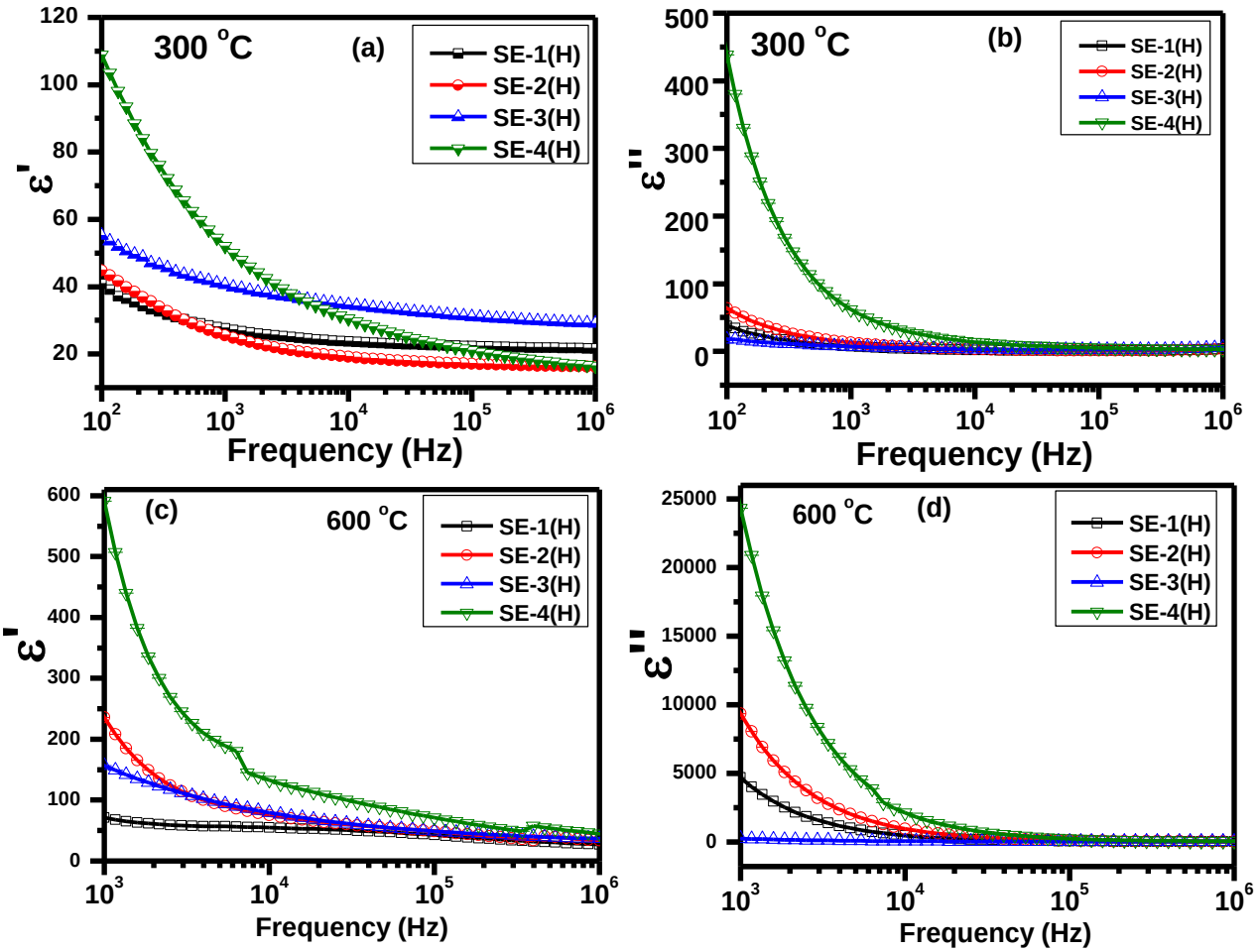

Fig. 4.33 Dielectric constant and losses of the **(a)** SE-1(H), **(b)** SE-2(H), **(c)** SE-3(H) and **(d)** SE-4(H) glass-ceramics at 300 and 600 °C with 1kHz-1MHz frequency range

At high temperature (600 °C), dielectric constant is increased at (1kHz) frequency and reduced the dielectric value with increasing frequency up to 1MHz that dielectric constant of these samples also depends on the temperature. On the other hand, the variation of the tangent loss of SE-samples is indicating the normal behavior of dielectric materials.[223] It is observed that the lowest dielectric constant with minimum loss found in SE-3(H) sample at room temperature, which is most likely due to the least hopping of charge carriers. The charge carriers of these glass-ceramics could be alkali metal or alkaline-earth metal ions**.** It may depend on many factors like stoichiometric ratio of both modifiers, structural homogeneity, the presence of modifiers content like Ca^{2+}, K^{+}, etc. in the

glass composition. Present glass-ceramics exhibit lower dielectric losses than mineral-derived glass-ceramics of similar composition.[10] The temperature dependence of dielectric constant and loss at 1kHz and 1MHz for all the SE-samples are presented in Fig. 4.34 (a)-(d).

At lower frequency (1kHz), dielectric constant and loss is increased with increasing the temperature from 300-600 °C. The increment of the dielectric constant is related to the thermally induced enhancement of oxygen vacancies. At higher frequency (1MHz), sufficient time for the motion of the ions and charge accumulation is responsible for increased dielectric constant at the temperature range (300-600 °C).[10,222] Dielectric constant is increasing after added ESP in composition with the temperature at low frequency and later stage gradually, it is decreased.

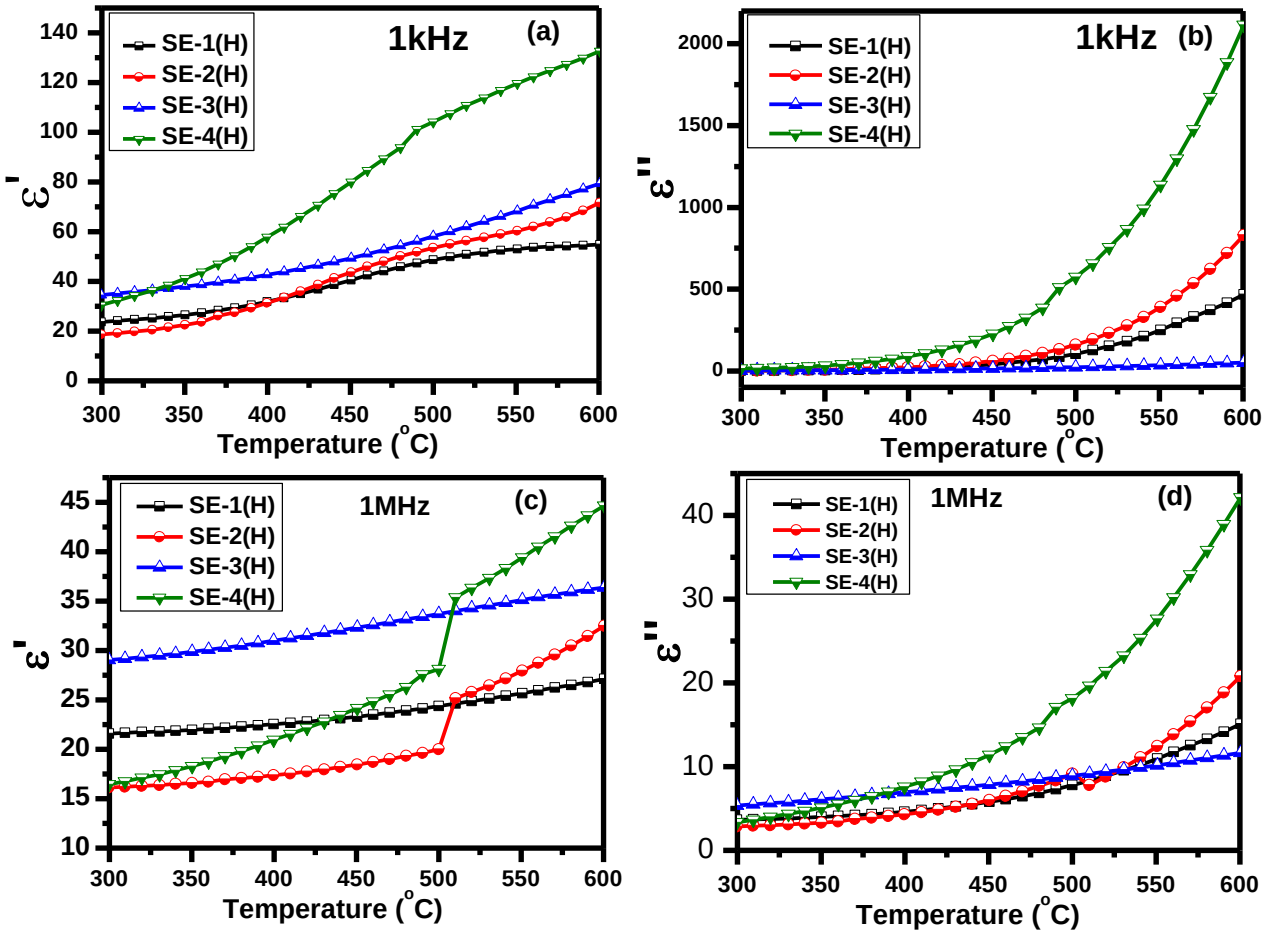

Fig. 4.34 (a)-(d) Dielectric constant and loss of the given glass-ceramics at (1kHz and 1MHz) with temperature (300- 600 °C)

4.4.7.1 σ_{dc} conductivity

Arrhenius plot is used to evaluate the σ_{dc} conductivity and activation energy of the heat-treated samples as shown in Fig. 4.35. Minimum σ_{dc} conductivity of the glass-ceramics samples is confirmed insulating nature of the glass-ceramics. SE-1(H) sample shows low σ_{dc} conductivity (5.26×10^{-7} S/m) at 400 °C due to the lower volume of non-bridging oxygen (NBOs) as compared to other samples. Secondly due to higher content of SiO_2 and low content of ESP (CaO) having higher glass-network connectivity. If temperature is raised >600 °C, the conductivity is increased up to 2.79×10^{-5} S/m. Maximum σ_{dc} conductivity observed in SE-4(H) sample after the addition of ESP (CaO). The conductivity of SE-4(H) glass-ceramic is higher at the high frequencies, which may be due to the easy hooping between ions. Hooping frequency may increase with increasing frequency; as a result, the conductivity increases gradually with frequency and temperature. However, the σ_{dc} conductivity increases with increasing CaO concentration in the SiO_2 content with respect to temperature (100-600 °C), due to the thermal vibration of the mobile charge carriers. With the increasing frequency dispersion in σ_{dc} conductivity is observed in the increasing trend.

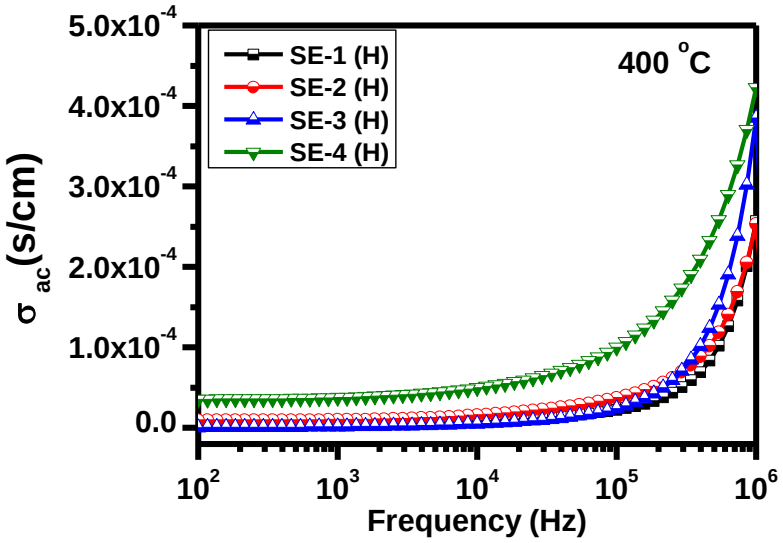

Fig. 4.35 σ_{dc} conductivity of the SE-1(H), SE-2(H), SE-3(H) and SE-4(H) glass-ceramics

4.4.7.2 Electrical impedance analysis

In Fig. 4.36 (a), the variation of Z' as a function of frequency (100Hz- 1MHz), SE-glass-ceramics at 600 °C is observed. It found that the addition of ESP (CaO) in SCLA and PSA composition, the magnitude of Z' (bulk-resistance) increases at low frequency (100 Hz) at 600 °C, and thereafter appears to merge in the high-frequency region. This is possible due to the release of space charge polarization with the rise in temperatures and frequencies.[195] This behavior shows that the conduction mechanism increases with increasing temperature and frequency (i.e., negative temperature coefficient). The coincidence of the value of Z' at higher frequencies at this temperature indicates a possible release of space charge. The space charge polarization occurs maximum at the low-frequency side for SE-3(H) as compared to all other samples. This may be due to the reduction in barrier properties of the materials with a rise in temperature which is responsible for the enhancement of conductivity of the materials. At the frequency range (10^5-10^6 Hz), Z' becomes independent of frequency.

Fig. 4.36 (b) shows the frequency dependence of Z'' (usually called a loss spectrum) of samples at 600 °C. The magnitude of Z'' decreases with an increase in frequency as well as high-temperature region after the addition of ESP in the composition. It shows that the magnitude of Z'' decreases and the entire peaks shift towards the lower frequency side. At higher frequencies, the contribution from predominate owing to the absence of the space charge effects of the different heat-treated samples. The individual contribution from each of these entities can be represented by equivalent parallel RC circuits connected in series. Each RC element of the equivalent circuit gives rise to a semicircle with its center lying on the real axis, if there is a single value of relaxation time, τ given by $\tau = 1/\omega$, where ω is the angular frequency corresponding to maxima in Z'' versus frequency plot.[224] The appearance of peaks in the loss spectrum at 600 °C temperature suggests the existence of the relaxation process of the different compositions. This may occur due to the immobile species at low temperatures and defects or vacancies at high temperatures. SE samples data have been

plotted of real and complex impedance spectrum (Z' versus Z'') at 600 °C, as shown in Fig. 4.36 (c). Thus, obtained results are provided actual electrical behavior of the heat-treated samples. Single semicircle arcs are observed for all the samples with different radius at high temperature (600 °C), which confirm the presence of the bulk effect of grain size in the system even after increasing the wt% of ESP in the main composition.

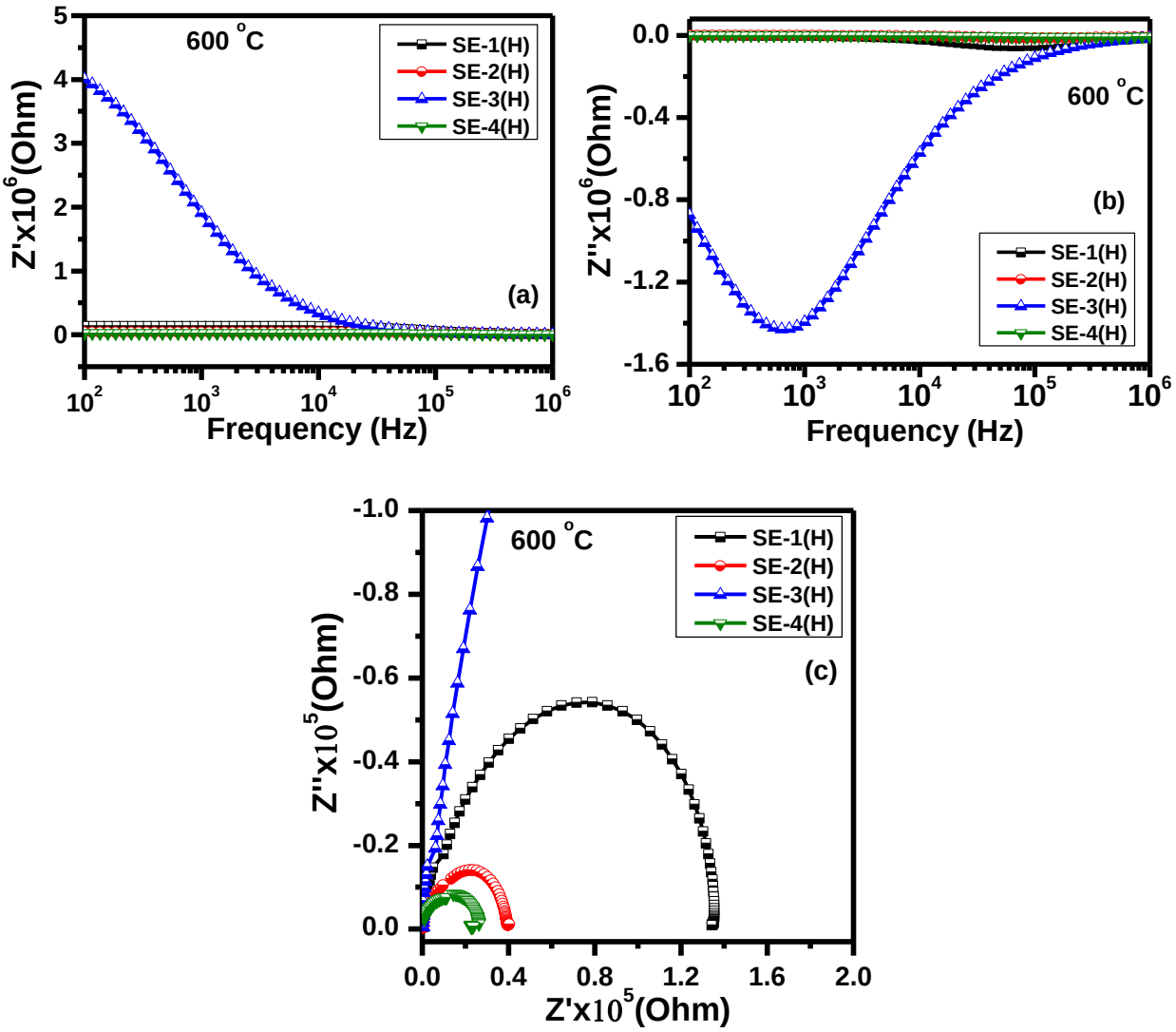

Fig. 4.36 (a) Real and **(b)** Imaginary impedance with frequency (1kHz-1MHz) at 600 °C **(c)** Cole-Cole plot of SE-1, SE-2, SE-3 and SE-4 samples

It is a well-known fact that if intercept point on the real axis shifts towards the origin indicates the decrease in the bulk resistance as the temperature increases. In this study, semicircle arcs also show the same trend that means bulk resistance of the materials is decreasing after increasing the

temperature. The electrical process taking place within the glass-ceramics can be equated (as an RC circuit) on the basis of the brick-layer model. Generally, the impedance data were used to evaluate the relaxation time (τ) of the electrical phenomena in the different compositions using this relation.

4.5 Interaction study of the WSA and similar mineral samples with Crofer 22 APU

Two samples wheat straw ash (WSA) and mineral oxides derived (MOD) were synthesized using WSA and exact same chemical composition using different minerals as given in table 4.15. Initially, WSA is processed at 1000 °C for 1 h to remove any volatile substance. Further, both the samples were made in similar experimental conditions as given in chapter 3. WSA glass-ceramic, MOD sample and Crofer 22 APU have been selected for interaction study. The powder WSA glass and mineral-based glasses were mixed with polyvinyl alcohol (PVA) and keep between two ultrasonically cleaned Crofer 22 APU sheets of size 1.0×1.0×0.2 cm to make the diffusion couple. This diffusion couple was kept at 900 °C for 1, 2, 10, 100 and 500 h.

4.5.1 EDS and ICP analysis

The chemical composition of the WSA was estimated by energy dispersive spectroscopy (EDS). To confirm the exact and precise chemical composition of the as-quenched WSA glass-ceramic was calculated using inductively coupled plasma (ICP-MS) technique. The composition of WSA and mineral-derived glass are more or less the same.

Table 4.15 chemical composition of WSA (wt%) and similar composition of mineral-derived sample analyzed by EDS

Samples label	**SiO_2**	**CaO**	**Na_2O**	**K_2O**	**MgO**
WSA	85	8	0.82	4.85	4.85
MOD-sample	85	8	0.82	4.85	4.85

However, both samples have a higher amount of SiO_2 with alkali and alkaline-earth metal, but some very minor trace elements are presented in the WSA, which is not detected by EDS.

Table 4.16 weight percentage (%) of different oxides presented in the as-quenched glass-ceramic of WSA and MOD calculated using ICP and EDS

Compounds	Elemental analysis (wt%)		
	WSA (ICP)	WSA (EDS)	MOD-sample (EDS)
SiO_2	84.94	84.53	85.40
CaO	8.02	4.85	9.50
Na_2O	0.62	1.46	1.25
MgO	0.82	1.83	0.55
K_2O	4.85	4.85	2.25
Al_2O_3	0.72	2.40	1.05

4.5.2 Thermogravimetric (TG) and CTE analysis

The thermal stability of the given WSA sample is checked using TGA experiment as shown in Fig. 4.37 (a). Initially, sample exhibits some weight loss i.e., 1.5% up to 350 °C. This weight loss is related to water molecules absorbed by the sample.

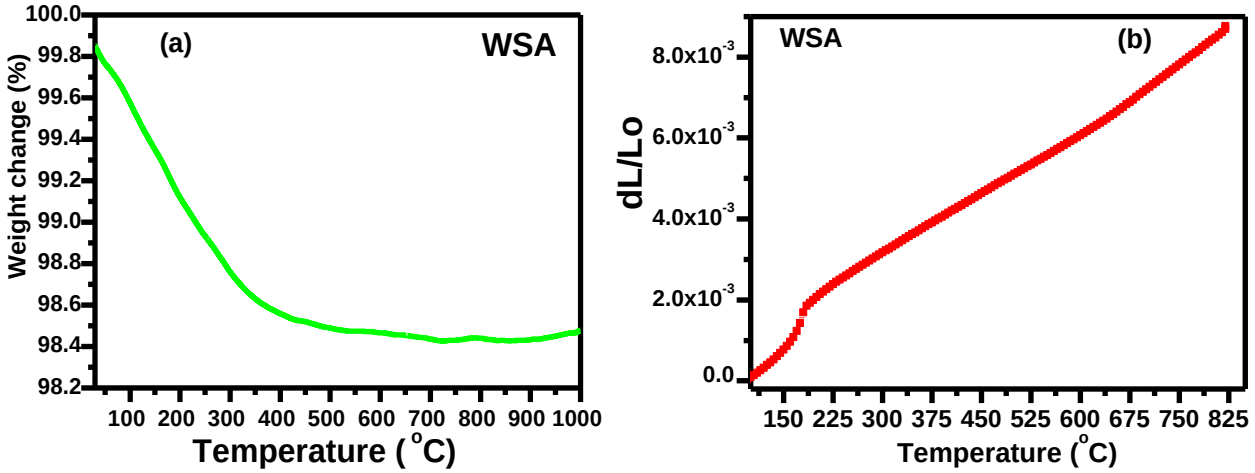

Fig. 4.37 (a) Thermal gravimetric (TG) curve and **(b)** CTE of the as-quenched WSA sample

After that, TGA curve does not show any trend with respect to temperature i-e., 350- 950 °C, which indicates the good thermal stability of WSA sample. Additionally, coefficient of thermal expansion (CTE) is a very essential parameter for sealing applications; normally, it should be in the range of 9-13×10^{-6}/K for SOFC application.[3,97,198] CTE of the as-prepared sample is 10×10^{-6}/K as shown in Fig. 4.37 (b). Usually, silica-rich glasses have low CTE, this amount of silica is the deciding factor for CTE in silicate glasses.[226] The presence of the modifying elements in the samples can increase the CTE due to the modifying overall structure of the glass-network means

the silicate-network. However, the small amount i-e., only ~3 wt% of modifiers are found in the WSA sample. XRD of the melt-quench sample (discussed in the next section) shows the presence of the tridymite crystalline phase. The tridymite phase has higher CTE as reported by Nurur *et al*.[227] Thus, CTE of the present sample may be arisen due to the presence of the crystalline phase as well as some trace elements and their bonding with other elements presented in glass-matrix.

4.5.3 X-ray diffraction analysis

The nature of the as-quenched samples derived from WSA and MOD sample is checked using X-ray diffraction. Additionally, powder of both the samples is used to make the diffusion couples (as shown in the experimental section) for interaction study. After exposure for different thermal cycles, the powders were taken from diffusion couple and investigated by XRD. X-ray diffraction patterns are given in Fig. 4.38 (a)-(c). The X-ray diffraction pattern of the as-prepared sample exhibits the broad halo along with some weak embedded crystalline peaks. These peaks are indexed with crystalline rhombohedral phases of Al_2O_3 (ICDD card no.00-042-1468). The volume fraction of rhombohedral Al_2O_3 crystalline phase is less than 2% as calculated from foolproof XRD software. It is also supported by ICP analysis as given in table 4.16. On the other hand, MOD-sample exhibits cristobalite crystalline phase with ICDD card no-(01-075-0923), which is given in Fig. 4.38 (c). This crystalline phase is very detrimental for sealing point of view, since during the thermal cycle, this phase showed a large volume change led to creating thermal stress at the interface of Crofer 22 APU and glass seal. After exposed at 900 °C for 500 h, the interface powder is taken from the diffusion couple for further experimentation. The XRD pattern of the exposed WSA sample (at 900 °C for 500 h) is shown in Fig. 4.38 (b). The XRD pattern is indexed with the tridymite crystalline SiO_2 phases. Interestingly, the Al_2O_3 crystalline phase, presented in the initial glass-ceramic, is completely either suppressed or dissolved in the matrix as indicated by XRD of 500 h exposed sample. Many researchers have reported that sometime the meta-stable crystalline

phase may dissolve to form a new crystalline phase in prolonged heat-treatment of glasses.[18,98] As heat-treatment evolved, either it dissolves or converts into more stable crystalline phase.

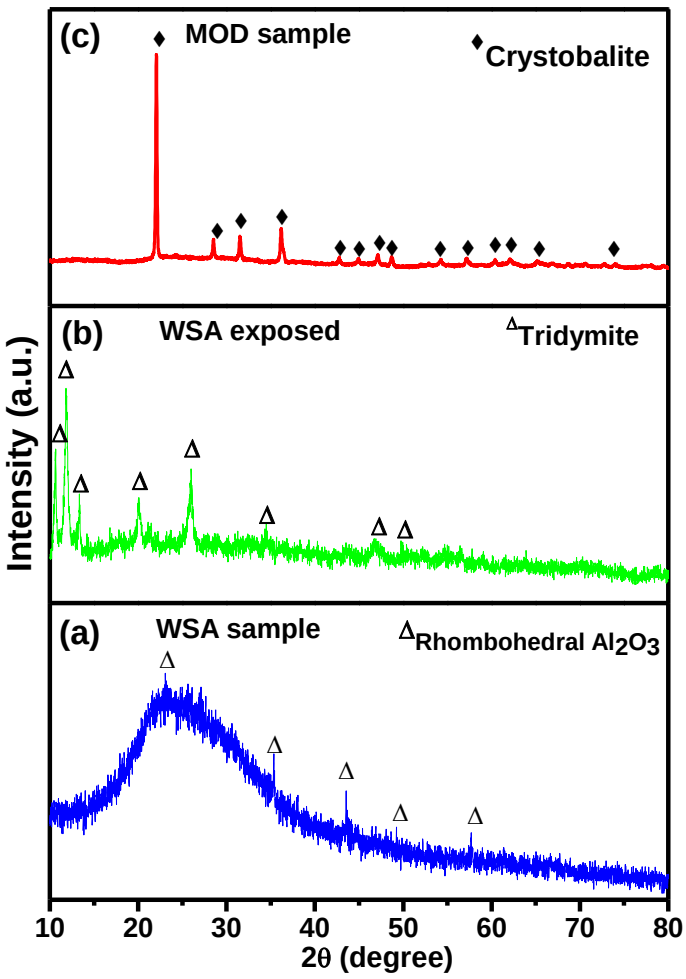

Fig. 4.38 XRD pattern of **(a)** as-prepared sample **(b)** after chemical interaction at 900 °C for 500 h and **(c)** MOD-sample derived using mineral oxides

The SiO_2 cristobalite phase is usually detrimental in SOFCs application point of view since large volume change occurs during thermal cycles, which led the thermal stresses. However, in the present case, the cristobalite phase is not formed. Moreover, In WSA sample, no other crystalline phases are formed even after 500 h exposed duration. Usually, chemical interaction for longer duration leads to the formation of many crystalline phases in the multi-component glasses/glass-ceramics with other components of SOFCs when glasses are made of mineral oxides[212,228,229] Conclusively, minimum reaction is taken place without forming any detrimental crystalline phase

at the interface between the sample and Crofer 22 APU. In this respect, the WSA derived glass-ceramic seems to be better alternate sealing materials than conventional glass-sealant formed using mineral oxides.

4.5.4 FTIR analysis

FTIR spectra are taken in the range of 4000-400 cm^{-1} of the as-prepared and exposed (900 °C/500h) samples as shown in Fig. 4.39 (a)-(c). FTIR spectra of as-prepared as well as exposed samples at 900 °C for 500 h exhibit some striking differences in the bands. For comparison, the FTIR spectra of MOD sample is also given in Fig. 4.39 (c). In the case of as-quenched and exposed samples, the bands are diffused particularly in the as-quenched sample. Exposed and MOD (as-quenched) samples exhibit sharp bands, particularly in MOD sample. Obviously, MOD sample is exhibiting fully cristobalite crystalline phase. In general, the broadness of bands is related to the presence of different structural units of glass-former (SiO_2) in the sample. However, in both the case, these bands are weak at the higher wavenumber. Most of the strong bands are present in the fingerprint region. The majority of bands belong to the SiO_4 polyhedra along with the hydroxyl group related bands in both the spectra. The band at 466-472 cm^{-1} belongs to Si-O-Si bending vibration.[10]

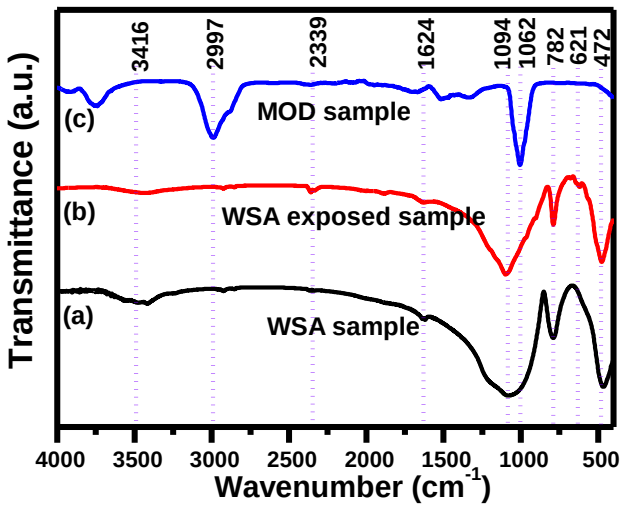

Fig. 4.39 FTIR spectra **(a)** as-prepared WSA **(b)** exposed glass-ceramic and **(c)** MOD as-quenched sample

The band at 790-782 cm^{-1} belongs to O-Si-O stretching vibration.[216] The strong band at 1062-1094 cm^{-1} is an asymmetric stretching vibration band of Si-O-Si.[5,215] The band at about, 1620-1629 cm^{-1} is the flexural vibration band of absorbed water H-OH.[230] The bands at 2997 cm^{-1} indicate the bending of Si-OH groups. The band at 3482-3414 cm^{-1} is arisen due to water absorbed by the sample. In comparison to the as-prepared sample with the exposed glass-ceramic sample exhibits two other weak bands at 685 and 621 cm^{-1}. The band at 685 cm^{-1} belongs to the inner vibration of Si-O-Si.[231] On the other hand, 621 cm^{-1} band is associated with chromium oxide. Additionally, all the bands shift towards the higher wavenumber in an exposed sample. It is associated with the diffusion of Cr and Fe from Crofer 22 APU to glass sealant. Since bonds between diffused species (Cr) and oxygen are stronger than bonds between silicon and oxygen, which will shift bands towards the higher wavenumber. The presence of the hydroxyl group, as observed in the FTIR spectra, it is responsible to promote the bonding between glass-sealant and interconnect. Initially, it may provide wettability between sealant and interconnect. Diffusion couple is prepared using sample powder of WSA glass with Crofer 22 APU and WSA, as shown in Fig. 4.40.

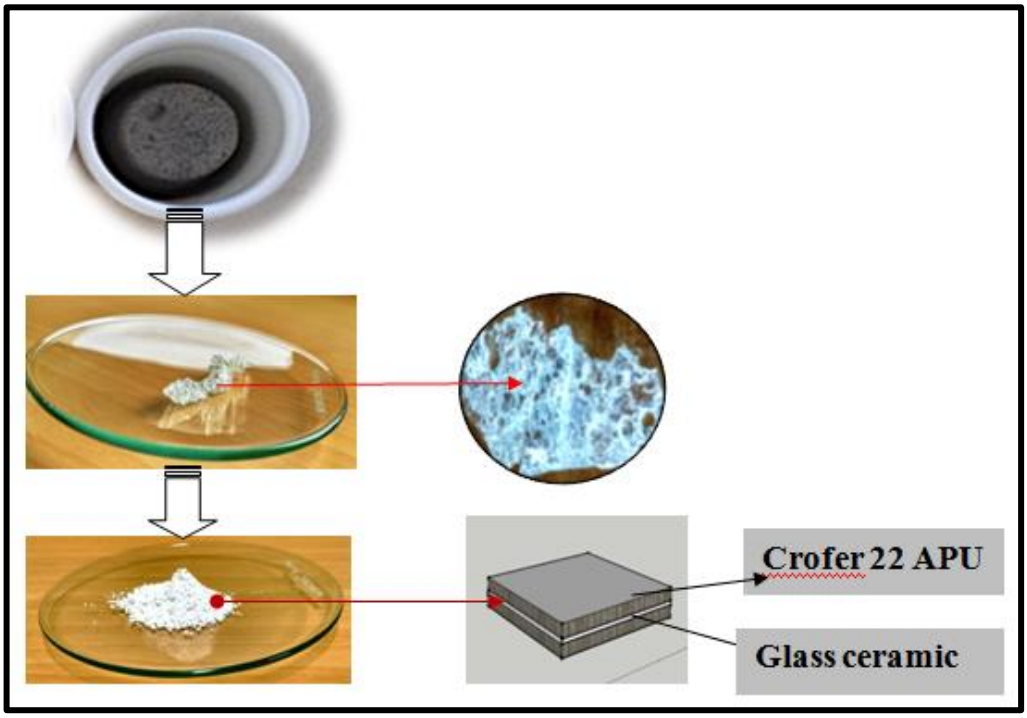

Fig. 4.40 Schematic design of diffusion couple of glass-ceramic samples with Crofer 22 APU

4.5.5 SEM/EDS analysis

The preparation of a diffusion couple is shown in a schematic diagram (Fig.4.40). A detailed investigation of the interface between glass-ceramic and Crofer 22 APU has been carried out after exposing diffusion couple at 900 ℃ for different time periods. Interestingly, MOD sample did not form any interface with interconnect material, So, SEM study couldn't be conducted on this diffusion couple. Fig. 4.41 (a)-(c) shows the SEM micrographs of the interface of glass-ceramic with Crofer 22 APU heat-treated at 900 ℃ for 10, 100 and 500 h exposed time duration. Initially, diffuse dendrite growth is clearly visible to the glass-ceramic side. As the time duration increased from 10 h to 100 h, it becomes clear and long in length as marked in Fig. 4.41 (a) and (b). Finally, in 500 h of exposure time, it becomes longer and clearer as shown in Fig. 4.41 (c). The dendrite types light gray rods correspond to the tridymite crystalline phase.

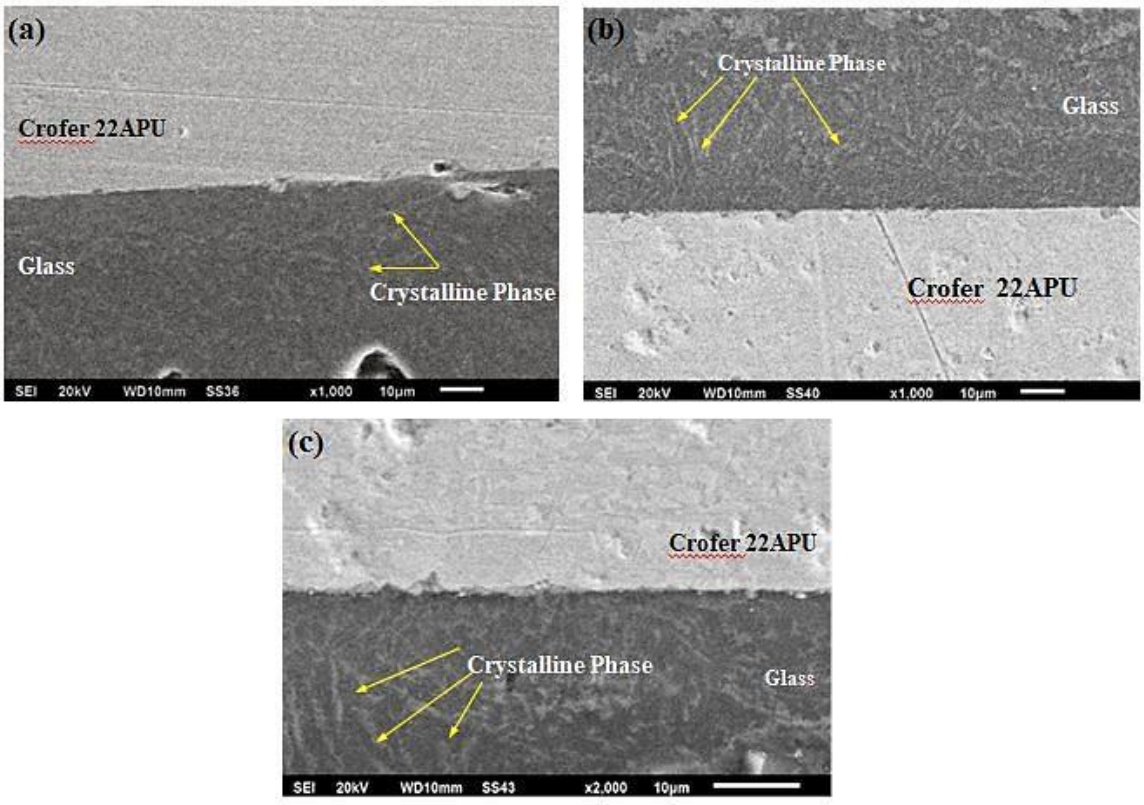

Fig. 4.41 SEM images of diffusion couple of WSA glass-ceramic with Crofer 22 APU: heat-treated for: **(a)** 10 h **(b)** 100 h and **(c)** 500 h

It is also supported by XRD. The interface is very smooth and free from porosity even after 500 h exposure with the five different thermal cycles. It is unusual since SiO_2 rich glasses and glass-ceramic usually form cristobalite and quartz crystalline phases after exposing many thermal cycles.

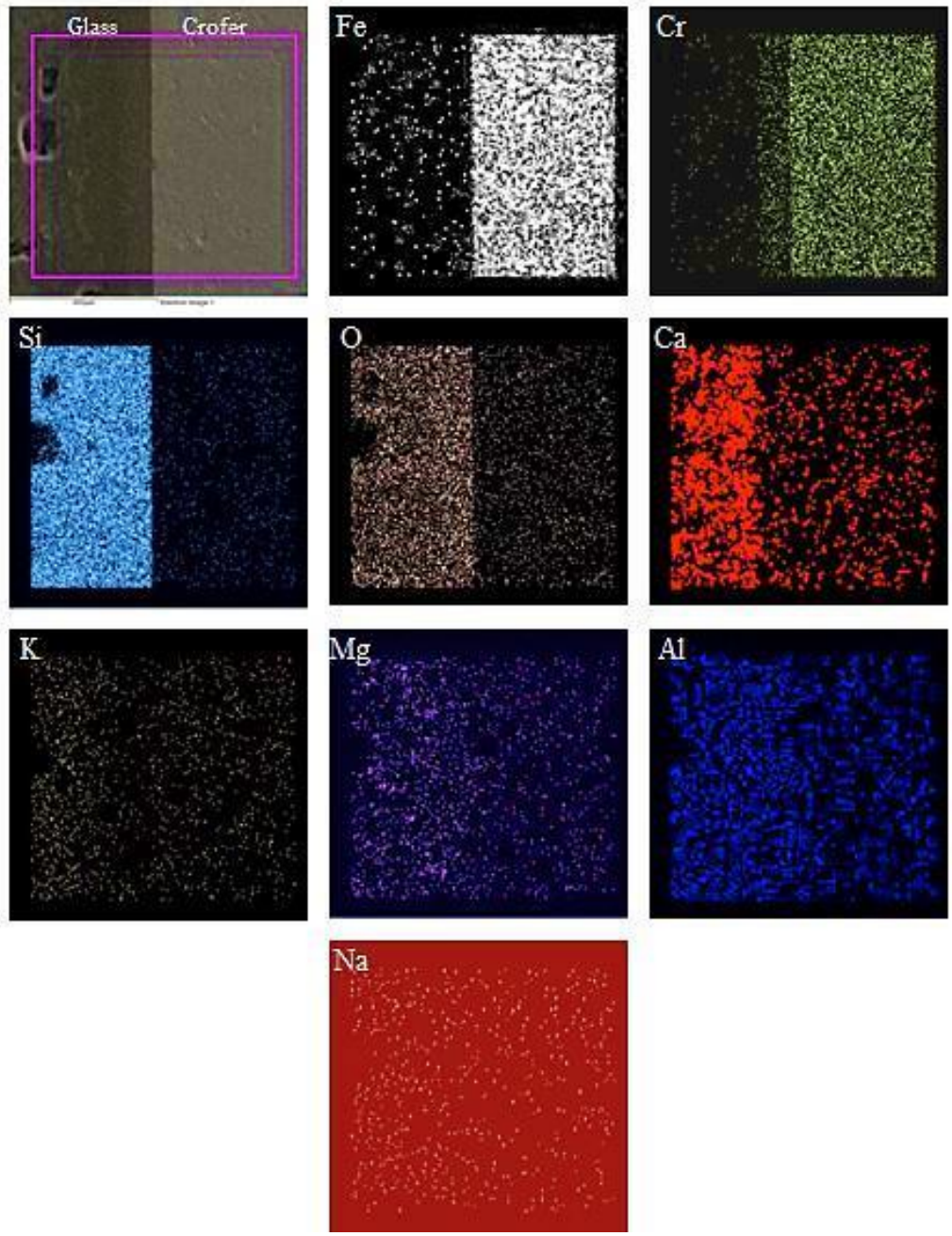

Fig. 4.42 Dot profile of different elements across the diffusion couple of WSA and Crofer 22 APU after heat-treatment at 900 °C for 500 h

The formation of these phases is very detrimental to SOFCs application point of view due to the big change in their volume fraction, particularly, cristobalite phase during thermal cycles. The big

change in their volume creates thermal stress at the interface leads delamination of the interface. In the case of the present study, a minimum chemical reaction between interconnect and glass-sealant has taken place.

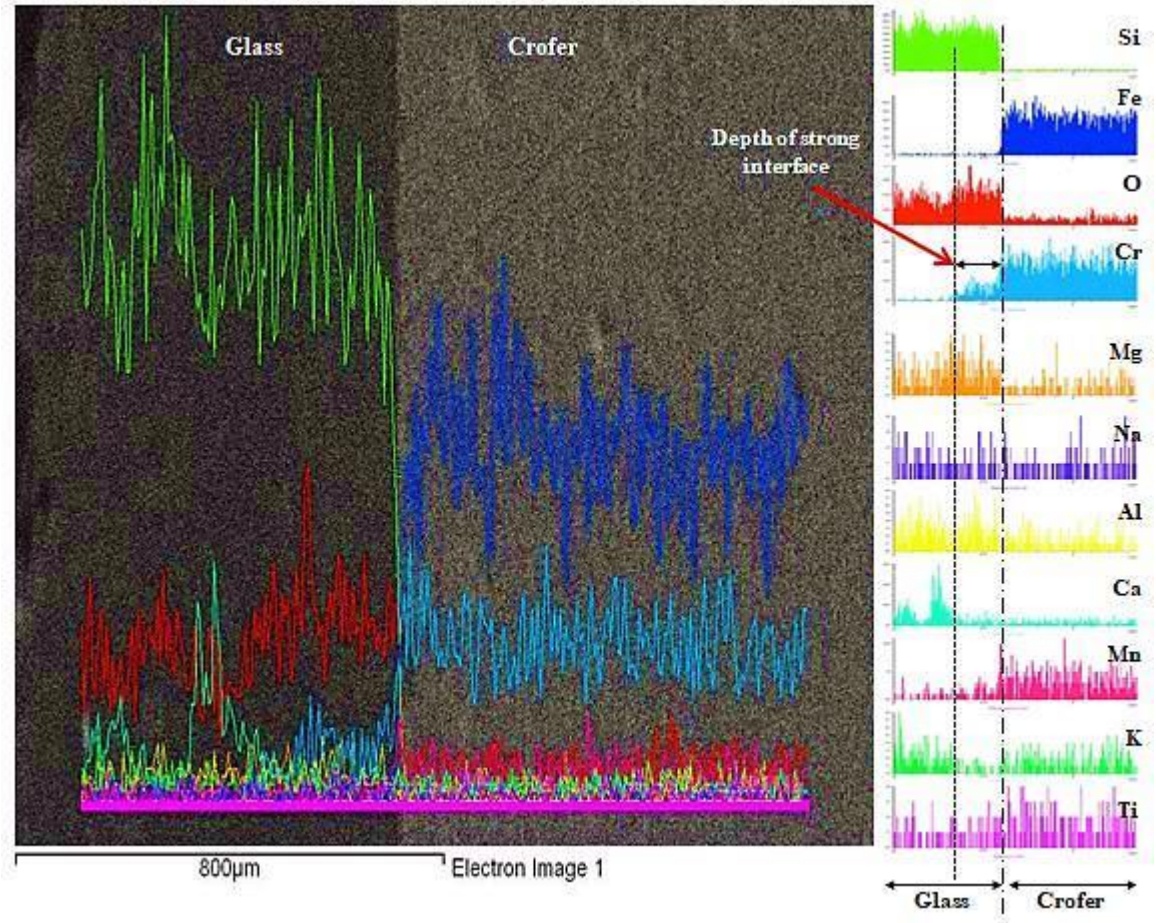

Fig. 4.43 Line profile of the different elements across the diffusion couple heat-treated at 900 °C after 500 h

It is showing good compatibility between both the components. Basically, once bonds are formed between SOFC components and glass-sealant then the vigorous reaction may form some crystalline phases, they change the CTE, which may de-laminate the interface. The dot mapping of the elemental distribution has been carried out and shown in Fig. 4.42. In the case of chromium distribution, a very interesting feature is observed, after uniform and equal distribution up to 160 µm followed by less dense and equally distributed chromium in the glass sealant. Similarly, calcium diffused from 200 µm glass side to interconnect side, whereas, alkali metals like K^+ and

Na^+ are equally distributed throughout the diffusion couple. Silicon and oxygen clearly show the interface boundaries in the dot-mapping of these elements to obtain a clear picture.

The line profile of different elements across the diffusion couple is also performed as shown in Fig. 4.43. It verifies from the dot mapping results. Interestingly, the present WSA glass-ceramic exhibits good bonding and smooth interface even after 500 h. It seems that the presence of some trace elements may play a crucial role in the formation of the interface. However, the role of trace elements in agricultural waste derived glass and glass-ceramic is not well-known yet.

4.5.6 Hardness of interface

The microhardness is measured across the interface at a different point as shown in Fig. 4.44. The microhardness of the Crofer 22 APU side varies from 130 to 190 HV. It is similar to earlier reports for the Crofer 22 APU. On the other hand, at the interface of glass-ceramic and Crofer 22 APU, microhardness increases and becomes 237 to 384 HV shown in table 4.17. At the boundary of glass-ceramic and Crofer 22 APU, microhardness is less than glass-ceramic and higher than the Crofer 22 APU. This clearly indicates that the bonding between glass-ceramic and Crofer 22 APU is semi-coherent in nature.[232] Towards the glass-ceramic side, microhardness is higher than the interface and Crofer 22 APU, i.e. 440-490 HV. Silicate glasses usually have the microhardness in above-said range, whereas borate glasses have higher microhardness.

Table 4.17 Hardness data of Crofer 22 APU, interface and WSA glass-ceramic after heat-treatment 500 h at 900 °C different points in Fig. 4.44

Hardness (HV) of the Crofer 22 APU, interface and glass-ceramic		
Crofer 22 APU	**Interface**	**Glass-ceramic**
156	237	439
190	384	490
130	343	475

In other words, the microhardness test clearly shows continuous and superior bonding between Crofer 22 APU and glass sealant even after 500 h exposed of the diffusion couple. Conclusively, the glass-ceramic derived from agricultural waste can be used as a sealant in SOFCs.

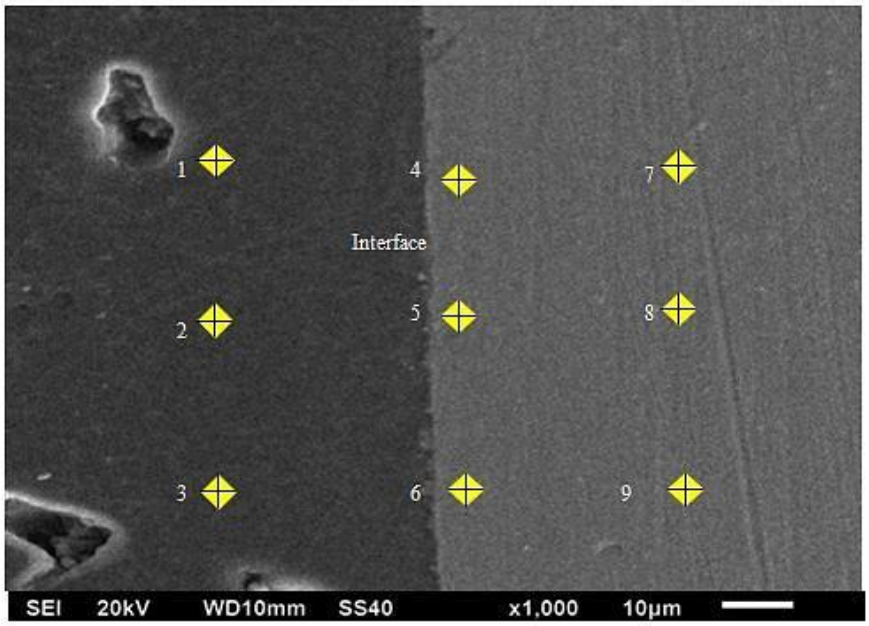

Fig. 4.44 Hardness of glass-ceramic, interface and Crofer 22 APU and glass-ceramic at different point

The comparative study of the WSA and mineral oxides based glass-ceramic have been done in the light of structural, mechanical and interaction behavior with Crofer 22 APU for SOFC application. WSA exhibits good thermal stability with insulating nature even at 700 $^{\circ}$C. The CTE of present WSA glass-ceramic is in the required range for SOFC application ~10 $\times 10^{-6}$/K. The major band of SiO_2 polyhedra with the presence of the hydroxyl group, which supports the wetting and adhesion between interconnect and WSA. While mineral oxides derived glass-ceramic of similar composition as WSA sample could not form the interface with interconnect. Semi-coherent interface is strong, smooth and well adhere to Crofer 22 APU even after five thermal cycles for the different time duration. The formation of a thin chromium layer (160 µm) at the interface as well as the presence of some trace elements might be responsible for strong bonding between Crofer 22 APU and glass-ceramic sealant derived from WSA. The present study demonstrates that agricultural wastes derived glass-ceramic over the mineral oxides based glass-ceramic can be promising sealant materials for SOFC's applications. The maximum microhardness at the interface is 384 HV.

Selected sample is checked interfacial study with Crofer 22 APU as the sealant for solid oxide fuel cells (SOFCs) applications. Some of the agro-food waste ashes are used for various applications

Chapter 5 Conclusions and future scope

Agro-food waste ashes are used as new sources of materials to synthesize glasses and glass-ceramics via melt-quench technique. These as-prepared glasses and glass-ceramics are characterized using different experimental techniques. Physical, thermal, optical and dielectric properties on agro-food waste ashes derived glasses and glass-ceramics have been carried out. Based on the obtained results and their analysis, the conclusions have been drowned and presented in this chapter. In the last section, future scope of the present work has also been given.

The addition of eggshell powder (ESP) in rice husk ash (RHA), sugarcane leave ash (SCLA), wheat straw ash (WSA) and peanut shell ash (PSA) increases the glass formation tendency with lower melting temperature. The prepared glasses are translucent having bluish tint due to the presence of trace transition elements. Inherently, present glasses exhibit lower density than mineral-derived glasses due to the presence of high porosity created due to the presence of organic substances in the agro-food waste ashes. Optical band gap of all the glasses is in the wide semiconductor range i.e. 3-4 eV. As-prepared glasses could not exhibit the proper glass transition temperature. Higher ESP containing glasses exhibit higher reactivity with the recrystallized alumina crucible during melting. Inherently presence of some trace elements for instance, Ti and Fe in the present glasses is responsible for good photoluminescence properties even without doping of rare-earth elements such as dysprosium (D_y), Erbium (E_r) and Samarium (S_m), etc. They may find application in the laser and white light-emitting diodes (LEDs).

All the as-prepared glasses convert into glass-ceramics by controlled heat-treatment. All glass-ceramics exhibit either silicate or aluminate based crystalline phases. At room temperature and 100 Hz frequency, they exhibit low/moderate dielectric constant in the range of 16-50 with minimum losses. Dielectric constant shows the independency up to certain temperature and frequency range in these glass-ceramics, which make them a good choice for microelectronic applications. Coefficient of thermal expansion (CTE) is found in the range of $6\text{-}16\times10^{-6}$/K depending on the

presence of different crystalline phases in the glass matrix. In all the synthesized glasses and glass-ceramics, 40RHA-60ESP glass shows good thermal and dielectric properties. Therefore, these glasses and glass-ceramics could be used as sealing materials for solid oxide fuel cells (SOFCs). Wheat straw ash (WSA) derived glass shows good adhesion with interconnect Since, it formed very good semi-coherent interface with Crofer 22 APU (interconnect). Interface between interconnect and glass seal was smooth, defect and crack-free, even up to 500 h with different thermal cycles. So, agro-food waste ashes could be used as sustainable and renewable resources to generate new engineering cost-effective materials. Utilization of these agro-food waste ashes provides a practical and environment-friendly way to convert them into value-added materials. Further, these materials could replace conventionally synthesized mineral-based products. This approach could also provide an effective solution to agro-food waste ashes related management problems. These agro-food waste ashes could be used as alternative resource materials to synthesize glasses, glass-ceramics and silicate-based ceramics for various engineering applications instead of mineral oxides-derived glasses.

Future Scope

Agro-food waste ashes exhibit the variable amount of different oxides such as SiO_2, CaO, K_2O, P_2O_5, etc. along with some trace elements. The presence of these trace elements influences the overall properties of the glass and glass-ceramics synthesized from these waste ashes. The exact amount of trace transition elements could not be accounted using energy dispersive spectroscopy. Therefore, for high-end applications, an instrument like x-ray photoelectron spectroscopy (XPS) is necessary to perform for evaluating the exact amount of elements presented in glasses and glass-ceramics derived from agro-food waste ashes before using them as high-performance materials. Moreover, the information about the local structural units in glasses can be calculated using electron scattring with pair distribution function. Secondly, these agro-food waste ashes derived glasses and glass-ceramics exhibit inherently porosity, so, absorption of acoustic waves, their

mechanical strength and durability can be studied to check their suitability and applicability as absorber and window materials. The presence of low atomic number elements and their oxides such as SiO_2, CaO, K_2O, P_2O_5, etc. could be used, in future as bioceramics and scaffold for bone generation and dentistry applications. Moreover, photoluminescence study could also be performed on these materials to check their utility as a host material for phosphors.

References

1 J. E. Shelby, *Introduction to Glass Science and Technology*, Royal Society of Chemistry, Cambridge, 2nd edn., 2005.

2 E. D. Zanotto, *Am. Ceram. Soc. Bull.*, 2010, **89**, 19–27.

3 J. W. Fergus, *J. Power Sources*, 2005, **147**, 46–57.

4 S. S. Raghavendra, G. R. Jadhav, K. M. Gathani and P. Kotadia, *J. Istanbul Univ. Fac. Dent.*, 2017, **51**, 128–137.

5 P. Jha and K. Singh, *Ceram. Int.*, 2015, **42**, 436–444.

6 H. R. Fernandes, A. Gaddam, A. Rebelo, D. Brazete, G. E. Stan and J. M. F. Ferreira, *Materials (Basel).*, 2018, **11**, 1–54.

7 H. Biricik, F. Aköz, I. Berktay and A. N. Tulgar, *Cem. Concr. Res.*, 1999, **29**, 637–643.

8 F. Bondioli, L. Barbieri, A. M. Ferrari and T. Manfredini, *J. Am. Ceram. Soc.*, 2010, **126**, 121–126.

9 S. Sankar, S. K. Sharma, N. Kaur, B. Lee, D. Y. Kim, S. Lee and H. Jung, *Ceram. Int.*, 2016, **42**, 4875–4885.

10 S. S. Danewalia, G. Sharma, S. Thakur and K. Singh, *Sci. Rep.*, 2016, **6**, 24617.

11 R. Benzerga, V. Laur, R. Lebullenger, L. Le Gendre, S. Genty, A. Sharaiha and P. Queffelec, *Mater. Res. Bull.*, 2015, **67**, 261–265.

12 S. K. Rajanna, M. Vinjamur and M. Mukhopadhyay, *Chem. Eng. Commun.*, 2017, **204**, 249–253.

13 D. Liu, D. Seeburg, S. Kreft, R. Bindig, I. Hartmann, D. Schneider, D. Enke and S. Wohlrab, *Catalysts*, 2019, **9**, 1–9.

14 K. Xu, Q. Sun, Y. Guo and S. Dong, *Appl. Surf. Sci.*, 2013, **276**, 796–801.

15 L. L. Devi, C. Basavapoornima, V. Venkatramu, P. Babu and C. K. Jayasankar, *Ceram. Int.*, 2017, **43**, 16622–16627.

16 S. Ibrahim and E. Mumtaz, *J. Phys. Conf. Ser.*, 2014, **8**, 35–41.

17 I. A. Cornejo, S. Ramalingam, J. S. Fish and I. E. Reimanis, *Am. Ceram. Soc. Bull.*, 2014, **93**, 24–27.

18 S. H. Javed, A. S. A. Umair and S. Tajwar, *J. Pakistan Inst. Chem. Eng.*, 2011, **39**, 51–54.

19 B. Aktas, M. Albaskar, S. Yalcin and K. Dogru, *Arch. Mater. Sci. Eng.*, 2016, **82**, 57–61.

20 I. H. Nayel, S. K. Burhan and M. S. Nasr, in *IOP Conf. Series: Materials Science and Engineering*, 2018, p. 012009.

21 C. A. Moraes, I. J. Fernandes, D. Calheiro, A. G. Kieling, F. A. Brehm, M. R. Rigon, J. A.

Berwanger Filho, I. A. Schneider and E. Osorio, *Waste Manag. Res.*, 2014, **32**, 1043–1048.

22 S. F. Lim and S. U. Matu, *Int. J. Energy Environ. Eng.*, 2015, **6**, 31–35.

23 X. Liu, X. Chen, L. Yang, H. Chen, Y. Tian and Z. Wang, *Res. Chem. Intermed.*, 2016, **42**, 893–913.

24 Y. Zhang, A. E. Ghaly and B. Li, *Am. J. Appl. Sci.*, 2012, **9**, 1757–1768.

25 A. Shrivas, D. Jain and R. Joshi, *Int. J. Sci. Technol. Eng.*, 2015, **2**, 89–107.

26 S. Niju, M. M. M. S. Begum and N. Anantharaman, *J. Saudi Chem. Soc.*, 2014, **18**, 702–706.

27 S. Sankar, N. Kaur, S. Lee and Y. Kim, *Ceram. Int.*, , DOI:10.1016/j.ceramint.2018.02.090.

28 R. Pode, *Renew. Sustain. Energy Rev.*, 2016, **53**, 1468–1485.

29 S. S. Hossain, L. Mathur, A. Bhardwaj and P. K. Roy, *Int. J. Appl. Ceram. Technol.*, 2019, **16**, 1069–1077.

30 V. Vishwakarma, D. Ramachandran, N. Anbarasan and A. M. Rabel, in *Materials Today: Proceedings*, 2016, vol. 3.

31 A. Gupta and J. P. Verma, *Renew. Sustain. Energy Rev.*, 2015, **41**, 550–567.

32 G. Najafi, B. Ghobadian, T. Tavakoli and T. Yusaf, *Renew. Sustain. Energy Rev.*, 2009, **13**, 1418–1427.

33 N. Sarkar, S. K. Ghosh, S. Bannerjee and K. Aikat, *Renew. Energy*, 2012, **37**, 19–27.

34 G. Sharma, M. Kaur, S. Punj and K. Singh, *Biofuels, Bioprod. Biorefining*, 2020, **13**, 1–23.

35 R. E. N. de Castro, R. M. de B. Alves, C. A. O. do Nascimento and R. Giudici, *Assessment of sugarcane-based ethanol production*, Web of Science, 2016.

36 R. M. Jorapur and A. K. Rajvanshi, *Biomass and Bioenergy*, 1995, **8**, 91–98.

37 I. J. Fernandes, D. Calheiro, A. G. Kieling, C. A. M. Moraes, T. L. A. C. Rocha, F. A. Brehm and R. C. E. Modolo, *Fuel*, 2016, **165**, 351–359.

38 A. R. Ibrahim, X. Li, Y. Zhou, Y. Huang, W. Chen, H. Wang and J. Li, *Int. J. Mol. Sci.*, 2015, **16**, 7960–7975.

39 A. Laca, A. Laca and M. Díaz, *J. Environ. Manage.*, 2017, **197**, 351–359.

40 C. Hernández, C. Escamilla-Alvarado, A. Sánchez, E. Alarcón, F. Ziarelli, R. Musule and I. Valdez-Vazquez, *Biofuels, Bioprod. Biorefining*, 2019, **13**, 1–17.

41 M. A. Perea-Moreno, F. Manzano-Agugliaro, Q. Hernandez-Escobedo and A. J. Perea-Moreno, *Sustain.*, 2018, **10**, 1–15.

42 R. Dungani, M. Karina, Subyakto, A. Sulaeman, D. Hermawan and A. Hadiyane, *Asian J. Plant Sci.*, 2016, **15**, 42–55.

43 R. Badar and S. A. Qureshi, *J. Bot.*, 2014, **2014**, 1–6.

44 S. Bharathiraja, J. Suriya, M. Krishnan, P. Manivasagan and S. K. Kim, in *Advances in Food and Nutrition Research*, Elsevier Inc., 2017, vol. 80, pp. 125–148.

45 G. C. Cordeiro, R. D. T. Filho, E. M. R. Fairbairn, L. M. M. Tavares and C. H. Oliveira, *Use Recycl. Mater. Build. Struct.*, 2004, **2**, 1–10.

46 R. Sindhu, E. Gnansounou, P. Binod and A. Pandey, *Renew. Energy*, 2016, **98**, 203–215.

47 H. Coutinho, J. Franco, M. Teresa, B. Pimenta, J. Luís, N. Carvalho, P. S. Graziano, C. E. V. R. Magalhães, O. A. Braunbeck, A. C. Vitti, O. T. Kölln and J. R. Neto, *Sci. Agric.*, 2013, **70**, 305–312.

48 Y. Zhang, A. E. Ghaly and B. Li, *Am. J. Eng. Appl. Sci.*, 2012, **5**, 98–106.

49 K. M. Omatola and A. D. Onojah, *Int. J. Phys. Sci.*, 2009, **4**, 189–193.

50 J. S. Lim, Z. Abdul Manan, S. R. Wan Alwi and H. Hashim, *Renew. Sustain. Energy Rev.*, 2012, **16**, 3084–3094.

51 S. Zhang, Q. Dong, L. Zhang and Y. Xiong, *Bioresour. Technol.*, 2015, **191**, 17–23.

52 E. Rohaeti, Hikmawati and Irzaman, *Mater. Sci. Technol.*, 2010, **1**, 265–272.

53 W. T. Tsai, M. K. Lee and Y. M. Chang, *Bioresour. Technol.*, 2007, **98**, 22–28.

54 H. S. Heo, H. J. Park, J. Dong, S. H. Park, S. Kim, D. J. Suh, Y. Suh, S. Kim and Y. Park, *J. Ind. Eng. Chem.*, 2010, **16**, 27–31.

55 W. Cai, R. Liu, Y. He, M. Chai and J. Cai, *Fuel Process. Technol.*, 2018, **171**, 308–317.

56 J. Alvarez, G. Lopez, M. Amutio, J. Bilbao and M. Olazar, *Fuel*, 2014, **128**, 162–169.

57 N. Liu, K. Huo, M. T. McDowell, J. Zhao and Y. Cui, *Sci. Rep.*, 2013, **3**, 1–7.

58 N. Kavitha, M. Balasubramanian and Y. D. Vashistha, *Trans. Indian Ceram. Soc.*, 2011, **70**, 115–118.

59 J. A. Adebisi, J. O. Agunsoye, S. A. Bello, I. I. Ahmed, O. A. Ojo and S. B. Hassan, *Sol. Energy*, 2017, **142**, 68–86.

60 Cornejo, Ivan A. Reimanis, Ivar E. Ramalingam, Subramanian, US Patent, US2015/0065329A1, 2015, 1–10.

61 S. Punj and K. Singh, *J. Mater. Sci. Mater. Electron.*, 2019, **30**, 3871–3881.

62 S. Yucel, D. Özçimen, P. Terziŏglu, S. Acar and C. Yaman, *Adv. Sci. Lett.*, 2013, **19**, 3477–3481.

63 K. Bogeshwaran, R. Kalaivani, S. Ashraf, G. N. Manikandan and G. E. Prabhu, *Int. J. ChemTech Res.*, 2014, **6**, 4337–4345.

64 S. Thakur and A. K. Gathania, *Indian J. Phys.*, 2015, **89**, 973–979.

65 T. Hossain, M. A. Salam, K. Ahmed and M. S. Habib, *Int. J. Chem. Math. Phys.*, 2019, **3**, 105–134.

66 A. N. Swami Nathen and S. Robert Ravi, *Int. J. Eng. Res. Appl.*, 2017, **7**, 76–79.

67 B. Mistry, *Int. J. Emerg. Technol. Adv. Eng.*, 2016, **6**, 2677–2679.

68 P. Jongpradist, W. Homtragoon, R. Sukkarak, W. Kongkitkul and P. Jamsawang, *Adv. Civ. Eng.*, 2018, **2018**, 1–11.

69 S. S. Banger, S. N. Phalke, A. Y. Gawade, R. S. Tambe and A. B. Rahane, *Int. J. Eng. Sci. Manag.*, 2017, **7**, 127–131.

70 S. W. Dhengare, S. P. Raut, N. V Bandwal and A. Khangan, *Int. J. Emerg. Eng. Res. Technol.*, 2015, **3**, 109–116.

71 A. I. Maulana, N. K. Wardani and D. Syamsidar, *MATEC web Conf.*, 2017, **97**, 1–8.

72 M. S. Ali, M. A. A. Hanim, S. M. Tahir, C. N. A. Jaafar, N. Mazlan and K. A. Matori, *Adv. Mater. Sci. Eng. Heat.*, 2017, **2017**, 1–10.

73 P. K. Mehta, in *Journal proceeding*, Peshawar, Pakistan, 1979, pp. 113–122.

74 I. K. Cisse and M. Laquerbe, *Cem. Concr. Res.*, 2000, **30**, 13–18.

75 R. Jauberthie, F. Rendell, S. Tamba and I. Cisse, *Constr. Build. Mater.*, 2000, **14**, 419–423.

76 M. Noushad, I. A. Rahman, a Husein and D. Mohamad, *Powder Technol.*, 2016, **299**, 19–25.

77 N. T. W. Pannangpetcha, K. Aranyika, K. Petcharoenb and A. Sirivat, *Prog. Rubber, Plast. Recycl. Technol.*, 2016, **31**, 145–169.

78 C. Balázsi, F. Wéber, Z. Kövér, E. Horváth and C. Németh, *J. Eur. Ceram. Soc.*, 2007, **27**, 1601–1606.

79 J. P. Nayak and J. Bera, *Phase Transitions*, 2009, **82**, 879–888.

80 M. Kaur and K. Singh, *AIP Conf. Proc.*, 2019, **2093**, 020033.

81 P. Jha, S. S. Danewalia, G. Sharma and K. Singh, *Mater. Sci. Eng. C*, 2018, **86**, 9–17.

82 S. S. Danewalia and K. Singh, *Ceram. Int.*, 2016, **42**, 11858–11865.

83 G. Kaur, O. P. Pandey, K. Singh, D. Homa, B. Scott and G. Pickrell, *J. Biomed. Mater. Res. - Part A*, 2014, **102**, 254–274.

84 K. Singh and D. Bahadur, *J. Mater. Sci. Mater. Med.*, 1999, **10**, 481–484.

85 A. Goel, S. Kapoor, R. R. Rajagopal, M. J. Pascual, H. W. Kim and J. M. F. Ferreira, *Acta Biomater.*, 2012, **8**, 361–372.

86 P. Balasubramanian, L. A. Strobel, U. Kneser and A. R. Boccaccini, *Biomed. Glas.*, 2015, **1**, 51–69.

87 G. Furtos, L. Silaghi-Dumitrescu, K. Lewandowska, A. Sionkowska and P. Pascuta, *Key Eng. Mater.*, 2016, **672**, 261–275.

88 J. S. Al-Sanabani, A. A. Madfa and F. A. Al-Sanabani, *Int. J. Biomater.*, 2013, **2013**, 1–12.

89 J. P. Nayak and J. Bera, *Adv. Mater. Res.*, 2012, **548**, 12–16.

90 M. Prakasam, J. Locs, K. Salma-Ancane, D. Loca, A. Largeteau and L. Berzina-Cimdina, *J. Funct. Biomater.*, 2015, **6**, 1099–1140.

91 K. Kaur, K. J. Singh, V. Anand, G. Bhatia and S. Singh, *Ceram. Int.*, 2016, **42**, 12651–12662.

92 R. Jayasree, J. Velkumar and T. S. Sampath Kumar, *Dent. Oral Craniofacial Res.*, 2018, **4**, 1–4.

93 M. G. Gandolfi, F. Siboni, T. Botero, M. Bossù, F. Riccitiello and C. Prati, *J. Appl. Biomater. Funct. Mater.*, 2015, **13**, 43–60.

94 W. F. Ho, H. C. Hsu, S. K. Hsu, C. W. Hung and S. C. Wu, *Ceram. Int.*, 2013, **39**, 6467–6473.

95 W. Leenakul, T. Tunkasiri, N. Tongsiri, K. Pengpat and J. Ruangsuriya, *Mater. Sci. Eng. C*, 2016, **61**, 695–704.

96 F. Naghizadeh, M. R. Abdul Kadir, A. Doostmohammadi, F. Roozbahani, N. Iqbal, M. M. Taheri, S. V. Naveen and T. Kamarul, *J. Non. Cryst. Solids*, 2015, **427**, 54–61.

97 M. K. Mahapatra and K. Lu, *J. Power Sources*, 2010, **195**, 7129–7139.

98 V. Kumar, S. Sharma, O. P. Pandey and K. Singh, *Solid State Ionics*, 2010, **181**, 79–85.

99 P. Jha and K. Singh, *Silicon*, 2015, **8**, 437–442.

100 S. S. Danewalia and K. Singh, *J. Am. Ceram. Soc.*, 2018, **101**, 2819–2830.

101 S. Singh, G. Kalia and K. Singh, *J. Mol. Struct.*, 2015, **1086**, 239–245.

102 Manupriya, K. S. Thind, K. Singh, V. Kumar, G. Sharma, D. P. Singh and D. Singh, *J. Phys. Chem. Solids*, 2009, **70**, 1137–1141.

103 N. Bansal, K. Pandey, K. Singh and B. C. Mohanty, *Vacuum*, 2019, **161**, 347–352.

104 G. Sharma and K. Singh, *Ceram. Int.*, 2019, **45**, 20501–20508.

105 P. Kaur, K. J. Singh, A. Kumar, H. Sood and S. Kaur, *Mater. Sci. Eng. C*, 2017, **83**, 177–186.

106 X. J. Xu, Y. L. Yue, H. T. Zhang and Z. Du, *Adv. Mater. Res.*, 2011, **306**, 531–534.

107 H. Aguiar, J. Serra, P. González and B. León, *J. Non. Cryst. Solids*, 2009, **355**, 475–480.

108 B. Aktas, M. Albaskar, S. Yalcin and K. Dogru, *Arch. Mater. Sci. Eng.*, 2016, **82**, 57–61.

109 M. R. Saeb, H. Rastin, H. A. Khonakdar, F. Simon, V. Goodarzi, P. V. P, D. Puglia, F. H.

Asl and K. Formela, *RSC Adv.*, 2017, **8**, 2218–2230.

110 D. A. Oliveira, P. Benelli and E. R. Amante, *J. Clean. Prod.*, 2013, **46**, 42–47.

111 J. A. Prasara and S. H. Gheewala, *J. Clean. Prod.*, 2016, **167**, 1020–1030.

112 W. Cheah, C. Ooi and F. Yeoh, *Mesoporous Biomaterails*, 2016, **3**, 27–38.

113 M. J. Gázquez, J. P. Bolívar, R. Garcia-Tenorio and F. Vaca, *Mater. Sci. Appl.*, 2014, **05**, 441–458.

114 A. Kumar, K. Mohanta, D. Kumar and O. Parkash, *Int. J. Eng. Sci.*, 2016, **2**, 86–90.

115 M. Jamil, A. B. M. A. Kaish, S. N. Raman and M. F. M. Zain, *Constr. Build. Mater.*, , DOI:10.1016/j.conbuildmat.2013.05.088.

116 J. R. Dodson, A. J. Hunt, V. L. Budarin, A. S. Matharu and J. H. Clark, *RSC Adv.*, 2011, **1**, 523.

117 Y. B. Seok, S. Nurbazilah, W. F. Hoon, S. B. Bin Mohamed, A. Humaizi, M. R. M. Juhari and W. N. F. W. Mohamad, *Environ. Asia*, 2016, **9**, 9–17.

118 S. Chandrasekhar, K. G. Satyanarayana, P. N. Pramada, P. Raghavan and T. N. Gupta, *J. Mater. Sci.*, 2003, **8**, 3159–3168.

119 S. F. Khor, M. H. A. M. Yusof, E. M. Cheng, M. A. Rojan, B. Johar, A. Chik, Z. A. Talib and B. Poobalan, *Int. J. Geomate*, 2016, **11**, 2150–2154.

120 S. Liu, X. Chen, A. Zhang, K. Yan and Y. Ye, *Bioresources*, 2014, **9**, 2328–2340.

121 V. B. Carmona, R. M. Oliveira, W. T. L. Silva, L. H. C. Mattoso and J. M. Marconcini, *Ind. Crops Prod.*, 2013, **43**, 291–296.

122 L. A. Pfaltzgraff, M. De bruyn, E. C. Cooper, V. Budarin and J. H. Clark, *Green Chem.*, 2013, **15**, 307.

123 U. Orlando, *Bioresour. Technol.*, 2002, **83**, 195–198.

124 L. Sun and K. Gong, *Ind. Eng. Chem. Res.*, 2001, **40**, 5861–5877.

125 R. Ghosh and S. Bhattacherjee, *J. Chem. Eng. Process Technol.*, 2013, **04**, 1–7.

126 E. Swatsitang and M. Krochai, *J. Met. Mater. Miner.*, 2009, **19**, 91–94.

127 P. Innocenzi, P. Falcaro, D. Grosso and F. Babonneau, *J. Phys. Chem. B*, 2003, **107**, 4711–4717.

128 U. Vijayalakshmi and S. Rajeswari, *Trends Biomater. Artif. Organs*, 2006, **19**, 57–62.

129 O. Olawale, A. Akinmoladun, F. Oyawale and A. Rejoice, *Int. J. Sci. Eng. Res.*, 2013, **4**, 2–5.

130 J. S. Le Blond, C. J. Horwell and C. Williamsond, Ben J.Oppenheimer, *J. Environ. Monit.*, 2010, **12**, 1459–1470.

131 A. Arumugam and V. Ponnusami, *J. Sol-Gel Sci. Technol.*, 2013, **67**, 244–250.

132 J. E. Kasmani and A. Samariha, *Middle-East J. Sci. Res.*, 2011, **8**, 823–825.

133 S. Norsuraya, H. Fazlena and R. Norhasyimi, *Procedia Eng.*, 2016, **148**, 839–846.

134 N. S. Trivedi, S. A. Mandavgane, S. Mehetre and B. D. Kulkarni, *Environ. Sci. Pollut. Res.*, 2016, **23**, 20243–20256.

135 J. Kumar, S. Kumar and S. S. Basarkar, *Int. J. Sustain. Built Environ.*, 2016, **5**, 312–333.

136 D. Shu-Ing and C. S. Choo, in *MUCET Conference proceeding*, 2015, pp. 1–5.

137 A. Bahrami, N. Soltani, M. I. Pech-Canul and C. A. Gutiérrez, *Crit. Rev. Environ. Sci. Technol.*, 2016, **46**, 143–208.

138 A. M. Qureshi, Y. V Sharma, S. R. Khan and B. M. Sontakke, *Int. J. Recent Innov. Trends Comput. Commun.*, 2015, **3**, 67–70.

139 L. R. Brun, M. Lupo, D. A. Delorenzi, V. E. Di Loreto and A. Rigalli, *Int. J. Food Sci. Nutr.*, 2013, **64**, 740–743.

140 P. S. Guru and S. Dash, *Adv. Colloid Interface Sci.*, 2014, **209**, 49–67.

141 W. T. Tsai, J. M. Yang, C. W. Lai, Y. H. Cheng, C. C. Lin and C. W. Yeh, *Bioresour. Technol.*, 2006, **97**, 488–493.

142 T. Vasan and S. Andavan, *J. Biosci. Informatics*, 2016, **4**, 118–133.

143 P. Milak, M. T. Souza, C. P. Bom and P. Mantas, *Cerâmica*, 2017, **63**, 490–493.

144 S. Tuscharoena, J. Kaewkhao, P. Limsuwana and W. Chewpraditkul, *Procedia Eng.*, 2012, **32**, 734–739.

145 S. Ruengsri, S. Insiripong, N. Sangwaranatee and J. Kaewkhao, *Prog. Nucl. Energy*, 2015, **83**, 99–104.

146 I. S. Mustafa, N. A. N. Razali, A. R. Ibrahim, N. Z. Yahaya and H. M. Kamari, *J. Intelek*, 2015, **9**, 1–6.

147 I. N. Sudiana, S. Mitsudo, T. Nishiwaki, P. E. Susilowati, L. Lestari, M. Z. Firihu and H. Aripin, *J. Phys. Conf. Ser.*, 2016, **739**, 012059 (1)-(7).

148 L. Lakshmi Devi and C. K. Jayasankar, *Ceram. Int.*, 2018, **44**, 14063–14069.

149 J. Kaewkhao and P. Limsuwan, *Procedia Eng.*, 2012, **32**, 670–675.

150 A. Jabbar, A. Al-nidawi, K. Amin, A. Zakaria, M. Hafiz and M. Zaid, *Results Phys.*, 2017, **7**, 955–961.

151 C. S. Lee, K. A. Matori, S. H. A. Aziz, H. M. Kamari, I. Ismail and M. H. M. Zaid, *Opt. - Int. J. Light Electron Opt.*, 2017, **136**, 129–135.

152 I. Zaitizila, M. K. Halimah, F. D. Muhammad and M. S. Nurisya, *Chalcogenide Lett.*, 2018,

15, 187–197.

153 G. Berkin, in *WIT Transactions on Ecology and the Environment*, WIT Press, 2008, vol. 109, pp. 521–527.

154 R. Patil, R. Dongre and J. Meshram, *J. Appl. Chem.*, 2014, **2278**, 26–29.

155 R. E. M. Khaidir, Y. W. Fen, M. H. M. Zaid, K. A. Matori, N. A. S. Omar, M. F. Anuar, S. A. A. Wahab and A. Z. K. Azman, *Optik (Stuttg).*, 2019, **182**, 486–495.

156 S. Thakur, N. Dhiman, A. Sharma and A. K. Gathania, *J. Electron. Mater.*, 2017, **46**, 2085–2089.

157 T. Wasanapiarnpong, B. Vorajesdarom, E. Rujirakamort, S. Nilpairach and C. Mongkolkachit, *Innov. Refract. Tradit. Ceram.*, 2011, **18**, 222028.

158 M. K. Naskar and M. Chatterjee, *J. Eur. Ceram. Soc.*, 2004, **24**, 3499–3508.

159 J. P. Nayak and J. Bera, *Silicon*, 2012, **4**, 57–60.

160 H. K. Tchakouté, C. H. Rüscher, S. Kong, E. Kamseu and C. Leonelli, *Constr. Build. Mater.*, 2016, **114**, 276–289.

161 F. Andreola, M. I. Martín, A. M. Ferrari, I. Lancellotti, F. Bondioli, J. M. Rincón, M. Romero and L. Barbieri, *Ceram. Int.*, 2013, **39**, 5427–5435.

162 E. R. Essien, V. N. Atasie and E. U. Udobang, *Bull. Mater. Sci.*, 2016, **39**, 1–5.

163 H. A. Saudi, S. M. Salem, S. S. Mohammad, A. G. Mostafa and M. Y. Hassaan, *Am. J. Phys. Appl.*, 2015, **3**, 97–105.

164 L. A. Q. Sierra and D. M. E. Sierra, *Jom*, 2019, **71**, 302–307.

165 R. S. Kumar, M. Vinjamur and M. Mukhopadhyay, *Int. J. Chem. Eng. Appl.*, 2013, **4**, 321–325.

166 T. Lee, R. Othman and F. Yeoh, *Biomass and Bioenergy*, 2013, **59**, 380–392.

167 Q. Tang and T. Wang, *J. Supercrit. Fluids*, 2005, **35**, 91–94.

168 A. O. Inegbenebor and F. A. Adeniji, *West Indian J. Eng.*, 2007, **30**, 17–26.

169 S. Nizamuddin, N. M. Mubarak, M. Tiripathi, N. S. Jayakumar, J. N. Sahu and P. Ganesan, *Fuel*, 2016, **163**, 88–97.

170 A. A. Salema, Y. K. Yeow, K. Ishaque, N. F. Ani, M. T. Afzal and A. Hassan, *Ind. Crop. Prod.*, 2013, **50**, 366–374.

171 N. H. Bateni, M. N. Hamidon, K. A. Matori, S. Pojprapai and P. Kantha, *J. Mater. Sci. Mater. Electron.*, 2014, **25**, 5491–5495.

172 N. S. M. Louis, A. Banu and S. Sudha, *Mater. Sci. An Indian J.*, 2014, **11**, 0974–7486.

173 B. Wang, M. Chen, J. Zhu, J. Tan, X. Fu, Y. Wang and S. Chen, *Procedia Environ. Sci.*,

2016, **31**, 12–17.

174 T. S. S. Kumar, R. Jayasree, P. S. K. Kavya, R. P. Nankar and D. Mukesh, 2015, **5**, 1–6.

175 F. Naghizadeh, N. Sultana, M. R. Abdul Kadir, T. M. Tengku Md Shihabudin, R. Hussain and T. Kamarul, *J. Nanomater.*, 2014, **2014**, 253185.

176 G. S. Ashworth and P. Azevedo, *Agriculture Issues and Policies Series*, nova science publishers, inc, New york, 2009.

177 C. M. Ajila, S. K. Brar, M. Verma, R. D. Tyagi, S. Godbout and J. R. Valéro, *Crit. Rev. Biotechnol.*, 2012, **32**, 382–400.

178 L. Lakshmi Devi and C. K. Jayasankar, *Ceram. Int.*, 2018, **44**, 14063–14069.

179 T. Lee, R. Othman and F. Y. Yeoh, *Biomass and Bioenergy*, 2013, **59**, 380–392.

180 S. S. Danewalia, G. Sharma, S. Thakur and K. Singh, *Sci. Rep.*, 2016, **6**, 24617.

181 M. K. Chhina and K. Singh, *Ceram. Int.*, , DOI:10.1016/j.ceramint.2019.12.195.

182 K. G. Patel, N. M. Misra and R. R. Shettigar, *Int. J. Chem. Eng. Appl.*, 2016, **7**, 344–347.

183 M. Baláž, *Acta Biomater.*, 2014, **10**, 3827–3843.

184 R. Yasothai and N. V Kavithaa, *Int. J. Sci. Environ. Technol.*, 2014, **3**, 1465–1471.

185 A. Bahrami, N. Soltani, C. A. Gutiérrez, N. Soltani and C. A. Gutiérrez, *Crit. Rev. Environ. Sci. Technol.*, 2016, **46**, 143–207.

186 Murakami et al., *Ciência e Tecnol. Aliment.*, 2007, **27**, 658–662.

187 A. Ibrahim, X. Li, Y. Zhou, Y. Huang and W. Chen, *Int. J. Mol. Sci.*, 2015, **16**, 7960–7975.

188 S. Singh and K. Singh, *J. Mol. Struct.*, 2015, **1081**, 211–216.

189 S. Khan and K. Singh, *Ceram. Int.*, 2019, **45**, 695–701.

190 G. Sharma and K. Singh, *Mater. Chem. Phys.*, 2020, **0254**, 122754.

191 K. Singh, N. Gupta and O. P. Pandey, *J. Mater. Sci.*, 2007, **42**, 6426–6432.

192 A. Goel, E. R. Shaaban, F. C. L. Melo, M. J. Ribeiro and J. M. F. Ferreira, *J. Non. Cryst. Solids*, 2007, **353**, 2383–2391.

193 K. Suzuki and K. Kijima, *Jpn. J. Appl. Phys.*, 2005, **44**, 2081–2082.

194 S. Khan and K. Singh, *Sci. Rep.*, 2020, **10**, 1089.

195 S. S. Danewalia, N. Gupta, S. Aggarwal and K. Singh, *J. Mater. Sci. Mater. Electron.*, 2017, **28**, 18986–18993.

196 M. Tiegel, R. Hosseinabadi, S. Kuhn, A. Herrmann and C. Rüssel, *Ceram. Int.*, 2015, **41**, 7267–7275.

197 W. Leenakul, T. Tunkasiri, N. Tongsiri, K. Pengpat and J. Ruangsuriya, *Mater. Sci. Eng. C*, 2016, **61**, 695–704.

198 N. Lahl, K. Singh, L. Singheiser and K. Hilpert, *J. Mater. Sci.*, 2000, **35**, 3089–3096.

199 M. F. Ferreira, B. A. E. Ben-arfa, H. R. Fernandes, I. M. M. Salvado and R. C. Pullar, 2017, 510–520.

200 C. L. Hwang and T. P. Huynh, *Constr. Build. Mater.*, 2015, **101**, 1–9.

201 M. Garai, N. Sasmal and B. Karmakar, *Indian J. Mater. Sci.*, 2015, **2015**, 1–7.

202 S. A. Hasan, S. M. Salman, H. Darwish and E. A. Mahdy, *Ceram. –Silikáty*, 2009, **53**, 165–170.

203 G. Sharma and K. Singh, *J. Mater. Cycles Waste Manag.*, 2019, **21**, 801–809.

204 P. Kubelka and F. Munk, *Zeitschrift für Tech. Phys.*, 1931, **12**, 593–601.

205 J. A. Duffy, *Phys. Chem. Glas.*, 2001, **42**, 151–157.

206 M. Abdel-Baki, F. A. Abdel-Wahab, A. Radi and F. El-Diasty, *J. Phys. Chem. Solids*, 2007, **68**, 1457–1470.

207 F. El-Diasty, F. A. Abdel Wahab and M. Abdel-Baki, *J. Appl. Phys.*, 2006, **100**, 093511.

208 Q. Zheng, Y. Zhang, M. Montazerian, O. Gulbiten, J. C. Mauro, E. D. Zanotto and Y. Yue, *Chem. Rev.*, 2019, **119**, 7848–7939.

209 B. Li, Z. Qing, Y. Li, H. Li and S. Zhang, *J. Mater. Sci. Mater. Electron.*, 2016, **27**, 2455–2459.

210 A. Prasad and A. Basu, *J. Adv. Res.*, 2013, **2**, 71–78.

211 S. Pandey, D. Kumar, O. Parkash and L. Pandey, in *Intech Open*, Web of Science, 2018, pp. 1–15.

212 N. Lahl, D. Bahadur, K. Singh, L. Singheiser and K. Hilpert, *J. Electrochem. Soc.*, 2002, **149**, 607–614.

213 M. Z. Firihu and I. N. Sudiana, *Pure Appl. Chem. Sci.*, 2017, **5**, 1–7.

214 G. Kaur, O. P. Pandey and K. Singh, *J. Non. Cryst. Solids*, 2012, **358**, 2589–2596.

215 A. G. Kalampounias, *Bull. Mater. Sci.*, 2011, **34**, 299–303.

216 M. I. M. Zamratul, A. W. Zaidan, A. M. Khamirul, M. Nurzilla and S. A. Halim, *Results Phys.*, 2016, **6**, 295–298.

217 A. Fluegel, D. A. Earl, A. K. Varshneya and T. P. Seward III, *Phys. Chem. Glas. Eur. J. Glas. Sci. Technol. B*, 2008, **49**, 245–257.

218 S. Rukzon, P. Chindaprasirt and R. Mahachai, *Int. J. Miner. Metall. Mater.*, 2009, **16**, 242–247.

219 P. C. D. B. Dingwell, *Am. Mineral.*, 1999, **84**, 465–476.

220 R. Salh, *Cryst. Silicon-Properties Uses*, 2011, **8**, 135–172.

221 H. Imai, K. Arai, H. Imagawa, H. Hosono and Y. Abe, *Phys. Rev. B*, 1988, **38**, 772–775.

222 G. Ganapathi Rao, B. Lakshmi Rekha, C. Arun Kumar, K. Jayant, K. Samatha and D. Madhava Prasad, *Appl. Phys. A Mater. Sci. Process.*, 2017, **123**, 1–8.

223 R. D. Shannon, *J. Appl. Phys.*, 1993, **73**, 348–366.

224 R. R. Raut, P. H. Salame, J. T. Kolte, C. S. Ulhe and P. Gopalan, *J. Mater. Sci. Mater. Electron.*, 2016, **27**, 730–737.

225 H. R. Fernandes, D. U. Tulyaganov, A. Goel, M. J. Ribeiro, M. J. Pascual and J. M. F. Ferreira, *J. Eur. Ceram. Soc.*, 2010, **30**, 2017–2030.

226 M. Elisa, B. A. Sava, A. Diaconu, L. Boroica, D. Ursu, I. Stamatin, F. Nastase, C. Nastase and C. Logofatu, *Glas. Phys. Chem.*, 2010, **35**, 596–601.

227 A. Nurur and H. Nakazawa, *Am. Mineral.*, 1978, **63**, 1252–1259.

228 G. Kaur, O. P. Pandey and K. Singh, *Int. J. Hydrogen Energy*, 2011, **37**, 3883–3889.

229 V. Kumar, S. Tyagi and K. Singh, *Indian J. Pure Appl. Phys.*, 2012, **50**, 335–338.

230 V. G. Plotnichenko, V. O. Sokolov and E. M. Dianov, *J. Non. Cryst. Solids*, 2000, **261**, 186–194.

231 P. Thuadaij and A. Nuntiya, *Procedia Eng.*, 2012, **32**, 1026–1032.

232 K. K. Chawla, *Interface, Composite Materials, Science and Engineering*, 2013, vol. 50.